9950 - 692

# INTEGRATED OPTICS TECHNOLOGY STUDY

# FINAL REPORT

PREPARED UNDER CONTRACT NO. 956157


APRIL 15, 1982

FOR

JET PROPULSION LABORATORY

CALIFORNIA INSTITUTE OF TECHNOLOGY



BY

B. CHEN, T. FINDAKLY, AND R. INNARELLA

TRW TECHNOLOGY RESEARCH CENTER

2525 E. EL SEGUNDO BLVD.
EL SEGUNDO, CALIF. 90245

# INTEGRATED OPTICS TECHNOLOGY STUDY

# FINAL REPORT

"This work was performed for the Jet Propulsion Laboratory, California Institute of Technology, sponsored by the National Aeronautics and Space Administration under Contract NAS7-100."

JUNE 18, 1982

FOR

JET PROPULSION LABORATORY

CALIFORNIA INSTITUTE OF TECHNOLOGY

BY

B. CHEN, T. FINDAKLY, AND R. INNARELLA

TRW TECHNOLOGY RESEARCH CENTER

*2525 E. EL SEGUNDO BLVD.*
*EL SEGUNDO, CALIF. 90245*

TABLE OF CONTENTS

# 1. INTRODUCTION AND SUMMARY

## 1.1 INTRODUCTION

This report summarizes the work performed under the Contract No. 956157 entitled "Integrated Optics Technology Study." The report describes and assesses the present status and near term potential of materials and processes available for the fabrication of single mode integrated electro-optical components. Issues included in the study are (1) host material and orientation (2) waveguide formation (3) optical loss mechanisms (4) wavelength selection (5) polarization effects and control (6) laser to integrated optics coupling (7) fiber optic waveguides to integrated optics coupling (8) sources (9) detectors. These issues are addressed separately in the following Sections 2 through 9. The goal of the study program is to provide a recommendation of the best materials, technology and processes for fabrication of integrated optical components for communications and fiber gyro applications.

Integrated optics technology has been advanced tremendously since its beginning in 1968. Until several years ago, most of the effort was concentrated on waveguide and device fabrication. Individual devices with optimum performance have been demonstrated using various waveguide materials and device configurations, while little attention was given to the device integration and coupling to the outside world. Recently, emphasis of the research effort is switched to apply those already developed technologies and to identify new technologies to be developed in order to satisfy system requirements. It is time for the researchers to examine the technology from the system point of view. Until the system requirements are clearly defined, it is difficult and risky to predict the future direction of material and device technology. At the end of each section of this report, we try to summarize the current status and technology trend. It is hoped that based on this report, system experts and technologists can work together to identify some most needed developmental programs.

## 1.2 SUMMARY AND RECOMMENDATIONS

In this section, we summarize the result of this study program. The objective of the program is to provide recommendation on the best materials technology and processes for the fabrication of integrated optical components for communications and fiber gyro applications. Throughout the text of this report, readers can find comments and conclusions drawn at the end of each section where specific issues are addressed. Here we will focus our attention on the subjects such as (1) substrate materials and waveguide fabrication techniques (2) reduction of waveguide losses (3) choices of single mode fibers and the polarization control (4) short wavelength systems versus long wavelength systems. We will try to point out the direction of future research effort specifically for fiber gyro and single mode communication systems applications.

### 1.2.1 Choice of Material System

In Section 2 and 3, we have discussed in great details on the materials and fabrication processes demonstrated during the last decade. Depending on the devices one may choose either active or passive substrate or waveguide materials. Once the material system is chosen, one of the waveguide fabrication techniques described in Section 3 can be adopted for the realization of the integrated optical circuit.

For fiber gyro application, the integrated optic processing chip may consist of optical switch, phase modulator, 3 dB beam splitter, and polarizer. The optical switch and modulator are active devices while the beam splitter and polarizer are passive devices. For active devices, $LiNbO_3$ is still considered as the best waveguide material and the in-diffusion of Ti metal forms a low loss optical waveguide. The total waveguide loss is estimated to be about 0.5 dB/cm at $\lambda$ = 830 nm and 0.2 dB/cm at $\lambda$ = 1300 nm. Until now, most researchers in the fiber gyro community are still using GaAlAs laser as the light source. At this wavelength, Ti:$LiNbO_3$ waveguides suffer the problem of optical damage. The effect of optical damage can be reduced to an insignificant level, if the power density inside the waveguide is less than $10^4$ W/cm$^2$ and the active devices are operated at an AC mode. Optical damage phenomenum is not observed at the operating wavelength of 1300 nm.

$LiNbO_3$ can also be used as the substrate material for passive devices. However, there are other passive material systems that have waveguide losses less than 0.1 dB/cm. If the fiber gyro processing chip does not require any active components, one can choose low loss optical glass substrates and the ion-exchange waveguide fabrication technique. Devices such as beam splitter and polarizer have been demonstrated using this technique with waveguide losses about 0.1 dB/cm.

Until now, fiber optical communication systems are primarily used as a point-to-point link. Thus the demand for integrated optic devices is not as critical as other applications. Again, $LiNbO_3$ and glass are the two prime material candidates for active and passive devices in single mode fiber optical systems.

For the next several years, $LiNbO_3$ and glass will continue to be the popular material systems for integrated optics applications. The research work on these two materials will be concentrated on the further reduction of waveguide losses. The absorption loss of bulk $LiNbO_3$ is about 0.3 dB/cm at $\lambda$ = 633 nm and it is not expected to total waveguide have losses less than 0.1 dB/cm even at $\lambda$ = 1300 nm. However, there is a good possibility of having stable glass waveguides with losses less than 0.01 dB/cm.

Two other material systems that have drawn a tremendous attention in integrated optics are laser annealed ZnO and III-V Semiconductors. Polycrystalline as well as single crystalline ZnO films have been fabricated on various substrate materials using various techniques. The most commonly used technique is the RF biased sputtering. The interest on ZnO waveguide is generated by the recent laboratory report of reduction of waveguide loss to 0.01 dB/cm using the laser annealing technique. As we conclude in Section 4, the effects of laser annealing on the electro-optic and piezo-electric properties of ZnO films are not known. We have some doubt that laser annealing would yield some adverse effects in this regard. More research work is needed to understand the annealing process and its effect on waveguide properties. It will be considered as a breakthrough in waveguide fabrication technique, if one can fabricate 0.01 dB/cm, single crystal, single mode ZnO waveguide.

One of the ultimate goals of integrated optics is to fabricate monolithic optical circuits on a single chip. To fulfill this technology challenge one has to use III-V semiconductor material systems, such as GaAs and InP. Only this class of material provides the opportunity to fabricate light source, detector together along with other integrated optic devices on one chip. Liquid phase epitaxy (LPE) is currently used in fabricating discrete as well as limited integrated optoelectronic devices. LPE does not have precise control of growth condition required for integrated optic devices. To really fabricate integrated optic circuits, one has to rely on the advanced molecular beam epitaxial (MBE) growth technique. This would require a well coordinated effort over several years at a sufficient funding level. For a laboratory equipped with MBE machines and growth expertise, this is definitely a research direction that promises a tremendous technology payoff. The payoff of MBE technology will not be limited to integrated optics only. the impact may be greater for certain electronic and optoelectronic devices. The problem facing semiconductor waveguides is the high absorption and free-carrier scattering losses. One has to operate these devices far away from the band gap.

### 1.2.2 Single Mode Optical Fiber

It is known that conventional circular core single mode optical fiber does not preserve the state of polarization over a long distance. On the other hand, most integrated optic devices do perform differently for different polarization states. During the last several years, a great amount of effort has been spent on the development of polarization preserving single mode optical fibers. Now, commercial fibers with beat length on the order of a few mm are available on a limited basis. These fibers have a built-in birefringence as a result of combination of anistropic strain induced birefringence and elliptical core waveguide birefringence. Research is still going on in this area with the goals of larger birefringence and lower attenuation loss. Polarization preserving property certainly is a desirable feature for fiber gyro application. As to high speed communication link, one does not have to worry about the output polarization state unless the homodyne detection scheme is used at the receiver end. Optical homodyne detection for optical fiber systems is still in its infancy. It is not yet clear if there is a real advantage over the commonly used detection scheme, at least in the wavelength region that glass fibers permit.

### 1.2.4 Choice of Operating Wavelength

Optical fiber communication systems are developed at a rapid rate. Short wavelength systems using GaAlAs light sources and Si detectors are already in field service all over the world. With the achievement of fiber loss of 0.4 dB/km at 1300 nm and 0.2 dB/km at 1550 nm, long wavelength systems are becoming very attractive. Germanium doped silica glass fibers have zero total dispersion at wavelengths ranging from 1300 nm to 1550 nm. A theoretical analysis has shown that for optical wavelength close to the minimum dispersion, single mode transmission system can be operated at 20-100 Gbps data rate over a distance greater than 100 km. Motivated by the improvement in fiber properties, there are tremendous on-going efforts on the development of long wavelength sources and detectors. Some long wavelength components are commercially available now with their performance comparable to the short wavelength counterparts.

Sections 8 and 9 give a detailed discussion on the state-of-the-art technology on the sources and detectors.

At the present time AlGaAs laser diodes and LED's have been used widely for short range optical data links (intraurban or shorter). This choice is aided by the commercial availability of low cost photo-detectors for the 800-900 nm spectral region. For high-data-rate long-haul applications, however, InGaAsP laser diodes, with their excellent match to the low-loss low-dispersion spectral region of fibers (1100-1700 nm) will eventually be the best choice of light source for optical fiber systems. They also appear to be less susceptible to degradation than GaAlAs diodes.

For optical gyro applications, where a short coherence length is required for freedom of interference of the optical beams with themselves due to the backward Rayleigh scattering, a super-radiant laser diode offers the best match. Super-radiant diodes can be obtained from most of the laser diodes by anti-reflection coating the mirror facets appropriately and by starting with a not too narrow stripe laser geometry capable of multimode oscillation.

It appears that the main efforts in source research should be concentrated in the areas of improving the mode stability of single-transverse and single-longitudinal mode laser diodes. This is of particular importance when lasers are modulated at several GHz frequencies. Other issues to be

addressed include higher output power and improved performance at higher currents and higher temperatures.

For short wavelength (800 - 900 nm) fiber systems, silicon photodiodes are used almost exclusively. The status of silicon photodiodes are very well-developed and high quality diodes (both p-i-n and APD's) are commercially available.

Most of the present investigation on photodetectors is concentrated toward long wavelength (1000 - 1600 nm) devices. The principal materials being used are germanium and several III-IV compounds (InGaAsP, GaAlAsSb). The problem areas of long wavelength photodiodes are high dark current, high excess noise and low useful avalanche gain. Ge APD performance has been improved by new diode structure ($n^+np$ and $p^+n$ instead of the conventional $n^+p$ structure). Effective ionization ratio of 0.6 - 0.7 over the 633 - 1500 nm wavelength was obtained. New structue has also been proposed for the InGaAsP APD where the absorbing and avalanche region are separated. The results obtained are very promising.

# 2. HOST MATERIAL AND ORIENTATION

Currently the electro-optical and acousto-optical material most commonly used in integrated optics applications is $LiNbO_3$. Other possible materials that can be used for the fabrication of active components include $LiTaO_3$, ZnO, GaAlAs/GaAs, InGaAsP/InP, ZnS/ZnSe/CdTe, $As_2S_3$ and other chalcogenide glasses. Magneto-optical materials have been used to fabricate waveguide devices such as Faraday rotators and modulators. Photo refractive materials have also been used to fabricate various passive integrated optic devices. However, these devices are less attractive for integrated optical circuits in comparison with electro-optical and acousto-optical devices. In this section, we will describe the electro-optical and acousto-optical effects of waveguide materials that can be used for active integrated optics devices.

## 2.1 LINEAR ELECTRO-OPTICAL MATERIALS

A linear electro-optic effect or Pockels effect is referred to as a change in the relative optical dielectric impermeability $B_{ij}$ proportional to an applied electric field $E_k$. The refractive index of a crystal is described by an index ellipsoid:

$$B_{ij}X_iX_j = 1 \equiv B_{11}X_1^2 + B_{22}X_2^2 + B_{33}X_3^2 + 2B_{23}X_2X_3 + 2B_{13}X_1X_3 + 2B_{12}X_1X_2$$

$$B_{ij} = B_{ji}$$

The electro-optic coefficient $r_{ij,k} \equiv r_{l,k}$ is defined by

$$\Delta B_{ij} = r_{ij,k}E_k$$

$$\Delta B_l = r_{lk}E_k$$

in which the indices i,j,k each are the rectangular coordinate axes 1,2,3 and l=(ij) refers to the six reduced combinations (11)=1, (22)=2, (33)=3, (23)=4, (13)=5, (12)=6. The electro-optic tensor matrices for all crystal symmetry classes are listed in Table 2-1. Table 2-2 lists most commonly used electro-optic materials and their properties.

Table 2-1. Electro-Optic Tensor Matrices (Handbook of Lasers)

*TRICLINIC – 1 – $C_1$*

$$\begin{pmatrix}\Delta B_{11}\\ \Delta B_{22}\\ \Delta B_{33}\\ \Delta B_{23}\\ \Delta B_{13}\\ \Delta B_{12}\end{pmatrix} = \begin{pmatrix} r_{11} & r_{12} & r_{13}\\ r_{21} & r_{22} & r_{23}\\ r_{31} & r_{32} & r_{33}\\ r_{41} & r_{42} & r_{43}\\ r_{51} & r_{52} & r_{53}\\ r_{61} & r_{62} & r_{63}\end{pmatrix} \begin{pmatrix} E_1\\ E_2\\ E_3\end{pmatrix}$$

(18) elements

*MONOCLINIC*

*$2 - C_2$*

$$\begin{pmatrix} 0 & r_{21} & 0\\ 0 & r_{22} & 0\\ 0 & r_{23} & 0\\ r_{41} & 0 & r_{43}\\ 0 & r_{52} & 0\\ r_{51} & 0 & r_{63}\end{pmatrix} \quad (2 \parallel X_2)$$

(8)

*$m - C_s$*

$$\begin{pmatrix} r_{11} & 0 & r_{13}\\ r_{21} & 0 & r_{23}\\ r_{31} & 0 & r_{33}\\ 0 & r_{42} & 0\\ r_{51} & 0 & r_{53}\\ 0 & r_{62} & 0\end{pmatrix} \quad (m \perp X_2)$$

(10)

*ORTHORHOMBIC*

*$222 - D_2$*

$$\begin{pmatrix} 0 & 0 & 0\\ 0 & 0 & 0\\ 0 & 0 & 0\\ r_{41} & 0 & 0\\ 0 & r_{52} & 0\\ 0 & 0 & r_{63}\end{pmatrix}$$

(3)

*$mm2 - C_{2v}$*

$$\begin{pmatrix} 0 & 0 & r_{13}\\ 0 & 0 & r_{23}\\ 0 & 0 & r_{33}\\ 0 & r_{42} & 0\\ r_{51} & 0 & 0\\ 0 & 0 & 0\end{pmatrix}$$

(5)

*TETRAGONAL*

*$4 - C_4$*

$$\begin{pmatrix} 0 & 0 & r_{13}\\ 0 & 0 & r_{13}\\ 0 & 0 & r_{33}\\ r_{41} & r_{51} & 0\\ r_{51} & -r_{41} & 0\\ 0 & 0 & 0\end{pmatrix}$$

(4)

*$\bar{4} - S_4$*

$$\begin{pmatrix} 0 & 0 & r_{13}\\ 0 & 0 & -r_{13}\\ 0 & 0 & 0\\ r_{41} & -r_{51} & 0\\ r_{51} & r_{41} & 0\\ 0 & 0 & r_{63}\end{pmatrix}$$

(4)

*$422 - D_4$*

$$\begin{pmatrix} 0 & 0 & 0\\ 0 & 0 & 0\\ 0 & 0 & 0\\ r_{41} & 0 & 0\\ 0 & -r_{41} & 0\\ 0 & 0 & 0\end{pmatrix}$$

(1)

*$4mm - C_{4v}$*

$$\begin{pmatrix} 0 & 0 & r_{13}\\ 0 & 0 & r_{13}\\ 0 & 0 & r_{33}\\ 0 & r_{51} & 0\\ r_{51} & 0 & 0\\ 0 & 0 & 0\end{pmatrix}$$

(3)

*$\bar{4}2m - D_{2d}$*

$$\begin{pmatrix} 0 & 0 & 0\\ 0 & 0 & 0\\ 0 & 0 & 0\\ r_{41} & 0 & 0\\ 0 & r_{41} & 0\\ 0 & 0 & r_{63}\end{pmatrix} \quad (2 \parallel X_1)$$

(2)

Table 2-1. Electro-Optic Tensor Matrices (Continued)
(Handbook of Lasers)

*TRIGONAL*

$3 - C_3$

$$\begin{pmatrix} r_{11} & -r_{22} & r_{13} \\ -r_{11} & r_{22} & r_{13} \\ 0 & 0 & r_{33} \\ r_{41} & r_{51} & 0 \\ r_{51} & -r_{41} & 0 \\ -r_{22} & -r_{11} & 0 \end{pmatrix} \quad (6)$$

$32 - D_3$

$$\begin{pmatrix} r_{11} & 0 & 0 \\ -r_{11} & 0 & 0 \\ 0 & 0 & 0 \\ r_{41} & 0 & 0 \\ 0 & -r_{41} & 0 \\ 0 & -r_{11} & 0 \end{pmatrix} \quad (2)$$

$3m - C_{3v}$

$$\begin{pmatrix} 0 & -r_{22} & r_{13} \\ 0 & r_{22} & r_{13} \\ 0 & 0 & r_{33} \\ 0 & r_{51} & 0 \\ r_{51} & 0 & 0 \\ -r_{22} & 0 & 0 \end{pmatrix} \quad (4)$$

*HEXAGONAL*

$6 - C_6$

$$\begin{pmatrix} 0 & 0 & r_{13} \\ 0 & 0 & r_{13} \\ 0 & 0 & r_{33} \\ r_{41} & r_{51} & 0 \\ r_{51} & -r_{41} & 0 \\ 0 & 0 & 0 \end{pmatrix} \quad (4)$$

$\bar{6} - C_{3h}$

$$\begin{pmatrix} r_{11} & -r_{22} & 0 \\ -r_{11} & r_{22} & 0 \\ 0 & 0 & 0 \\ 0 & 0 & 0 \\ 0 & 0 & 0 \\ -r_{22} & -r_{11} & 0 \end{pmatrix} \quad (2)$$

$622 - D_6$

$$\begin{pmatrix} 0 & 0 & 0 \\ 0 & 0 & 0 \\ 0 & 0 & 0 \\ r_{41} & 0 & 0 \\ 0 & -r_{41} & 0 \\ 0 & 0 & 0 \end{pmatrix} \quad (1)$$

$6mm - C_{6v}$

$$\begin{pmatrix} 0 & 0 & r_{13} \\ 0 & 0 & r_{13} \\ 0 & 0 & r_{33} \\ 0 & r_{51} & 0 \\ r_{51} & 0 & 0 \\ 0 & 0 & 0 \end{pmatrix} \quad (3)$$

$\bar{6}m2 - D_{3h}$

$$\begin{pmatrix} 0 & -r_{22} & 0 \\ 0 & r_{22} & 0 \\ 0 & 0 & 0 \\ 0 & 0 & 0 \\ 0 & 0 & 0 \\ -r_{22} & 0 & 0 \end{pmatrix} \quad (m \perp X_1) \quad (1)$$

*CUBIC*

$432 - O$

$$\begin{pmatrix} 0 & 0 & 0 \\ 0 & 0 & 0 \\ 0 & 0 & 0 \\ 0 & 0 & 0 \\ 0 & 0 & 0 \\ 0 & 0 & 0 \end{pmatrix} \quad (0)$$

$23$ and $\bar{4}3m - T$ and $T_d$

$$\begin{pmatrix} 0 & 0 & 0 \\ 0 & 0 & 0 \\ 0 & 0 & 0 \\ r_{41} & 0 & 0 \\ 0 & r_{41} & 0 \\ 0 & 0 & r_{41} \end{pmatrix} \quad (1)$$

Table 2-2. Some Electro-Optic Materials and Their Properties (Quantum Electronics, A. Yariv)

| Material | Room Temperature Electrooptic Coefficients in Units of $10^{-12}$ m/V | Index of Refraction[a] | $n_i^3 r_i$, in Units of $10^{-12}$ m/V | $\varepsilon/\varepsilon_0$ (Room Temperature) | Point-Group Symmetry |
|---|---|---|---|---|---|
| KDP ($KH_2PO_4$) | $r_{41}=8.6$<br>$r_{63}=10.6$ | $n_o=1.51$<br>$n_e=1.47$ | 29<br>34 | $\varepsilon_3^S \parallel c=20$<br>$\varepsilon \perp c=45$ | $\bar{4}2m$ |
| $KD_2PO_4$ | $r_{63}=23.6$ | ~1.50 | 80 | $\varepsilon \parallel c \sim 50$ at 24°C | $\bar{4}2m$ |
| ADP ($NH_4H_2PO_4$) | $r_{41}=28$<br>$r_{63}=8.5$ | $n_o=1.52$<br>$n_e=1.48$ | 95<br>27 | $\varepsilon \parallel c=12$ | $\bar{4}2_1m$ |
| Quartz | $r_{41}=0.2$<br>$r_{63}=0.93$ | $n_o=1.54$<br>$n_e=1.55$ | 0.7<br>3.4 | $\varepsilon \parallel c \sim 4.3$<br>$\varepsilon \perp c \sim 4.3$ | 32 |
| CuCl | $r_{41}=6.1$ | $n_o=1.97$ | 47 | 7.5 | $\bar{4}3m$ |
| ZnS | $r_{41}=2.0$ | $n_o=2.37$ | 27 | ~10 | $\bar{4}3m$ |
| GaAs at 10.6 $\mu$ | $r_{41}=1.6$ | $n_o=3.34$ | 59 | 11.5 | $\bar{4}3m$ |
| ZnTe at 10.6 $\mu$<br>CdTe at 10.6 $\mu$ | $r_{41}=3.9$<br>$r_{41}=6.8$ | $n_o=2.79$<br>$n_o=2.6$ | 77<br>120 | 7.3 | $\bar{4}3m$<br>$\bar{4}3m$ |
| ZnSe | $r_{33}=30.8$<br>$r_{13}=8.6$<br>$r_{41}=1.8$ | $n_o=2.29$<br>$n_o=2.3$ | $n_e^3 r_{33}=328$<br>26 | $\varepsilon \perp c=98$<br>9.1 | $\bar{4}3m$ |
| $LiNbO_3$ | $r_{22}=3.4$<br>$r_{42}=28$ | $n_e=2.20$ | $n_o^3 r_{22}=37$<br>$\frac{1}{2}(n_e^3 r_{33}-n_o^3 r_{13})=112$ | $\varepsilon \parallel c=50$ | 3m |
| GaP | $r_{41}=0.97$ | $n_o=3.31$ | $n_o^3 r_{41}=29$ | | $\bar{4}3m$ |
| $LiTaO_3$ (30°C) | $r_{33}=30.3$<br>$r_{13}=5.7$ | $n_o=2.175$<br>$n_e=2.180$ | $n_e^3 r_{33}=314$ | $\varepsilon \parallel c=43$ | 3m |
| $BaTiO_3$ (30°C) | $r_{33}=23$<br>$r_{13}=8.0$<br>$r_{42}=820$ | $n_o=2.437$<br>$n_e=2.365$ | $n_e^3 r_{33}=334$ | $\varepsilon \perp c=4300$<br>$\varepsilon \parallel c=106$ | 4mm |
| ZnO at 632.8 nm | $r_{33}=2.6$ | $n_e=2.015$ | $n_e^3 r_{33}=21.3$ | 8.15 | 6mm |

[a]Typical value

## 2.2 ACOUSTO-OPTICAL MATERIALS

For acousto-optical waveguide devices, performance usually is characterized by the figure of merit, $M_2$

$$M_2 \equiv n^6 p^2 / \rho v^3$$

where n is the index of refraction, p the strain-optic tensor element, $\rho$ the density, and $v$ the acoustic velocity. It is important to note that parameters n, p, and $v$ are all related to tensor quantities and vary with crystal orientation. Table 2-3 lists selected acousto-optic materials and their properties. This table includes figures of merit $M_1$, $M_2$ and $M_3$. $M_1$ and $M_3$ are defined in a slightly different way.

$$M_1 \equiv n^7 p^2 / \rho v$$

$$M_3 \equiv n^3 p^2 / \rho v^2$$

In order to maximize the device performance, one may choose a special crystal cut that gives the highest figure of merit. On the other hand, the integrated optical devices thus fabricated should retain their low optical and acoustic losses. Among all the materials listed in Table 2-3, $LiNbO_3$ has the lowest acoustic attenuation of <0.03 dB/μsec at 500 MHz.

## Table 2-3. Selected Acoustic-Optic Materials (Handbook of Lasers)

| *Material* | *Approximate range of optical transmission* ($\mu$) | *Wavelength of measurement* ($\mu$) | *Index of refraction n* | *Acoustic wave polarization and direction* | *Acoustic velocity* ($\times 10^5$ *cm/sec*) | *Optical wave polarization and direction*[b] | *Figures of merit*[a] $M_1$ | $M_2$ | $M_3$ | *Acoustic attenuation at 500 MHz*[c] (*dB/μsec*) | *Comments* |
|---|---|---|---|---|---|---|---|---|---|---|---|
| Fused silica[d] ($SiO_2$) | 0.2–4.5[e] | 0.633 | 1.46 | long. | 5.96 | perpendicular | 1.0 | 1.0 | 1.0 | 1.8[f] | Reference material |
| | | | | shear | 3.76 | parallel or perpendicular | 0.12 | 0.31 | 0.2 | | |
| Water[d] $H_2O$ | 0.2–0.9[g] | 0.633 | 1.33 | long. | 1.5 | parallel or perpendicular | 6.1 | 106 | 24 | 75.[h] | |
| $D_2O$ | 0.2–1.8[g] | | | | | | | | | | |
| $\alpha$-$HIO_3$[i] | 0.3–1.8 | 0.633 | 1.98 | long. [001] | 2.44 | perpendicular [010] | 13.6 | 55. | 32 | 0.6 | Water soluble |
| $PbMoO_4$[j] | 0.4–5.5 | 0.633 | 2.39 | long. [001] | 3.66 | parallel or perpendicular [100] | 15.3 | 23.7 | 24.9 | 1.2 | |
| $LiNbO_3$[d] | 0.5–4.5 | 0.633 | 2.20 | long. [11$\bar{2}$0] | 6.57 | | 8.3 | 4.6 | 7.5 | <0.03[k] | Optical damage[l] |
| $TiO_2$[d] | 0.45–5.5[l] | 0.633 | 2.58 | long. [11$\bar{2}$0] | 7.86 | perpendicular [0001] | 7.9 | 2.6 | 6.2 | | |
| $TeO_2$[m] | 0.35–5.[n] | 0.633 | 2.27[n] | long. [001] | 4.26 | perpendicular [010] | 18.5 | 22.8 | 25.6 | 1. | |
| | | | | shear. [110] | 0.617 | parallel or perpendicular [001] | 8.8 | 525. | 85. | 3. | |
| GaP[d] | 0.6–10.0 | 0.633 | 3.31 | long. [110] | 6.32 | parallel | 75. | 29.5 | 69. | <1. | |
| | | | | shear [100] | 4.13 | parallel or perpendicular [010] | 17.4 | 16. | 25.7 | | |
| $As_2S_3$ glass[d] | 0.6–11.[e] | 1.15 | 2.46 | long. | 2.6 | perpendicular | 78. | 230 | 182. | 11.[p] | |
| $Ge_{33}Se_{55}As_{12}$ glass[q] | 1.–14. | 1.06 | 2.7 | long. | 2.52 | parallel or perpendicular | 53. | 164. | 128. | 1.8 | |
| Ge[r] | 2.–20.[e] | 10.6 | 4.0 | long. [111] | 5.50 | parallel | 1,270. | 540. | 1,380. | 4.2 | |
| | | | | shear [100] | 3.51 | parallel or perpendicular | 182. | 190. | 308. | 0.8 | |
| Te[s] | 5.–20[e] | 10.6 | 4.8 | long. [11$\bar{2}$0] | 2.2 | parallel in [0001] | 1,320 | 2,920 | 3,550 | "a few"[p] | Soft |
| ZnO | | 0.633 | 2.015 | long. | 6.0 | | | | | | |

# 3. WAVEGUIDE FORMATION

Optical waveguides are structures that confine and direct the optical signals in a region of higher index of refraction than its surrounding medium. One good example of optical waveguide is the optical fiber which has been widely used for transmission of wideband optical information over tens kilometers. Most of the fibers developed have circular cross-sections for both the fiber core and clad. The optical confinement in the fiber core is achieved by increasing the index of refraction in the core region. On the other hand, the optical waveguides of interest to integrated optics are usually asymmetric either in the planar or channel waveguide structures. Most waveguides considered here are single mode waveguides for TE and TM polarizations. Figure 3-1 shows various structures of optical waveguides that have been investigated in integrated optics. Figure 3-1(a) depicts a planar waveguide which is the simplest and most basic waveguide structure. The thin film sandwiched between the substrate and superstrate has the highest index of refraction, thus providing the guiding region. In the case of Figure 3-1(a), the superstrate is air with index of refraction of 1. The typical thickness of the waveguide is on the order of the wavelength of the optical signal to be transmitted. The index of refraction of the thin film optical waveguide can be homogeneous or graded with certain profiles. The index profile is primarily determined by the waveguide fabrication process. The channel waveguides, Figure 3-1 (d)-(g), are three dimensional waveguides with cross-sections of a few square μm. In the channel waveguide case, the guided modes are not TE nor TM. However, the longitudinal component of the electrical field (or magnetic field) is much smaller than the transverse component. One can therefore approximate the mode structure by a TE (or TM) polarization.

Figure 3-1 (a), (b), and (c) illustrate various planar waveguide structures: (a) asymmetric air-guide-substrate, $n_g > n_s > n_o$; (b) symmetric optical waveguide, $n_g > n_s$; (c) composite waveguide structure, $n_g > n_s$, and $n_g > N_o$; (d), (e), (f) and (g) illustrate various channel waveguide structures; (d) and (e) are ridge waveguides with $n_g > n_s$ for (d), and $n_a$, $n_b < n_o$ for (e); (f) embedded channel waveguide, $n_g > n_s$; (g) inverted ridge waveguide $n_a$, $n_b > n_s$.

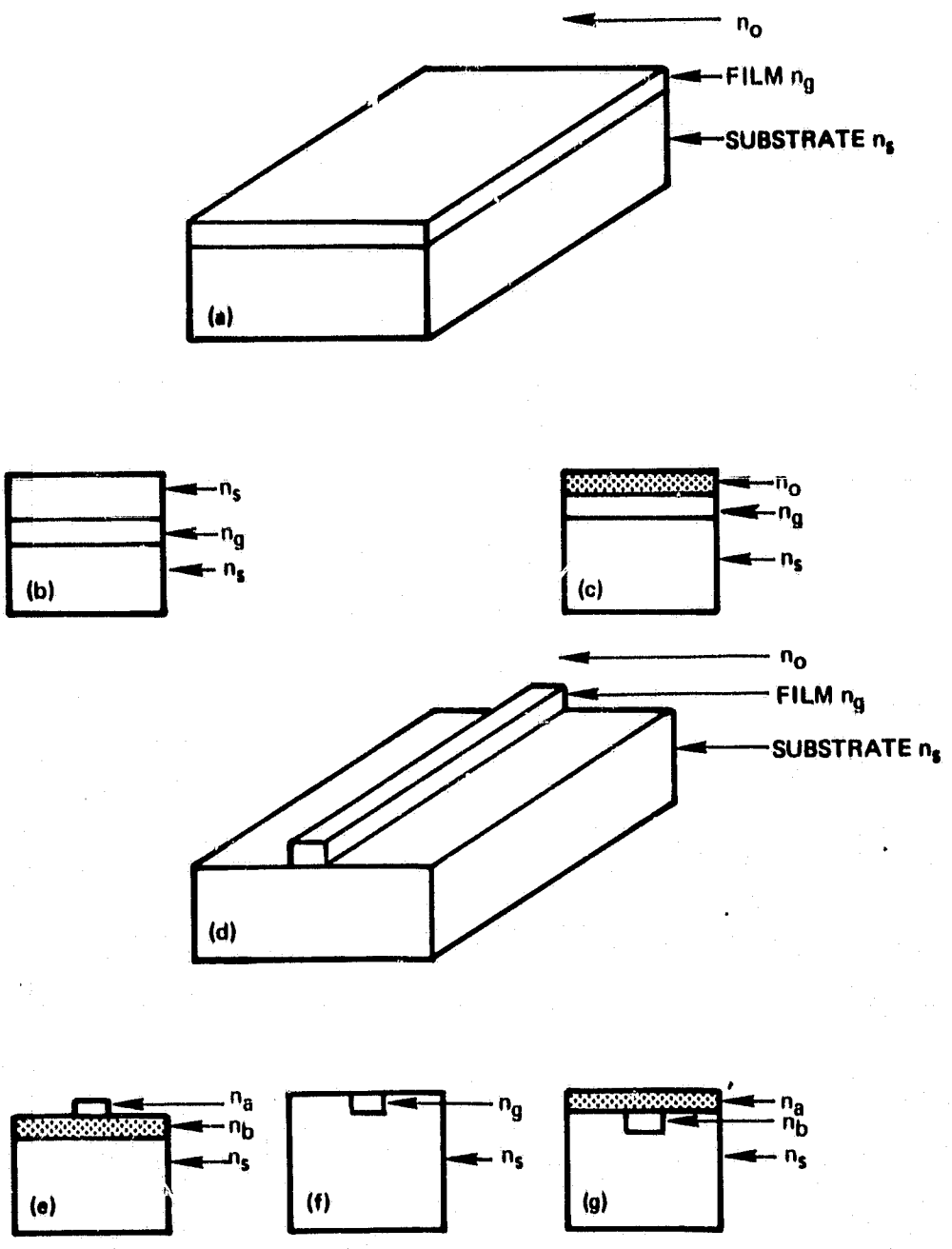


Figure 3-1. Various Waveguide Structures

Since the name of "INTEGRATED OPTICS" was coined in 1968, many waveguide fabrication techniques have been proposed and used to form various optical waveguides on different substrates. Unfortunately, a large number of waveguides fabricated are not suitable for any practical applications due to large waveguide propagation losses. A good optical waveguide should have propagation loss less than 1 dB/cm. In this section we try to summarize all the fabrication processes reported to date with emphasis on the ones that generate low loss waveguide. We can classify all the fabrication processes into three categories: (1) thin film deposition (2) epitaxial growth, and (3) modification.

## 3.1 THIN FILM DEPOSITION

Within this category, the optical waveguides are formed by deposition of a layer of high index of refraction. This deposition can be done by evaporation (thermal evaporation, electron-beam evaporation), RF sputtering, spin and dip coating, and chemical vapor deposition.

### 3.1.1 Evaporation

Two standard methods of thin-film deposition by evaporation are thermal and electron-beam evaporation. Evaporation techniques have been known in the optical coating field for a long time. Various dielectric films, both high and low index, have been used for protective coating as well as interference filters. These thin film coatings are more than adequate for most optics applications. The requirements on the surface roughness scattering and absorption losses are much more stringent for the integrated optics. This is simply because the optical light is travelling within the thin film waveguide rather than perpendicular to the thin film. As a result evaporation is used only for electrode fabrication, deposition of masks or diffusion sources.

ZnS films have been deposited on glass substrate by E-beam evaporation.[1] The substrate was held at room temperature during evaporation and the ZnS films were amorphous. The films had a loss of more than 5 dB/cm, attributed to the long tail of the absorption edge. E-beam evaporation has also been used to fabricate low loss glass waveguides on fused quartz substrate.[2] A special glass Planer CAS 10 was used as the evaporation source. Results of two different runs were reported, the first one

with a deposition rate of 3.8 nm/s and a thickness of 2.05 μm, the second one with 2.6 nm/s and 0.91 μm thickness. The 0.91 μm thick waveguide can support only one mode while the 2.05 μm thick one supports two modes. The refractive index of the glass film is estimated to be 1.469 at $\lambda$ = 632.8 nm. The measured waveguide losses were 1.2 ± 1 dB/cm at $\lambda$ = 676.4 nm and 4.3 dB/cm at $\lambda$ = 476.2 nm.

### 3.1.2 RF Sputtering

RF sputtering is a popular technique of fabricating low loss dielectric waveguides. The sputtering process is quite well understood[3] and precise control of various sputtering parameters is obtainable with commercial sputtering systems. Several sputtering modes can be obtained by making appropriate electrical connections to the J-head (substrate table). These sputtering modes include RF sputtering, RF bias sputtering, RF sputtering with J-head grounded, and RF sputter-etch. Depending on the sputtering gases used, reactive sputtering can modify the chemical composition of the deposited films.

RF sputtering was first used to deposit 7059 glass on ordinary glass slides.[4] Corning 7049 glass is a pyrex type of glass with bulk composition $SiO_2$ 50.2%, BaO 25.1%, $B_2O_3$ 13.0%, $Al_2O_3$ 10.7% and $As_2O_3$ 0.4%. The refractive index of bulk 7059 glass is about 1.53. Because of the change of composition during the sputtering process the refractive index of sputtered film was determined to be 1.62 by the Brewster angle measurement. Films sputtered with 100% Ar gas were brown and lossy because of oxygen deficiency. When 100% oxygen gas was used, the waveguide loss was reduced to less than 1 dB/cm. The use of oxygen as sputtering gas reduces the deposition rate. This is attributed to the formations of high concentration of negative ions of O or $O_2$, which act as electron traps.[5] The electron affinities of $O^-$ and $O_2^-$ are 1.47 eV and 0.43 eV, respectively. These are the additional energy required to support the discharge.

In the steady state of the sputtering, the ratio of the effective sputtering rates of different constituents must be equal to the ratio of their concentrations in the target. If this is not the case, then for the faster sputtering constituents, the number of atoms on the surface available for sputtering becomes less and less. Consequently their sputtering rates are reduced gradually until equilibrium is reached. For the lower

sputtering rate constituents the situation is just the opposite. The sputtering rates are increased to reach the equilibrium value. On the deposition side, however, the ratio of deposition rates of different constituents does not follow this rule since the sticking coefficients are different for different constituents. Even for a single component target, the sticking coefficient may change with the substrate material and sputtering conditions. This effect explains the fact that sputtered 7059 glass films having their composition and refractive indices different from that of the bulk material. It was observed that the sputtered 7059 glass films have a different barium oxide content than the bulk.[6] It was also observed that the refractive index of sputtered films varied as a function of the power level at which the deposition was done.[7] The film refractive index at $\lambda$ = 632.8 nm could vary from 1.53 (the bulk refractive index) to 1.585 as the RF sputtering power density was changed from 0.5 W/cm$^2$ to 4.0 W/cm$^2$. It was also observed that the film refractive index depended on substrate material. Under similar sputtering conditions, the film index was 1.61 for fused quartz substrate, 1.55 ~ 1.56 on micro glass slides, and 1.55 on Nd-doped glass substrates.[8] 7059 glass waveguide is most successful material fabricated by RF reactive sputtering technique. It has been used by many research groups to fabricate various passive waveguide devices. This popularity is partially due to the commercial availability of 7059 glass as sputtering target. Another type of glass film reported by RF reactive sputtering is barium-silicate glass.[9] The sputtering target is formed by hot-pressing of a mixture of barium carbonate and silica. The sputtered films exhibited low waveguide loss and the refractive index of the film was controlled by varying the ratio of barium oxide to silicon dioxide in the sputtering target. The film index varied from 1.48 to 1.62 simply by varying the barium oxide content from 0 to 40 wt. percent.

Nd-glass thin film waveguide is an attractive active medium for Nd thin film laser. Nd-glass films have been prepared by RF sputtering of barium crown Nd-glass on a heated corning 7059 glass substrate.[10] Clear films were obtained only when the target glass is sodium-free. When AO 1838 Nd-glass target (the constituents are $SiO_2$, $Na_2O$, $K_2O$, BaO, $Al_2O_3$, $Li_2O$, and $Sb_2O_3$) was used, the sputtered film was brown.[11] The brownish color was attributed to the oxygen deficiency of alkali-oxides. The heat of dissociation of these alkali-oxides is much smaller than other oxides.

The brownish color can be annealed away by heating the film at 500°C for 15 hours in air. The propagation losses of these waveguides were measured to be 0.5 dB/cm at $\lambda$ = 632.8 nm and 0.15 dB/cm at $\lambda$ = 1064 nm. An attractive feature is that a gain of 1 $cm^{-1}$ at $\lambda$ = 1064 nm was obtained when the waveguide is pumped with dye laser coupled into the waveguide. With a 1 $cm^{-1}$ net gain (the waveguide loss has already been taken into account), one should be able to use it as the active medium for Nd-thin film lasers of either the distributed-feedback type or the Bragg-reflector type. The laser threshold requires the round trip total loss less than the gain, i.e., 1 $cm^{-1}$ = 4.34 dB.

Aluminum oxide films RF sputtered onto single crystal quartz substrate have been used in thin film second harmonic generation experiments.[12] The index of refraction at $\lambda$ = 546.1 nm, measured by ellipsometry technique, was n = 1.663. Waveguide loss was estimated to be about 40 dB/cm.

$Ta_2O_5$ is a high index of refraction material, a desirable feature for integrated optics applications, for example, Lunenberg Lenses. Film index as high as 2.08 at $\lambda$ = 632.8 nm was obtained by RF reactive sputtering of Ta metal target.[13] If a small amount of $N_2$ is introduced in the sputtering chamber, the resulting film index can be varied from 1.85 to 2.13 depending on the $N_2/O_2$ ratio. Optical waveguide loss < 1 dB/cm was reported. Another way of changing the film index is to add some low index oxides into the $Ta_2O_5$ sputtering target. $SiO_2$-$Ta_2O_5$ composite waveguide films have been deposited on Corning Vycor glass substrates from a target consisting of $SiO_2$ and $Ta_2O_5$.[14] Five sputtering targets containing 0, 25, 50, 75, and 100 mol% $Ta_2O_5$ were used to deposit films of refractive index ranging from 1.46 to 2.08 at $\lambda$ = 632.8 nm. Propagation loss of less than 0.8 dB/cm was obtained for films thicker than 1 μm. Waveguide loss was reduced by post-deposit annealing in air for 12 hours at 450°C.

Another high index waveguide film material is $Nb_2O_5$, which can be fabricated by RF reactive sputtering of either Nb metal or $Nb_2O_5$. An early experiment with $Nb_2O_5$ film showed high waveguide loss, 20 dB/cm at $\lambda$ = 632.8 nm.[15] X-ray diffraction analysis indicated that the film contained small, randomly oriented crystallites, which gave rise to a large scattering loss. By reducing the substrate temperature during the sputtering process, one can obtain an amorphous film with low propagation loss.

Waveguide loss can be further reduced by laser annealing. For a 100% $O_2$ sputtering, a refractive index of 2.297 was measured. For both $Ta_2O_5$, and $Nb_2O_5$ cases, the reactive sputtered films have their index of refraction about 94% of the value for the anodic oxide films. This is probably due to a lower film density. It is important to note that the film density depends on many sputtering conditions. It is not a surprise that different laboratories report different results on waveguide characteristics.

### 3.1.3 Spin and Dip Coating

Thin film optical waveguides have been deposited on glass substrates from liquid solutions. Solid films were formed after a slow evaporation of the solvents. Similar to the coating of photoresist in photolithographic process, the liquid films are coated on solid substrates by spin or dip coating. Final film thickness is primarily determined by the solid content, viscosity and spinning speed. Various materials were used,[16] including polyurethane, polystyrene, epoxy, photoresist, and organo-metallic solutions. This coating is usually done at room temperature and cured at an elevated temperature varying from 50°C to 100°C. Waveguide losses less than 1 dB/cm at $\lambda$ = 632.8 nm can be easily obtained with all the materials mentioned above except photoresist. Photoresists provide the advantage that channel waveguide structure can be easily fabricated using well developed photolithographic technique. However, photoresists, such as Kodak KPR,[16] Shipley AZ1350,[17] are too lossy ($\geq$7 dB/cm) to be practical waveguide materials. Waveguide loss can be reduced by removing the photo-sensitizer, which also reduces the photosensitivity.

Films fabricated from liquid solutions are usually soft and susceptible to to chemical attack. The coating technique does not have the control of film thickness and uniformity required for integrated optics devices. Because of the ease of fabrication, some of these films are used as diffusion source[18] or overlay coating to reduce the waveguide surface scattering.[19] A spin coating technique is also used to deposit organic films followed by a polymerization process. This type of fabricated technique is classified as "Modification" process and is discussed in Section 3.3.

### 3.1.4 Chemical Vapor Deposition

Silicon oxynitride films deposited on fused silica by chemical vapor deposition has at one time been considered as a potential integrated optics medium.[20] SiON is a glassy, amorphous, stable silicon-oxygen-nitrogen polymer of adjustable composition. The index of refraction can be varied between those of deposited $SiO_2$ ($n = 1.455$ at $\lambda = 546$ nm) and deposited $Si_3N_4$ ($n = 1.98$). SiON films were deposited at 850°C in a conventional RF — heated silica tube reactor from a one atmosphere ambient typically comprising 0.2 to 0.5% nitric oxide, 0.02 to 0.07% silane, and the remainder nitrogen. The SiON composition was controlled by the $NO/SiH_4$ concentration ratio. Deposition of 1200 to 8000 Å thick waveguide film was achieved in 2 to 10 min. Films of $n = 1.48 - 1.54$ had very low loss, <4 dB/cm at $\lambda = 632.8$ nm. However, higher refractive index films were not so successful as the surface cracked easily. By using low vapor pressure CVD technique, excellent quality films of $Si_3N_4$ were reported. Silicon wafers were used as substrates, and the $Si_3N_4$ was separated from the substrate by a steam-oxide $SiO_2$ buffer layer.[21] No evidence of cracks was observed for film thickness less than 4000Å. For a film thickness of 3212Å, two (TE) waveguide modes with propagation losses of <0.1 dB/cm ($TE_0$) and 6 dB/cm ($TE_1$) were observed. Extension of optical fields into the Si substrate was shown to be the major loss mechanism. This explains the fact that the loss for $TE_1$ mode is much higher than the loss of $TE_0$ mode.

## 3.2 EPITAXIAL GROWTH

This technique allows one to fabricate single crystalline films for integrated optics, and in particular, active optical devices such as switches, modulators and scanners. It has been and it will continue to be a big challenge to material scientists to refine the growth technique such that low loss waveguide devices can be constructed. A successful development of low loss waveguides on GaAs or InP material systems will certaintly brighten the prospect of fabricating monolithic integrated optic circuits. There are two methods available today for forming single crystal films, namely epitaxial growth and modification by diffusion or ion-exchange. In spite of the recent intensive research, neither method is satisfactory of a monolithic circuit. Many more years of elaborate work is needed to understand and improve the fabrication processes.

### 3.2.1 Epitaxial Growth by RF Sputtering

ZnO films have been prepared by RF sputtering of a ZnO target in $O_2$ - Ar mixtures on various substrate materials. The technology was developed originally for applications in the acoustic field, where ZnO served as a good transducer medium. Sputtered ZnO film is a polycrystalline film with columnar crystallite structure typically 100Å in a dimater. For the films to show electro-optic and electro-mechanic properties, it is necessary that all the crystallites be oriented in the same direction, so that the associated effects of these crystallites can be accumulated coherently for device application. ZnO film is known to have a strong tendency to grow with C-axis normal to the substrate surface. A complete C-axis normal orientation with small deviation requires special growth condition under a certain temperature, vapor pressure, growth rate, etc.

ZnO thin films have been employed as optical waveguides for many integrated optics experiments.[22,23] Early experiments yielded extremely high optical propagation loss (20 to 50 dB/cm),[24] even after gentle polishing of the film surface. This is believed to be due to the columnar structure which results in a rough surface proportional to a film thickness. Optical losses also arise due to voids among crystallites. Although the optical waveguide properties depend strongly on the film deposition process, it is generally recognized that high optical quality film (<5 dB/cm) occurs only for nearly epitaxial films. Recently nearly epitaxial film exhibiting low optical losses has been observed after annealing the RF sputtered ZnO film with a $CO_2$ laser.[25] Waveguide loss for the fundamental mode of a three-mode waveguide was reduced to 0.01 dB/cm. A laser annealing process is believed to induce coalescence of neighboring crystallites, thus improving the film density uniformity and orientation. Effects on the electro-optic, acousto-optic, and nonlinear characteristics of laser annealed ZnO films are yet to be determined.

### 3.2.2 Epitaxial Growth by Melting

Epitaxial growth by meling (EGM) has been used to grow $6Bi_2O_3:TiO_2$ waveguides on $Bi_{12}GeO_{20}$, and $LiNbO_3$ waveguides on $LiTaO_3$. This is one of the simplest method of epitaxial single crystal film growth, achieved by either dipping the substrate into a bulk melt or melting a power or lacquer suspension on the substrate. This technique is attractive for integrated

optics for two reasons: first, the waveguide material with index of refraction larger than that of the substrate often has a lower melting point. Secondly, the film grown by EGM always has a transition region which minimizes the lattice mismatch problem. The refractive index profile is somewhere between the exponential function of some diffused waveguides and the step function of the uniform waveguide.

In the grwoth of various sillenites on bismuth germanate ($Bi_{12}GeO_{20}$) substrate,[26] substrates were dipped in a super-cooled melt (825 to 930°C) at a growth rate of 1 to 2 μm per minute. Sillenites used were bismuth gallate ($12Bi_2O_3:Ga_2O_3$) or bismuth titanate ($6Bi_2O_3:TiO_2$).

For the growth of $LiNbO_3$ on $LiTaO_3$ substrate,[27] the $LiNbO_3$ powder was first spread over the $LiTaO_3$ substrate and then heated up to 1300°C to melt the powder. The sample was cooled slowly at a rate of about 20°C/h. The top surface of the as-grown film was rough, and required special polishing before the waveguiding phenomenum was observed. An electro-optic modulator was fabricated using this technique.[28] The EGM method was improved by first suspending $LiNbO_3$ powder in a lacquer, and then painting the $LiNbO_3$-lacquire on the $LiTaO_3$ substrate.[29] As the sample temperature was raised to 1270°C, the coating first turned black as the organic lacquer was decomposed. It then became transparent and glossy indicating the melting of $LiNbO_3$. Within a few minutes, the glassy appearance disappeared, and the solid solution was formed. An improvement in film uniformity was obtained.

Despite the simplicity of forming high index single crystalline films, the EGM does not produce any waveguides with good optical properties for integrated optics applications.

### 3.2.3 Liquid Phase Epitaxy (LPE)

Liquid phase epitaxial growth of thin films has been successfully developed in the semiconductor industry, and it seems reasonable to apply it to optical waveguide fabrication. However, the LPE technique is still limited to the growth of semiconductor films primarily for the fabrication of opto-electronic devices.

The first growth of $LiNbO_3$ films on $LiTaO_3$ by LPE technique was demonstrated using a $Li_2O$-$V_2O_5$ flux.[30]. A C-cnt $LiTaO_3$ substrate was dipped into a molten mixture containing 50 mol% $Li_2O$, 40 mol% $V_2O_5$, and 10 mol% $Nb_2O_5$. This mixture was heated to about 1100°C and cooled slowly to the growth temperature of about 850°C. A transparent and colorless $LiNbO_3$ film with with thickness ~3 μm was grown epitaxially onto the substrate, the waveguide supported seven TE and TM modes. Measurements of the modal indices indicated that the film was an uniform waveguide having constant indices $n_o$ = 2.288 and $n_e$ = 2.191 at $\lambda$ = 632.8 nm. Waveguide losses of 5 and 11 dB/cm were measured for $TM_o$ and $TE_o$ modes, respectively. Different flux systems were tried:[31] $Li_2B_2O_4$-$Li_2Nb_2O_6$ and $Li_2WO_4$-$Li_2Nb_2O_6$ flux systems produced films rich in Li; $K_2WO_4$-$Li_2Nb_2O_6$ and $WO_3$-$Li_2Nb_2O_6$ flux system produced films rich in Nb.

Ridge channel waveguides were fabricated by liquid phase heteroepitaxial growth of GaAlAs on GaAs.[32] A channel was first etched into the GaAs substrate, over which was grown as $Ga_{0.7}Al_{0.3}As$ layer as a low index confinement and smoothing layer, followed by a second high index GaAs layer to fill the channel. The guides were reported to be low loss because the smoothing layer removed most of the scattering losses. Electro-optic modulation has been performed at 1.15 μm in double heterostructures of GaAs-GaAlAs channel guide of width only 0.15 to 0.2 μm.[34]

Another optical waveguide fabricated by LPE technique is that of gallium-and iron-garnet films developed originally for magnetic bubble memory devices. Optical waveguide and magneto-optical waveguide switches have been successfully demonstrated. Because of the abrupt interface between the film and substrate, good lattice matching is required for the LPE growth. The garnet family has a good range of lattice parameters and refractive indices to allow a "mix-and-match" set of waveguide structures. Garnet films as-grown are smooth, uniform and pin-hole free, thus eliminating the scattering losses. However, the absorption losses varied from 1 to 5 dB/cm, depending on the impurity content of the melt.[34] A magneto-optic switch was fabricated on $Eu_3Ge_5O_{12}$ waveguide epitaxially grown on $Gd_3Sc_2Al_3O_{12}$ substrate.

Other waveguide materials fabricated by LPE method include yttrium aluminum garnet on sapphire,[35] and a KDP:ADP layer on KDP substrates.[36] Unfortunately, these films are not suitable for integrated optics applications because of difficulty of obtaining good quality films or water attack of ADP and KDP.

### 3.2.4 Vapor Phase Epitaxy (VPE) and Metal-Organic Chemical Vapor Deposition (MOCVD)

The VPE and MOCVD are two alternative techniques of growing semiconductor films primarily for the fabrication of optoelectronic devices. Unlike the LPE method, the materials to be deposited are carried by a gas, usually $H_2$. The deposition is slower than that of LPE method. As a result, one has the control of thickness and doping profile of each deposited layer. A strip-loaded waveguide was fabricated by first growing a high-index lightly doped layer of GaAs on a heavily doped $n^+$ layer followed by etching to form a strip-line.[37] Waveguide loss at 1.16 μm was 4.5 dB/cm. An electro-optic directional coupler switch was fabricated on a planner VPE GaAs layer fabricated in a similar fashion.[38] Lateral confinement was obtained by depositing an Au-Pt Schottky barrier film, which also was used as electrodes.

### 3.2.5 Molecular Beam Epitaxy (MBE)

MBE is a powerful technique in growing single crystal films with precise control of stoichiometry thickness, deposition rate, and dopant concentration. Growth is performed in a high vacuum chamber where the substrate is kept at an elevated growth temperature. Molecular species are evaporated and directed toward the substrate by separate source chambers. Slow growth rate allows one to control the process down to a few atomic layers. This method was used to fabricate GaAs double heterostructure lasers and other devices. MBE was also used to fabricate GaAs CW-DH laser taper coupled to a passive $Ga_{1-x}Al_xAs$ waveguide layer inside the cavity.[39] The taper coupler approached 100% coupling efficiency and the waveguide loss of the passive layer was about 4 dB/cm. MBE is one of the most promising technique for the monolithic integrated optic circuit. Currently, GaAlAs laser devices made by MBE are as good as other lasers made by LPE or MOCVD. However, MBE is still having problems in growing InGaAsP layered structures.

## 3.3 MODIFICATION

Optical waveguides can also be formed by increasing the index of refraction of the substrate surface through diffusion, ion-exchange, ion-implantation, polymerization, etc. It has been found that the most popular waveguides used in integrated optics are fabricated using one of methods in this category, for example, Ti diffused $LiNbO_3$ waveguide and ion-exchanged glass waveguide.

### 3.3.1 Out-Diffusion

$LiNbO_3$ and $LiTaO_3$ are among the best waveguide materials for active integrated optic devices due to their unique electro-optic, acousto-optic and nonlinear optic characteristics. The first waveguides on $LiNbO_3$ and $LiTaO_3$ were fabricated by out-diffusion of lithium and oxygen atoms.[40] $LiNbO_3$ and $LiTaO_3$ crystals can be grown in a slightly nonstoichiometric form, $(Li_2O)_\nu\ (M_2O_5)_{1-\nu}$, where M may be Nb or Ta and $\nu$ ranges from 0.48 to 0.50. It is known experimentally that for a small change of $\nu$ in $LiNbO_3$ and $LiTaO_3$, the ordinary refractive index remains unchanged while the extraordinary refractive index ($n_e$) increases approximately linearly as $\nu$ decreases. For $LiNbO_3$, $dn_e/d\nu = -1.63$ and for $LiTaO_3$, $dn_e/d\nu = -0.85$. Reduction of $Li_2O$ concentration at the surface caused by out-diffusion forms a high-index guiding layer. $Li_2O$ out-diffusion waveguides have been demonstrated when the crystals were heated at high temperature (850-1200°C) in vacuum or in air. If the out-diffusion process was carried out in vacuum, the crystals became black after the process. Discoloration could be removed by reheating the sample at high temperature in air or in oxygen environment. Waveguide layers thus formed had a $\Delta n_e \sim 10^{-3}$ and a thickness of few to several hundred μm. They usually support a large number of guided modes and are not practical for most applications. As discussed in next section, in-diffusion of Ti metal has been chosen as the preferred approach of fabricating optical waveguides on $LiNbO_3$ substrate.

As a matter of fact, the existence of out-diffusion of $Li_2O$ at high temperature creats a problem for integrated optic devices. Planar out-diffusion waveguide may cause optical leakage or cross-talk between the useful optical waveguide channels. Several papaers have been published on lithium out-diffusion suppression describing techniques such as annealing the sample in $Li_2CO_3$,[41] or $LiNbO_3$[42] powders before or after the diffusion,

placing a cruicible of $Li_2O$ upstream in the gas flow,[43,44] and wetting the incoming gas flow during diffusion.[45]

### 3.3.2 In-Diffusion

Until now, the in-diffusion process is the most common technique of fabricating waveguides on $LiNbO_3$ and $LiTaO_3$. A metal film such as Ti, Nb, Mn, Fe, Co, Cu, Zn, Mg, etc., is first deposited on the substrate, followed by thermal diffusion at tempertures ranging from 850 to 1100°C. A good number of papers have been published on the diffusion of various metals into $LiNbO_3$ and $LiTaO_3$ under various diffusion conditions. Of the two substrate materials, $LiTaO_3$ is a less desirable material to work with because its Curie temperature (~610°C) is well below the diffusion temperatures used. As a result, the crystal must be repoled after diffusion. However, the optical damage threshold of $LiTaO_3$ waveguides is about two orders of magnitude higher than that of $LiNbO_3$ waveguides.

In 1974, optical waveguides in $LiTaO_3$ were reported by in-diffusion of Nb metal,[46] and optical waveguides in $LiNbO_3$ were demonstrated by in-diffusion of various transition metals.[47] The majority of integrated optical directional couplers, modulators, switches, and mode converters are fabricated based on the Ti in-diffusion $LiNbO_3$ waveguide technique. Single mode optical waveguides are easily obtained by diffusing 200 to 400 Å of Ti metal. The resulting waveguides have propagation losses less than 1 dB/cm.

X-ray photoelectron spectroscopy has been used to determine the valence state of titanium atom in $LiNbO_3$.[48] Experimental results indicated that the in-diffused Ti metal in $LiNbO_3$ was all tetravalent, i.e., Ti ions are fully ionized. There are no electrons in partially filled d-orbitals to absorb the electromagnetic energy at visible wavelengths. This explains the measurement of low optical losses fabricated by Ti diffusion into $LiNbO_3$. The spectrum of X-ray photoelectron spectroscopy did not show evidence of $Ti^{+4}$ ion distributed among various different sites. Based on these measurements, one would conclude that Ti ions are bonded chemically in the lattice in the center of oxygen octahedra. However, it is not conclusive that the Ti ions are incorporated chemically into $LiNbO_3$ as substitutional impurities on Nb or equivalent sites. Absorption loss of channel waveguide is measured to be less than 0.3 dB/cm at 632.8 nm and is expected to decrease at longer wavelength.[49] The predominant loss mechanism is attributed to scattering losses.

X-ray microanalyzer has also been used to determine the refractive-index change and profile of Ti diffused $LiNbO_3$ waveguides.[50] Several conclusions are drawn from this study. (1) $\Delta n_o$ and $\Delta n_e$ are identical at 0.75% Ti-concentration. For the Ti concentration smaller than 0.75%, $\Delta n_o > \Delta n_e$, and for Ti concentration higher than 0.75%, $\Delta n_e > \Delta n_o$. (2) The diffusion profiles were Gaussian distributions with diffusion depth less than a few microns. The maximum refractive index change of waveguide made at 970°C for 7 h are $\Delta n_e = 3.05 \times 10^{-2}$ and $\Delta n_o = 7.7 \times 10^{-3}$ for a Ti film of 800 Å.

### 3.3.2 Ion Exchange

The ion exchange process is different from the diffusion in that anions from an external source exchange with anions in the glass or crystal lattice. The ion exchange technique has been used successfully for fabricating low loss waveguides on various glass substrate. This technique is also currently used by Nippon Sheet Glass Co. to fabricate commercial SELFOC lenses. The first optical waveguide fabricated by this method was by ion-exchange from a mixture of salts into a borosilicate glass plate.[51] An external electrical field was used to enhance the ion migration rate. A mixture of thallium, sodium and potassium salts were used, the ion-exchange occured between the $Tl^+$ ions in the melt and $Na^+$ and $K^+$ ions in the glass. After a while, the mixture of salts was then replaced with a sodium and potassium mixture to form a buried waveguide by reversing the ion-exchange process. The resulting waveguide has a graded bell shaped refractive index profile supporting many waveguide modes. Total waveguide propagation loss was $\leq$0.1 dB/cm. The external electrical field effect allows one to control the ion-exchange process for a desirable waveguide structure. At higher temperatures, the ion-exchange process becomes faster following the thermodynamics principles. However, darker films are formed from dissociated metal, and the nitric acid formed by $NO_2$ will etch the glass surface.[52] Table 3-1 is a list of ions and their characteristics that have been used in fabrication of glass waveguides. Table 3-2 is a comparison of various ion-exchange process.

Ion-exchange of Ag into $LiNbO_3$ has demonstrated a three-mode waveguide in an X-cut crystal.[53] There was no waveguide formed on Y-cut wafers even after extended period of treatment. Optical losses on X-cut waveguides

Table 3-1. Relevant Ion-Exchange Parameters

| Ion | Electronic Polarizability ($\lambda$=D) $Å^3$ | Ionic Radius Å | Salts | Melting Point °C | Decomposition Point °C | Index Increase |
|---|---|---|---|---|---|---|
| $Na^+$ | 0.41 | 0.95 | $NaNO_3$ | 307 | 380 | |
| $Li^+$ | 0.03 | 0.65 | $LiNO_3$<br>$(LiSO_4)(K_2SO_4)$<br>0.8 .2 | 264<br>524 | 600 | 0.01<br>0.015 |
| $T\ell^+$ | 5.2 | 1.49 | $T\ell NO_3$<br>$T\ell SO_4$ | 206<br>632 | 430 | 0.1<br>0.1 |
| $Cs^+$ | 3.34 | 1.65 | $CsNO_3$ | 414 | | 0.03 |
| $Ag^+$ | 2.4 | 1.26 | $AgNO_3$ | 212 | 444 | 0.09 |
| $Rb^+$ | 1.98 | 1.49 | $RbNO_3$ | 310 | | 0.015 |
| $K^+$ | 1.33 | 1.33 | $KNO_3$ | 334 | 400 | 0.009 |
| $Ag^+$ | 2.4 | 1.65 | Silver Film | | | 0.001 |
| $Ag^+$ | 2.4 | 1.65 | Silver Film Field Assisted | | | 0.025 |

Table 3-2. Comparison of Various Ion-Exchange Processes

| Ion Used | Index Increase $\Delta n$ | Waveguide Losses at dB/cm | Compatibility with Commercial Glasses | Feasibility for Fabricating Buried Layers | Fabrication Difficulties or Hazzards |
|---|---|---|---|---|---|
| $Li^+$ | 0.01 | >1db/cm | poor | poor | No |
| $Cs^+$ | 0.03 | >1dB/cm | Good | Possible with an Electric Field | Toxic |
| $Rb^+$ | 0.015 | (High?) | Good | poor | Fire |
| $Ag^+$ | 0.09 | >2dB/cm | very poor | possible | No |
| $K^+$ | 0.009 | $\leq$0.2 | very good | poor | No |
| $Tl^+$ | 0.1 | $\leq$0.1 | very good | Possible with an Electric Field | Toxic |

were higher than 6 dB/cm. Ion-exchange of lithium and thallium also resulted in optical waveguides on both $LiNbO_3$ and $LiTaO_3$ crystals.[54] Change in refractive index occurred for extraordinary index only, and for X-cut crystals only.

Proton ion exchange has been introduced recently as a new method of creating large increases in the extraordinary refractive index of $LiNbO_3$. Very large increases in $n_e$ (about 0.12) have been obtained in this method by treating X-cut and Z-cut samples in benzoic acid at low temperatures (110-249°C) for a few hours. Low loss waveguide (0.5 dB/cm) were reported following this method in X-cut crystals. Treatment of Y-cut samples resulted in surface deformations and no waveguides were reported in that orientation.

### 3.3.4 Ion-Implantation

Several different types of optical waveguides have been fabricated by ion-implantation. One of the problems associated with ion-implantation is that the high energy particles create defects which result in scattering losses. Thermal annealing is usually used to reduce the damage effect. Channel waveguides on fused quartz were formed by $Li^+$ implantation through a PMMA electron resist mask.[55] Waveguide loss after annealing was about 3 dB/cm.

$LiNbO_3$ implanted with 60 KeV Ne or Ar ions showed up to 10% decrease in refractive index, attributed to polarization effect of damanged lattice structure.[56] No individual measurements were reported of effects on the two refractive indices, or effects of possible annealing damage on the index change. Later, the effect of ion-implantation on $LiNbO_3$ was examined in a greater detail.[57] Optical waveguides were formed by generating a subsurface low-index layer, 2 to 4 μm below the surface by He implantation. It was noted that the electro-optic coefficient, $r_{33}$, was reduced by about 60%. In another attempt to maintain the crystalline structure, He ion-implantation was used to delineate a channel waveguide structure on a planar Ti diffused waveguide.[58] Even though the high e-o and a-o coefficients are retained, the process is more cumbersome than direct diffusion of Ti channels.

Light ions (proton, helium, boron) were also used to form waveguides in ZnTe.[59] Waveguide formation is the result of macroscopic implantation and the microscopic property changes due to induced damage effect. Low optical losses, 1 to 4 dB/cm were measured. ZnTe material does not have particular interest to integrated optics applications.

### 3.3.5 Others

There are many other modification techniques available to fabricate reasonably good optical waveguides, including polymerization by photolocking, stress, metal cladding. It is almost impossible to exhaust all the techniques published in literatures. Sone of the techniques are of little interest, anyhow, for practical device applications.

## 3.4 RECOMMENDATIONS

There are all together close to 1000 publications on the fabrication and characterization of optical waveguides for integrated optics applications. They are only a few techniques are still used by researchers. The most critical selection criterium is the ability of fabricating low los (<1 dB/cm) optical waveguides. Depending on the substrate and waveguide materials used, one would choose different fabrication technique. Based on this study, several conclusions on the waveguide fabrication can be drawn:

a) RF sputtering is good for 7059 glass, $Ta_2O_5$, and $Nb_2O_5$ films, waveguide loss is usually about 1 dB/cm. These waveguides are primarily used for passive integrated optic devices.

2) RF sputtering is also good for ZnO single crystal films. ZnO film is potentially an attractive waveguide material. The biggest concern is on the reduction of waveguide scattering losses. Laser annealing provides a promising means to achieve this goal. More work is needed in this area.

3) Ion-exchange is attractive for glass waveguides due to its simplicity and good results on optical losses. Single mode channel waveguides with losses less than 0.1 dB/cm have already been demonstrated. There is no reason that one cannot fabricate waveguides with losses on the same order of magnitude as glass fibers $\leq$ dB/km. If it is realized, the glass waveguides certainly can be used for passive laser gyroscope application.

4) Ti diffusion into $LiNbO_3$ is still considered as one of the best techniques to fabricate waveguide devices, in particular, electro-optic and acousto-optic devices. Optical damage associated to $LiNbO_3$ will no longer be a problem when the operating wavelength is shifted to beyond 1 μm. For most high data rate long haul system, the optical wavelength will be around 1.3 μm to fully capitalize the advantages of optical fibers.

5) One of the ultimate goals of integrated optics is to fabricate monolithic optical circuits on one chip, e.g. GaAs or InP. Liquid phase epitaxy is currently used to fabricated discrete as well as limited integrated optoelectronic devices. LPE does not have precise control of growth condition required for integrated optic devices. To really fabricate integrated optic circuits, one has to rely on the advanced molecular beam epitaxial growth technique. This would require a well coordinated effort over several years at a sufficient funding level. The payoff of MBE technology will not be limited to integrated optcs only, the impact may be greater for electronic and optoelectronic devices. Another problem facing semiconductor waveguides is the high absorption and free-carrier scattering losses. One has to operate these devices far away from the band gap.

## 3.5 FINE LINE PHOTOLITHOGRAPHY

The definition of optical guided wave circuitry is currently made possible as a result of major advances in pattern generation of micro-electronics circuitry in the last two decades. While tolerances in integrated optical circuitry are more critical than those required in micro-electronics, the state-of-the-art of pattern generation has become sufficient to meet the high resolution needed in integrated optics. The common practice used in integrated optic device fabrication is to generate the designed circuit on a photomask. Subsequently, the waveguide pattern is transferred to the substrate material using contact photolithography technique. The contact printing technique can faithfully reproduce the waveguide pattern with minimum or non-measurable distortions. Here we describe the state-of-art techniques of fabricating photomasks.

Optical lithography is historically the first method used in micro-electronics, and continues to be a popular technique in that field. The method used for pattern definition by optical means (considered primitive in today's standards) was the Rubylith cutting and exposure method. The pattern, scaled up by a certain ratio is cut on a large Rubylith sheet taped on a screen in front of a green light source. The exposure of green light through

a reduction lens onto photo sensitive emulsion plate produces an image of the Rubylith pattern on the emulsion plate. The procedure can also be repeated to further down scale the image size through different reduction lenses. This technique has two limitations. The first relates to the diffraction limits of the lenses, and the second limitation is imposed by the resolution limits and edge sharpness of emulsion films. The latter is the more serious of the two, and because of that, good quality lines narrower than 5 μm are not obtained by this method.

A more advanced method of mask making uses an optical machine called pattern generator. These machines primarily consist of a processor controlled rectangular exposure opening through which UV light is exposed on a photoresist coated mask plate through an intermediate lens system. The mask plate coated with chromium or iron oxide is fixed on a precision stage monitored by mechanical or interferometric means. Due to the limitations imposed by the image field of the lenses, typically 10 mm in diameter, large area masks are generated by successive exposures. Upon completion of a programmed exposure, the pattern is developed and etched through the metallic film yielding high quality patterns. The use of photo-sensitive polymer resists allows the formation of sharp and smooth edges. The line width and line spacing are on the order of 0.8 - 1.0 μm, controlled within 0.25 μm, and the edge smoothness of <0.1 μm is achieved. Off axial alignment shifts between connecting exposure boxes (when image size is greater than 10 mm) is typically 0.25 - 0.5 μm.

Scanning E-beam lithography is another method of writing high resolution patterns on radiation sensitive polymer films. Both negative and positive electron resists are used. It employs a scanning electron microscope with the electron beam focused down to less than 0.1 μm in diameter. The image field of the E-beam is smaller than that of the optical pattern generator, it is typical that 1x1 $mm^2$ before electron lens aberrations become too large. For large patterns, the substrate must therefore be moved from exposure to exposure according to a digitized program processor. In order to maintain high accuracy between neighboring exposure rectangles, the substrate motion is detected interferometrically and corrections are made to the beam position. Typical off axis misalignment between boxes (also known as butting error) is <0.15 μm. Line widths as small 0.25 μm with edge roughness of no greater than 0.10 μm are possible due to the large depth of focus of the E-beam. Such parameters are typically quoted by commercial E-beam mask suppliers.

## REFERENCES


1. P.K. Tien, R. Ulrich, and R.J. Martin, "Modes of Propagating Light Waves in Thin Deposited Semicondictor Films," Appl. Phys. Lett 14, 291 (1969).

2. R. Th. Kersten and W. Rauscher, "A Low Loss Think Film Optical Waveguide for Integrated Optics Made by Vacuum Deposotion," Opt. Comm. 13, 189 (1975).

3. J.L. Vossen and J.J. O'Neill, "RF Sputtering Process," RCA Review, 29, 149 (1968).

4. J.E. Goel and R.D. Standley, "Sputtered Glass Waveguides for Integrated Optics," Bell System Tech. J. 48, 3445 (1969).

5. P.D. Davidse and L.I. Maissel, "Dielectric Thin Films through RF Sputtering," J. Appl. Phys. 37, 574 (1966).

6. T. Nishimura, Y. Murayana, K. Dota, and H. Matsumaru, Digest of 3rd Symp. on the Deposition of Thin Films by Sputtering, Rochester, Bendix Corp. 1969, pp. 96-106.

7. C.W. Pitt, "Sputtered Glass Optical Waveguides," Opt. Lett. 9. 401 (1973).

8. B. Chen, Ph.D Dissertation, Cornell University, 1976.

9. J.E. Goell, "Barium Silicate Films for Optical Integrated Circuits," Appl, Opt. 12, 737 (1973).

10. H. Yajima, S. Kawase, and Y. Sekimoto, "Amplification at 1.06 μm Using a Nd-glass Thin Film Waveguide," Appl. Phys. Lett. 21, 407 (1972).

11. B. Chen and C.L. Tang, "Nd-glass Thin Film Waveguide, An Active Medium for Nd Thin-Film Laser," Appl. Phys. Lett. 28, 435 (1976).

12. B. Chen, C.L. Tang, and J.M. Telle, "CW Harmonic Generation in the UV Using a Thin-Film Waveguide on a Nonlinear Substrate," Appl. Phys. Lett., 25, 495 (1974).

13. H. Terui and M. Kobayashi, "Refractive-index-adjustable $SiO_2$-$Ta_2O_5$ Films for Integrated Optical Circuits," Appl. Phys. Lett., 32 666 (1978).

14. S.J. Ingrey, W.D. Westwood, Y.C. Cheng, and J. Wei, "Variable Refractive Index and Birefringent Waveguides by Sputtering Tantalum in $O_2$-$N_2$ Mixture," Appl. Opt., 14 2194 (1975).

15. S.J. Ingrey and W.D. Westwood, "Birefringent Waveguides prepared by Reactive sputtering of Niobium in $O_2$-$N_2$ Mixtures," Appl. Opt., 15, 607 (1976).

16. R. Ulrich and H.P. Weber, "Solution Deposited Thin Films as Passive and Active Light Guides," Appl. Opt., 11, 428 (1972).

17. D.B. Ostrowsky and A. Jacques, "Formation of Optical Waveguides in Photo Resist Films," Appl. Phys. Lett., 18, 556 (1971).

18. B. Chen, "A New Technique for Waveguide Formation in $LiNbO_3$," Thin Solid Films, 64 (1979).

19. S. Dutta, H. Jackson and J.T. Boyd, "Extremely Low-Loss Glass Thin-Film Optical Waveguides Utilizing Surface Coating and Laser Annealing," J. Appl. Phys., 52, 3873 (1981).

20. M.J. Rand and R.D. Standley, "Silicon Oxynitride Films on Fused Silica for Optical Waveguides," Appl. Opt., 11, 2482 (1972).

21. W. Stutius and W. Streifer, "Silicon Nitride Films on Silicon for Optical Waveguides," Appl. Opt., 16, 3218 (1977).

22. T. Shiosaki, S. Fukuda, K. Sakai, H. Kuroda, and A. Kawabata, "Second Harmonic Generation in As-Sputtered ZnO Optical Waveguide," Jap. J. Appl. Phys., 19, 2391 (1980).

23. S. Zemon, R.R. Alfano, S.L. Shapiro, and E. Conwell, "High-Power Effects in Nonlinear Optical Waveguides," Appl. Phys. Lett., 21, 327 (1972).

24. P.K. Tien, "Lightwaves in Thin Films and Integrated Optics," Appl. Opt. 10, 2395 (1971).

25. S. Dutta, H.E. Jackson, J.T. Boyd, F.S. Hickernell and R.L. Davis, "Scattering Loss Reduction in ZnO Optical Waveguides by Laser Annealing," Appl. Phys. Lett. 39, 206 (1981).

26. A.A. Ballman, H. Brown, P.K. Tien, and R.J. Martin, "The Growth of Single Crystalline Waveguiding Thin Films of Piezoelectric Sillenites," J. Crystal, Growth, 20, 251 (1973).

27. S. Miyazawa, "Growth of $LiNbO_3$ Single Crystal Film for Optical Waveguides," Appl. Phys. Lett. 23, 198 (1973).

28. S. Fukunishi, N. Uchinda, S. Miyazawa and J. Noda, "Electro-Optic Modulation of Optical Guided Waves in $LiNbO_3$ fabricated by EGM Method," Appl. Phys. Lett., 24, 424 (1974).

29. P.K. Tien, S. Riva-Sanseverino, R.J. Martin, A.A. Ballman, and H. Brown, "Optical Waveguide Modes in Single Crystalline $LiNbO_3$-$LiTaO_3$ Solid Solution Films," Appl. Phys. Lett., 24, 503 (1974).

30. S. Miyazawa, S. Fushimi and S. Kondo, "Optical Waveguide of $LiNbO_3$ Thin Film Growth by Liquid Phase Epitaxy," Appl. Phys. Lett., 26, 8 (1975).

31. P.K. Tien and A.A. Ballman, "Research in Optical Films for the Applications of Integrated Optics," J. Vac. Sci, Tech. 12, 892 (1975).

32. W.T. Tsang and S. Wang, "Mode Properties of GaAs-$Ga_{1-x}Al_xAs$ Heterstructure Inverted Optical Waveguides," Appl. Phys. Lett., 28, 665 (1976).

33. F.K. Reinhart and B.I. Miller, "Efficient GaAs-$Ga_{1-x}Al_xAs$ Double-Heterstructure Light Modulators," Appl. Phys. Lett., 20, 36 (1972).

34. P.K. Tien, R.J. Martin, S.L. Blank, S.H. Wempie and L.J. Varnerin, "Optical Waveguides of Single Crystal Garnet Films," Appl. Phys. Lett., 21, 207 (1972).

35. P.K. Tien, R.J. Martin, R. Wolfe, R.C. Le-Craw, and S.L. Blank, "Switching and Modulation of Light in Magneto-Optic Waveguides of Garnet Films," Appl. Phys. Lett., 21, 394 (1972).

36. V. Ramaswamy, "Epitaxial Electro-Optic Mix-Crystal $(NH_4)_xK_{1-x}H_2PO_4$ Film Waveguide," Appl. Phys. Lett., 21, 183 (1972).

37. F.A. Blum, D.W. Shaw, and W.C. Holton, "Optical Striplines for Integrated Optical circuits in Epitaxial GaAs," Appl. Phys. Lett., 25, 116 (1974).

38. J.C. Campbell, F.A. Blum, D.W. Shaw, and K.L. Lawley, "GaAs Electro-Optic Directional-Coupler Switch," Appl. Phys. Lett., 27, 202 (1975).

39. F.K. Reinhart and A.Y. Cho, "Molecular Beam Epitaxial Layer Structures for Integrated Optics," Opt. Comm., 18, 79 (1976).

40. I.P. Kaminow and J.R. Carruthers, "Optical Waveguiding Layers in $LiNbO_3$ and $LiTaO_3$," Appl. Phys. Lett., 22, 326 (1973).

41. S. Miyazawa, R. Guglielmi and A. Carenco, "A Simple Technique for Suppressing $Li_2O$ Out-Diffusion in Ti:$LiNbO_3$ Optical Waveguide" Appl. Phys. Lett., 31, 742 (1977).

42. B. Chen and A.C. Pastor, "Elimination of $Li_2O$ Out-Diffusion Waveguide in $LiNbO_3$ and $LiTaO_3$," Appl. Phys. Lett., 30, 570 (1977).

43. T.R. Ranganath and S. Wang, "Suppression of $Li_2O$ Out-Diffusion from Ti-Diffused $LiNbO_3$ Optical Waveguides," Appl. Phys. Lett., 30, 376 (1977).

44. R.J. Esdaile, "Closed-Tube Control of Out-Diffusion During Fabrication of Optical Waveguides in $LiNbO_3$," Appl. Phys. Lett., 33, 733 (1978).

45. J.L. Jackel, V. Ramaswamy and S.P. Lyman, "Elimination of Out-Diffused Surface Guiding in Titanium Diffused $LiNbO_3$," Appl. Phys. Lett., 38, 509 (1981).

46. J.M. Hammer and W. Phillips, "Low Loss Single Mode Optical Waveguides and Efficient High Speed Modulators of $LiNb_xTa_{1-x}O_3$ on $LiTaO_3$," Appl. Phys. Lett., 24, 545 (1974).

47. R.V. Schmidt and I.P. Kaminow, "Metal Diffused Optical Waveguides in $LiNbO_3$," Appl. Phys. Lett., 25, 458 (1974).

48. T.P. Pearsall, S. Chiang, and R.V. Schmidt, "Study of Titanium Diffusion in Lithium-Niobate Low-Loss Optical Waveguides by X-ray Photoelectron Spectroscopy," J. Appl. Phys. 47, 4794 (1976).

49. A.M. Glass, I.P. Kaminow, A.A. Ballman, and D.H. Olson, "Absorption Loss and Photorefractive-Index Changes in Ti:$LiNbO_3$ Crystals and Waveguides," Appl. Opt., 19, 276 (1980).

50. M. Minakata, S. Saito, M. Shibata, and S. Miyazawa, "Precise Determination of Refractive-Index Changes in Ti-Diffused $LiNbO_3$ Optical Waveguides," J. Appl. Phys., 49, 4677, (1978).

51. T. Izawa and H. Nakagome, "Optical Waveguide Formed by Electrically Induced Migration of Ions in Glass Plates," Appl. Phys. Lett., 21, 584 (1972).

52. T.G. Gialorenzi, E.J. West, R. Kirk, R. Ginther and R.A. Andrews, "Optical Waveguides Formed by Thermal Migration of Ions in Glass," Appl. Opt., 12, 1240 (1973).

53. M.K. Shah, "Optical Waveguides in $LiNbO_3$ by Ion-Exchange Technique," Appl. Phys. Lett., 26, 652 (1975).

54. J. Jackel, "High-An Optical Waveguides in $LiNbO_3$: Thallium-Lithium Ion-Exchange," Appl. Phys. Lett., 37, 739 (1980).

55. J.E. Goell, R.D. Standley, W.M. Gibson and J.W. Rodgers, "Ion Bombardment Fabrication of Optical Waveguides Using Electron Resist Masks," Appl. Phys. Lett., 21, 72 (1972).

56. D.T.Y. Wei, W.W. Lee, L.R. Bloom, "Large Refractive Index Change Induced by Ion-Implantation in Lithium Niobate," Appl. Phys. Lett., 25, 329 (1974).

57. G.L. Desterfanis, J.P. Gailliard, E.L. Liegon and S. Valette, "The Formation of Waveguides and Modulators in $LiNbO_3$ by Ion-Implantation," J. Appl. Phys. 50, 7898 (1979).

58. J. Heibei and E. Voges, "Fabrication of Strip Waveguides in $LiNbO_3$ by Combined Metal Diffusion and Ion Implantation," Topical Meeting on Integrated and Guided Wave Optics, Incline Village, NE, Jan. 1980.

59. S. Valette, G. Labrunie, J-C, Deutsch, and J. Lizet, "Planar Optical Waveguides Achieved by Ion-Implantation in Zinc Telluride: General Characteristics," Appl. Opt., 16, 1289 (1977).

# 4. OPTICAL LOSS MECHANISMS

Loss mechanisms in integrated optical waveguides can be classified in two major categories, namely, absorption, or conversion of the light energy into heat, and scattering, or light escaping the bound modes. Absorption consists of three types: intrinsic, impurity, and atomic defect color centers. Scattering also consists of three types: intrinsic volume scattering, boundary scattering, and index inhomogeneity. Certain other effects such as optical damage and fabrication irregularities may cause additional losses as will be described later.

## 4.1 ABSORPTION

Intrinsic absorption originates due to charge transfer bands in the UV region and vibration of multi-phonon bands in the near IR. If these bands are sufficiently strong, their tails will extend into the spectral region of interest in optical communications (800-1600 nm). In most cases, the IR bands are located beyond 4 μm, and are narrow. On the other hand, the UV bands are stronger and potentially more troublesome in the wavelength range of interest.

Impurity absorption arises predominantly from transition metal ions present in the bulk or diffused during the waveguide formation. Absorption of these ions varies for different materials as does their valence states. In glassy materials, OH ions contribute to absorption around 725, 950, 1250 and 1390 nm.

The third type of absorption is atomic defects which include species deliberately added to the material composition, such at Ti, whose plus-three valence state has strong absorption in the visible while titanium plus-four does not.

## 4.2 SCATTERING

All transparent materials scatter light due to frozen-in thermal fluctuations of constituent atoms. This causes density and hence refractive index fluctuations. This intrinsic effect is believed to represent the fundamental limit to attenuation in waveguides. A second source of index inhomogeneity scattering arises from aggregation of certain compositions after their reduction from ionic form into atomic form and their subsequent

nucleation and formation of colloidal scattering centers as in the case of silver and titanium diffused waveguides.

In addition to these scattering loss mechanisms, one can have radiation losses associated with the waveguide circuitry and boundaries. In the context of thin film-substrate waveguides, the sources of such losses are due to surface irregularities, two dimensional pattern definition, bends, and curvature. These are engineering desigr problems and have no fundamental limitation on the total attenuation. Nevertheless, they contribute significantly to the total losses unless they are properly minimized.

## 4.3 LOSS MEASUREMENTS

The measurement of losses in integrated optical circuitry continues to be an issue of accuracy. While fiber losses can be measured with high accuracy over long segments of fiber, such is not easily accommodated in short thin film waveguides. The main difficulty is the uncertainty of the input and output coupling efficiencies. This uncertainty clouds the measurements of both absorption and scattering losses of short waveguides, especially when the losses are low. Absorption is usually measured by calorimetric methods, whereby the induced heat is detected by a thermocouple and correlated with the sample geometry, mass and propagating power. Total loss is measured by making power-distance measurements. Excitation of power is done through a prism coupling, end focusing, or fiber pigtailing. In our opinion, none of these methods allows precise knowledge of the amount of power coupled into the waveguide, and with the exception of end focusing, none are accurately or easily reproducible.

In the prism coupling method, the wave is coupled into the out of the waveguide with a pair of prisms clamped tightly on the surface of the waveguide. In channel waveguides, a lens must be used to focus the beam to a spot size comparable to the channel width. This method of excitation is made possible primarily as a result of evanescent field coupling. As such it is very sensitive to an air or liquid filled gap between the prism and the substrate surface. For efficient coupling, this gap must be on the order of the wavelength or less. In practice, the optical contact between these two surfaces is very sensitive to the optical flatness of both surfaces, and may vary from region to region. Such variations account for considerable changes in the coupling efficiencies at different points.

Therefore, when the prism separation is changed to measure the output power as a function of distance, variations in the coupling efficiencies inevitably lead to measurement inaccuracies, and often discrepancies. In our opinion, even the most elaborate setups providing special pressure point contacts are not accurate enough or reproducible, and all such measurements cannot be seriously assumed reliable. A figure near $\pm$0.5 dB/cm is often quoted (questionably) to describe the resolution of this method when measuring losses estimated at 1 dB/cm. (Numbers in general are amusingly rounded around these figures).

The second method of loss measurement involves the detection and monitoring of the scattered light along the travel length, usually with a detector or a light carrying conduit positioned closely to the surface of the waveguide. This method is more accurate and the limitations are systematic arrising from the noise level of the opto-electronic detection system, and background. Over short distances (few mm), however, random scattering centers within the guide or on its surface cause considerable perturbations that affect the measurements in two ways; first causing variable intensities of the scattered light which have to be averaged out by statistical means, and second, it may change the directionality of the radiating pattern and therefore the scattered power relayed to the detector. Nevertheless, if the various noise sources are minimized, and with use of a sensitive linear detector, this method yields reasonably accurate results.

The third method of estimating the losses is carried out by making input-output measurements by the end focusing method. In this case, the sample ends are polished, and the input power is excited with a lens, and the output power is collected with a second lens. Power at the output side is then measured and the sample is removed and the power is remeasured. In this situation, two corrections to these measurements are made, the first accounts for the Fresnel reflections at both ends, and the second for the coupling efficiency at the input end. Coupling efficiency in this case presents an uncertainty factor. It can be theoretically estimated from the knowledge of the waveguide and focusing lens parameters. It can also be measured, but in a tedious way. One way of measuring it is by cutting a thin slice of the sample, and polishing both ends. If the slice is thin

(short) enough, the propagation losses can be neglected, and the input-output powers are different only by the amount of light not coupled into the guide. This method is in a way similar to fiber loss measurements, but it requires the additional cutting and polishing. Otherwise, it is a fairly good method of loss measurement.

## 4.4 MATERIALS VERSUS LOSS: PROBLEMS AND OUTLOOK

In this section, we focus our attention to loss aspects related to various material-waveguide combinations, outline major problem areas, and project some expectations. In specific, we consider Ti:$LiNbO_3$, glasses, ZnO and polymers as potential building blocks in hybrid integrated optic circuitry.

### 4.4.1 Ti:$LiNbO_3$

A major limitation to integrated optical devices built by Ti diffusion or $LiNbO_3$ is the photorefractive effect, also known as optical damage. It is thought to be caused by charge transfer from optically excited impurities within the band gap to metastable trapping sites.[1,2]. This effect manifest itself in refractive index changes in the material upon exposure to visible light intensities in excess of $1x10^{-4}$ $mW/\mu m^2$. Due to this localized laser induced changes in the extraordinary index, the propagating beam diverges gradually as its wave front becomes distorted by index inhomogeneities. Contribution of this effect to the total loss is not known, as other geometrical imperfections may scatter the light in a similar way. Typically, single mode Ti:$LiNbO_3$ channel waveguides exhibit 1 dB/cm total loss. Of this, about 0.3 dB/cm is attributed to bulk absorption at 6328 nm. The rest results from Ti impurity absorption scattering from intrinsic, geometric, and photorefractive effects. It has been pointed out that the diffused Ti impurities do not increase the absorption or level of optical damage from that of the original substrate.[1,2]. With the application of an electric field of few KV/cm, however, the sensitivity to the photorefractive effect is greatly increased in the Ti diffused layers in comparison to similar fields applied to the bulk crystal.[1] It has also been observed that Ti indiffused waveguide are more susceptable to optical damage than outdiffused waveguides.[3]. Optical damage decreases for longer wavelengths and becomes negligibly small beyond 1 μm.[2] Recently, a

technique for suppressing the out-diffusion in Ti diffused waveguides by carrying the diffusion in humid atmosphere has been found to improve the susceptibility of Ti-diffused waveguides to optical damage as a result of the presence of $H^+$ ions.[4] In this case, the photorefractive sensitivity is improved by a factor of 2-5 by introducing humidity in the diffusion process. This phenomena is not very well understood at this point, but work is in progress to gain greater understanding of this effect.[4]

### 4.4.2 Glass Waveguides

Glass waveguides can be expected to yield lowest losses for integrated optical patterns among the other materials commonly used in integrated optics. At present, typical glass waveguide losses are in the range of 0.01 - several dB/cm, depending on the type of glass and process used in the waveguide fabrication. It is our belief that very low glass waveguides can be fabricated provided that certain important considerations are recognized in the glass selection and process used. To elaborate on this, we shall consider the problem areas associated with glass waveguides formed in two different methods; namely ion exchange and film deposition.

In the ion exchange process, the selection of bulk glass and exchanging ions greatly influences the loss. Bulk transmission is important for obvious reasons. This issue has not unfortunately been of major convern to researches of this field, when indeed it is a very important one. Consider, for example, an optical quality glass bulk having 0.975 transmission over 1 cm thickness. It follows that the bulk loss for this type of glass is about 0.1 dB/cm which constitutes an absolute minimum achievable. Other losses arising from impurity diffusion, scattering etc. will add to that figure by certain amounts, some of which are still related to the bulk composition. Remember that 0.1 dB/cm is 10,000 dB/km, which is astoundingly high for fiber optics, and reflects loss in fiber optics prior to 1970. While the comparison here is not fair, it is justifiable from the material point of view where both (bulk glass and fiber preform) use $SiO_2$ as a major constituent. Fiber raw material, however, is far more refined from transition metal ions thus yielding much lower losses. These ions contribute not only to absorption of the basic substrate, but can be even more harmful in the process of waveguide fabrication by ion exchange. An excellent example of this situation is $Ag^+$ ion exchanged waveguides. The

presence of metastable ions such as Fe, Sb and As even in few ppm act as strong reducing agents whereby they donate electrons while jumping through the valence states. These electrons are attracted to the $Ag^+$ ions, and upon combination, the $Ag^+$ ions are reduced to metallic atoms, which aggregate and form submicroscopic cyrstals in the form of colo'dal color centers, repsonsible for the yellowish colora.ion or staining often observed in $Ag^+$ ion exchanged waveguides. This type of chemical reaction is described by the following:[5]

$$Ag_2O + 2FeO \xrightarrow{(heat)} Fe_2O_3 + 2Ag$$

$$2Ag_2O + As_2O_3 \xrightarrow{(heat)} As_2O_5 + 4Ag$$

Losses induced by this type of reaction are very high, typically several dB/cm in $Ag^+$ ion exchanged waveguides. This underlines the importance of minor constituents in the glass materials and suggests that the selection of both glass material and doping impurity have to be considered simultaneously in order to minimize the loss. While most transition metal ions can be minimized by starting with high purity materials in glass production, some constituents like As are intentionally introduced in the process for certain purposes such as bubble and inclusion removal, a common procedure followed in optical glass manufacturing. Modern technological Advances in glass manufacturing can be utilized to substitute that procedure without using As, which will understandably add to the cost of material, as does the use of ultra pure raw materials.

Other examples of loss factors of ion exchanged waveguides are those relating to structural ionic size disparity. For example, when Li ions are used as the exchanging ions, the glass network in the surface Li diffused layer collapses around the small size Li ions at temperatures below the glass transition temperature resulting in surface distortion evident by microcracks. Glass structure and diffusion temperature become crucial factors in producing low losses in this case.

Taking these considerations into account, general guidelines can be established for the production of low loss ion exchanged waveguides, these can be summarized as follows:

1. The starting bulk material must be:
   a. very low on transition metal ions
   b. free of bubbles and oclusions
   c. have high index homogeniety
   d. stress and striae free
   e. compatible with the exchanging ions
   f. be of silicate base with 10-15% sodium oxide.
2. Preferred exchanging ions are $K^+$ and $Tl^+$ for $Na^+$
3. Glass structure should enable fast ion exchange at relatively low temperature.

The second type of glass waveguides is formed by film deposition (sputtering) of a higher index glass on a glass substrate or oxidized silicon. In this case, the bulk loss or transmission is of secondary importance, but the sputtered source purity is important. Generally, since only small amounts of material is used, it is more economical to use in high purity form than would be the case if the whole substrate were to be of high purity. In such cases, however, the film surface quality is most important. In general, sputtered glass films have relatively high surface irregularity after sputtering, and exhibit fairly high loss at that point (typically several dB/cm). It has been reported recently that laser annealing of the film surface yields considerable reduction in the scattering losses of such waveguides.[6,7] For example, sputtered high purity 7059 glass film (about 1 μm thick) exhibited 7.2 dB/cm losses after deposition. When annealed with a $CO_2$ laser radiation, the loss was reduced to 0.2 dB/cm. This loss was further reduced to 0.01 dB/cm after coating the film with an index matching liquid.[7] This indicates the influence of surface roughness on the total loss. It should be pointed out that these experiments were conducted on planar films, and it is yet to be determined if this procedure can be effective in channel waveguiding structures. Nevertheless, these results are quite encouraging, suggesting that such a technique might be useful with ion exchange waveguides where two dimensional confinement is not a problem. This of course must be done such that the localized annealing does not purturb the original waveguide parameters that are sensitive to further heat treatment.

### 4.4.3 ZnO Films

ZnO films are also sputtered or CVD deposited on various substrates such as quartz, oxidized Si or sapphire. Films grown on sapphire by CVD or rf sputtering yielded optical losses of 0.5-1 dB/cm,[8,9,10,11] and 1-2 dB cm resulted in ZnO films sputter deposited on amorphous oxidized silicon.[12] The laser annealing method described earlier for reducing scattering losses in glass yielded considerable reduction of losses in ZnO films sputter deposited on amorphous Si substrates.[13] Losses in the range of 2.5-6.0 dB/cm after deposition were reduced by $CO_2$ laser annealing to 0.01-0.03 dB/cm,[13] for the fundamental mode of waveguides supporting three modes. Losses of the higher order modes were also reduced by not substantially, and this was explained on the bases of modal field confinement difference between the various modes due to the large index difference between ZnO and air. It is not clear yet how annealing may affect the electro-optic and piezo-electric properites of the ZnO film, and no data has been reported on the subject, although it is speculated that such annealing would yield adverse effects in that regard.

### 4.4.4 Polymer Films

Polymer films are another class of waveguides that exhibit low loss. In planar forms a loss of 0.4 dB/cm was reported for the early demonstration of such waveguides for organosilicon films[14]. These materials were further incorporated with a photolocking technique in writing channel waveguides upon UV exposure. Earlier experiments reported a loss of 0.2 dB/cm for 4 μm wide channels.[15] More recently, further refinement of the polymers yields lower losses (0.05 dB/cm) for channel waveguides 10 μm wide.[16] The usefulness of such waveguides is limited to the visible region beyond which the absorption becomes prohitively high. Furthermore, these films are usually soft and vulnerable to scratches and humidity. Nevertheless they are useful in special prototype demonstration cases such as the integrated optical ring gyro.[16]

## REFERENCES


1. A.M. Glass, I.P. Kaminow, A.A. Ballman, and D.H. Olson, "Absorption Loss and Photorefractive Index Changes in $LiNbO_3$ Crystals and Waveguides", Appl. Opt., 19, 276, 1980.

2. A.M. Glass, I.P. Kaminow, A.A. Balman, and D.H. Olson, "Absorption Loss and Photorefractive Index Changes in $LiNbO_3$: Ti Crystals and Waveguides", paper $TuD_5$, Topical Meeting on Integrated and Guided Wave Optics, Jan. 1980, Incline Village, Nevada.

3. R.L. Holman, P.J. Cressman, and J.F. Revelli, "Chemical Control of Optical Damage in $LiNbO_3$", Appl. Phys. Lett., 32, 280, 1978.

4. J.L. Jacket, D.H. Olson, and A.M. Glass, "Optical Damage Resistance of Monovalent Ion Diffused $LiNbO_3$ and $LiTaO_3$ Waveguides", J. Appl. Phys., 52, 4855, 1981.

5. See for example: "Colored Glasses" by W.A. Weyl, the Scholar Press Limited, Ilkley, Yorkshire, 1978.

6. S. Dutta, H.E. Jackson, and J.T. Boyd, "Reduction of Scattering from a Glass Thin Film Optical Waveguide by $CO_2$ Laser Annealing", Appl. Phys. Lett., 37, 512, 1980.

7. Ibid, "Extremely Low Loss Glass Thin Film Optical Waveguides Utilizing Surface Coating and Laser Annealing", J. Appl. Phys., 52, 3873, 1981.

8. D.J. Channin, J.M. Hammer and M.T. Duffy, "Scattering in ZnO-Sapphire Optical Waveguides", Appl. Opt., 14, 923, 1975.

9. T. Shiosaki, S. Ohnishi, Y. Hirokawa, and A. Kawabata, "As-grown CVD ZnO Optical Waveguide on Sapphire", J. Appl. Phys. Lett., 33, 406, 1978.

10. T. Shiosaki, S. Ohnishi, and A. Kawabata, "Optical Properties of Single Crystaline ZnO Film Smoothly CVD Deposited on Intermediately Sputtered Thin ZnO Film on Sapphire", J. Appl. Phys., 50, 3113, 1979.

11. T. Mitsuyu, S. Ono, and K. Wasa, "Structure and SAW Properties of RF-Sputtered Single Crystal Films and ZnO on Sapphire", J. Appl. Phys., 51, 2464, 1980.

12. F.S. Hickernell, "Low Loss ZnO Optical Waveguide on Amorphous Substrates", Digest of the Topical Meeting on Integrated and Guided Wave Optics, WB6-1, 1980.

13. S. Dutta, H.E. Jackson, J.T. Boyd, F.S. Hickernell, and R.L. Davis, "Scattering Loss Reduction in ZnO Optical Waveguides by Laser Annealing", Appl. Phys. Lett., 39, 206, 1981.

14. P.K. Tien, G. Sonolinsky and R.J. Martin, "Thin Organo-Silicon Films for Integrated Optics", Appl. Opt., 11 637, 1972.

15. E. Chandross, C.A. Pryde, W.J. Tomlinson, and H.P. Weber, "Photo Locking - a New Technique for Fabricating Optical Waveguide Circuits", Appl. Phys. Lett., 24 72, 1974.

16. J. Haavisto and G.A. Pajer, "Resonance Effects in Low Loss Ring Waveguides" Opt. Lett., 5, 510, 1980.

# 5. WAVELENGTH SELECTION

Since the first report of 20 dB/km optical fiber in 1970[1], glass fiber manufacturing techniques have been advanced to produce fibers with attenuation loss close to its theoretical limit. A loss of 0.2 dB/km at a wavelength of 1550 nm was reported in 1979[2]. The fiber, consisting of $SiO_2$ cladding and $GeO_2$-doped silica core, was fabricated by the modified chemical vapour deposition (CVD) technique using ultrapure starting materials. The total fiber dispersion, the sum of waveguide dispersion and material dispersion, became zero at wavelength around 1270 nm. At this wavelength, the fiber loss was measured to be 0.6 dB/km. On the other hand the fiber losses at GaAlAs laser wavelengths, $\lambda$=800-900 nm, were about 2 dB/km. It becomes quite evident that long wavelength optical communications systems can be operated at higher data rate over a longer distance without repeater than the short wavelength systems. In a recent announcement, Bell Telephone Laboratories has demonstrated[3] a repeaterless transmission system at 274 MBit/s over 101 km using single mode fiber, 1.3 μm InGaAsP laser diodes and InGaAs PIN diodes. When the transmission rate was raised to 420 Mbit/s, the system length without a repeater became 84 km. A theoretical analysis[4] has shown that for optical wavelength close to the minimum dispersion, single mode fiber transmission system can be operated at 20-100 Gbit/s data rate over a distance greater than 100 km. Motivated by the progress in fiber fabrication, sources and detectors for long wavelength operations have been studied extensively for the last several years. Some long wavelength devices are available commercially with performance comparable with short wavelength devices.

The choice of operating wavelength for optical systems is determined by many factors such as data rate, power budget, temperature sensitivity, coupling to integrated optical devices, etc. Table 5-1 is a list of system parameters that will be affected by the operating wavelength.

Table 5-1 Comparison of Operating Wavelength

| System Parameters | Short Wavelength (800-900 nm) | Long Wavelength (1100-1700 nm) |
|---|---|---|
| Data Rate | Low, <100 Mbps | High, >100 Mbps |
| Repeater Spacing | Short, <10 km | Long, >10 km |
| Receiver Sensitivity | Good, Si APD | PIN-FET or other APD's not as sensitive as Si APD |
| Laser-Fiber-IO Device Coupling | More critical | Less critical |
| IO Waveguide Losses | Higher (both scattering and absorption losses) | Lower |
| Drive Power | Lower ($\propto\lambda^2$) | Higher |
| Optical Damage in $LiNbO_3$ | Yes | No |

## REFERENCES


1. F.P. Kapron, D.B. Keck, and R.D. Mauer, "Radiation Losses in Glass Optical Waveguides", Appl. Phys. Lett., 17, 423 (1970).

2. T. Miya, Y. Terunuma, T. Hosaka and T. Miyashita, "Ultimate Low-Loss Single Mode Fiber at 1.55 μm", Elect. Lett., 15, 106 (1979).

3. Bell Telephone Laboratory announcement in CLEO/OFC April 13-16, 1982, Pheonix, AZ.

4. C. Lin and D. Marcuse, "Dispersion in Single Mode Fibers: the Question of Maximum Transmission Bandwidth", IOOC 81, paper TUC5, April 27-29, I981, San Francisco, CA.

# 6. POLARIZATION EFFECTS AND CONTROL

In various sensor applications, single mode fibers are attractive principally because they have a single well defined phase velocity and polarization state, small variations in which can be readily detected. Whereas this is true in a circularly symmetric stress free straight fiber, in practice, a degree of ellipticity invariably exists, accompanied by a nonuniform stress induced birefringence associated with stress asymmetry leading to birefringence. Such birefringence effects are caused by various internal and external perturbations. Internal effects include core deviation form circular cross-section[1,2,3,4] and intrinsic lateral stress components.[5] External effects include lateral force,[6,7] twisting,[8] bending,[9,10] and temperature. As a result of such perturbations, the fiber supports two orthogonally polarized nondegenerate $HE_{11}$ modes, generally of elliptical polarization. Due to this slight difference between their phase velocities, the fiber appears to be brefringent. Consequently, in the absence of extraneous coupling mechanism, the output state of polarization varies cyclically along the fiber length with a period $L_p = 2\pi/\Delta\beta$, where $\Delta\beta$ is the difference in propagation constants of the two orthogonal modes.[11,12,13] This distance $L_p$ has been conveniently called the beat length corresponding the coupling length through which the energy alternates between the two modes. Clearly, by increasing $\Delta\beta$, the birefringence length is reduced. Only mechanical perturbations with periods comparable to $L_p$ can couple the energy from one polarization to the other. To avoid coupling, the value $L_p$ should be made smaller than the perturbation periods that are introduced by various effects such as drawing, bends, twists etc. The state of polarization may also change with time due to thermal fluctuations and inter-mode coupling, a serious problem in interferometric applications.

The evolution of the state of polarization (SOP) in single mode fibers as a results of the various above-mentioned effects can be traced by mathematical methods such as Jones matrix, time domain methods, or coherency matricies. The complexity of such procedures makes it difficult to follow the evolution of the state of polarization at various points of a birefringent network. The Poincare sphere[14] representation has been found most useful in visualizing the evolution of the state of polarization and the computation of the output phase response of birefringent networks of both

coupled and uncoupled waves.[11,15,16] Since single mode fibers at rest are fully determinate two mode systems, the degree of polarization is always preserved due to the absence of depolarizing effects (except time varying thermal fluctuations). As a result, all birefringent effects on the state of polarization can be described as a rotation of the Poincaré sphere.[16] Referring to the Poincaré sphere geometry shown in Figure 6-1a, the states of linear polarization lie on the equatorial plane at longitude $2\phi$, and states of left-right circular polarization lie on the upper-lower poles. All other left-right elliptical polarizations lie on the upper-lower hemisphere at latitude $\pm 2\psi$, respectively. The main sources of birefringencies and their effect on the state of polarization as visualized on the Poincaré sphere are described below:

1. Deviations of the refractive index distribution from circular symmetry (core ellipticity, fiber bends) cause linear birefringence. Their effect on the SOP is to rotate the Poincaré sphere with an angular velocity $\Delta\beta=\beta_1-\beta_2$, where $\beta_1$ and $\beta_2$ are the local wavevectors of the two nondegenerate modes. The axis ($\Delta\beta$) of this rotation lies in the equatorial plane at longitude determined by the azimuths of the principle axes of birefringence.

2. A twist of a birefringent index distribution causes the vector $\Delta\beta$ to rotate in the equatorial plane at a rate $2\tau$ about the polar axis, where $\tau$ is the twist rate.

3. Stresses of internal or external origin may induce optical activity in the fiber material. Its influence on the SOP is to rotate the Poicaré sphere about the polar axis at a rate $\alpha=k^+ - k^-$ where $k^+$ and $k^-$ are the wave vectors of the two circularly polarized modes of the optically active, but otherwise ideal fiber.

These three effects cannot be treated separately, since finite rotations are not additive. Rather, the three effects must be added differentially and then integrated. The vector addition-integration of these effects yields a vector evolving along cycloidal trajectories[8,11,16] as shown in Figure 6-1b.

Active control of the SOP of ordinary circular single mode fibers has been reported.[17] This method employs a polarimeter and two electromagnetic fiber squeezers which introduce variable amounts of stress birefringence directly into the fiber, compensating for the effects of changing intrinsic fiber birefringence. A second method of stabilizing the SOP of circular fibers is fiber twisting.[18] Since the shear strain associated with a twist

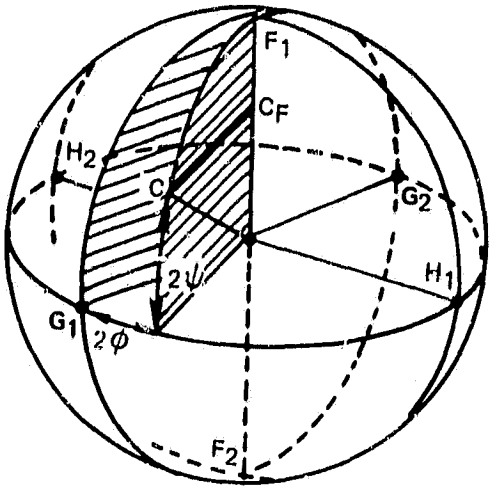


Figure 6-1a. Any combination of two waves, $F_1$, $F_2$, can be represented by a point C on the generalized Poincare sphere.

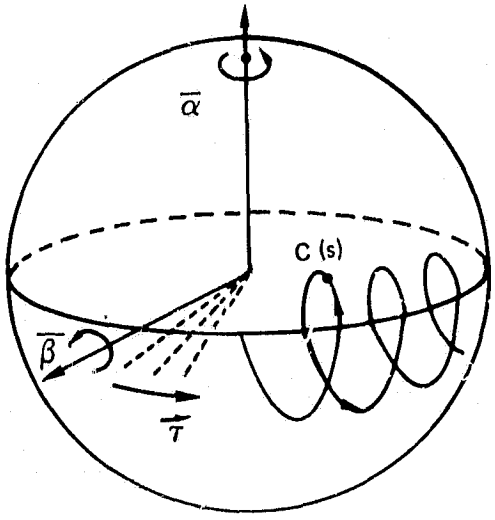


Figure 6-1b. In a monomode fiber, the combined effects of birefringent $\beta$, optical activity $\alpha$, and twist $\tau$ result in cycloidal trajectories C(s).

$^{\tau}$ elasto-optically induces a circular birefringence, strong twists ($\alpha_{\tau} >> \Delta\beta$ and $\beta_b$) modifies the eliptically birefringent fiber into a predominantly circularly birefringent medium. This technique has provided successful in current sensing[18] and optical isolation[19] applications in conjunction with Faraday rotation.

Attempts to modify the circular cross section of the fiber core into an elliptical core resulted into a slight improvement in the polarization performance of these fibers.[20,21] This is because of the fact that changing the core geometry into elliptical or even rectangular does not significantly alter the difference in the propagation constants of the two fundamental modes of orthogonal polarizations. This reasoning is supported by theoretical analysis of square-rectangular waveguides in which even a large change in the geometrical factor does not appreciably separate the first two cross polarized modes.[22] It was therefore found that noncircular geometry and the associate stress induced birefringence introduced during drawing are not sufficient to improve the polarization performance, and the enhancement of the anisotropic strain birefringence is necessary to achieve polarization maintaining fibers.[20]

Enhancement of anisotropic strains in single mode polarization maintaining fibers was first demonstrated by anisotropically straining a noncircular cladding of a circular core preform.[1,21,23] Two methods were first used to accomplish this. In the first method,[21] flats are ground on the substrate preform tube prior to deposition and formation of cladding. The cladding and core are then deposited, and tube collapsed subsequently yielding a circular core and an elliptical cladding. The cladding is strained because of the difference in thermal expansion between the cladding and the silica substrate tube, thus breaking the circular symmetry of the strain and causing birefringence. An alternative technique to this method[23,24] (known as the exposed cladding technique), is to expose two opposite sides of the doped cladding of a circular preform after collapse. The preform can be either slot ground or etched after collapse yielding strain induced birefringence also resulting from thermal expansion gradient between core-cladding and jacketing tube. The index difference $\Delta n$ between the two orthogonal axis obtained by these methods has been estimated at about 4-5 x $10^{-5}$, yeilding a beat length on the order of 10 mm at 0.5 $\mu$m

for borosilicate fibers, and about $3.2 \times 10^{-4}$ in germanosilicate fibers yielding a beat length of about 1.5 mm. Shorter beat lengths have been obtained in more heavily doped core (Ge+P) having a core cladding index difference $\Delta n = 0.065$, collapsed elliptically with approximate core dimensions of $0.85 \times 2.14 \mu m$,[25] yielding a birefringent index difference of $8 \times 10^{-4}$ and a beat length of 0.75 mm. The above mentioned techniques yield good polarization maintaining fibers, preserving the polarization over few hundred meters under practical conditions of random twists bends etc. While it has been indicated that the losses appear to increase as the birefringence increases, it is suggested that these losses are not intrinsic even at high doping levels.[12] Recent measurements indicate that Rayleigh scattering can introduce in excess of 2 dB/km of loss at 1.5 μm for heavily doped germanium fibers.[26]

## 6.2 POLARIZATION ASPECTS OF INTEGRATED OPTICAL DEVICES

Integrated optical devices in general process different polarizations with different efficiencies for several reasons, most notable of which are: the inherent birefringencies and lack of electro-optic symmetry of waveguide materials; the near rectangular cross section of optical waveguides, and the structural composition of integrated optical circuitry such as overlays, corrugations, etc. Performance of these devices is further complicated when they are linked to conventional singlemode fibers whose output is elliptically polarized due to the reasons discussed in Section 6.1. This situation gives rise to both TE and TM polarizations to be present in the guided structure. The first issue, that of performance difference for TE and TM modes in optical waveguides can not be avoided since it is dictated mainly by boundary conditions which are different for the two orthogonal polarizations. The second issue, relating to fiber output ellipticity can be resolved in three ways:

1. The use of a polarizer.
2. The use of a polarization preserving fiber.
3. The construction of thin film devices that are polarization independent in their operation.

Several configurations are presently used to achieve switching and modulation in integrated optical structures. The most common types are:

1. Directional couplers (mode interference).

2. Mach-Zender interferometer.

3. Electro-optic Bragg switching (planar).

4. Electro-optic phase modulators.

Type (1) utilizes modal coupling between two closely spaced channels and yields a modulated output when the modal dispersion of the guided modes is altered by electro-optical effects. In this configuration, the output of only one channel can be controlled with high extinction ratio.[27] While this is well suited for modulation purposes, it cannot be expected to be adequate for switching purposes since complete switching is not achieved due to the presence of unwanted power in the orthogonal polarization. The main reason for this is the fact that the electro-optically induced phase shift cannot be made identical for both polarizations for any crystal orientation.

In $LiNbO_3$, regardless of the crystal orientation, it has been concluded that low cross talk electro-optic couplers cannot be realized when both polarizations are present, and an optimum situation is obtained for X-cut crystals with an X-directed applied field and propagation at $14^o$ off the Z-axis.[27] In GaAs, however, it has been indicated that the $(\bar{1}12)$ cut appears to be the most promising in that regard whereby when the electric field is applied parallel to the Y-axis, the resulting electro-optic phase shift and thereby the switching efficiency is the same for both TE and TM modes.[27] In this orientation, however, the electro-optic coefficient of GaAs is relatively small requiring approximately three times the switching voltage required for the optimized X-cut $LiNbO_3$ orientation at $14^o$.

The second type of structures employing Y-branching junctions and electro-optically induced phase shifts appears to yield effectively zero crosstalk using either X or Y cut $LiNbO_3$ crystals, assuming perfectly fabricated patterns. Specially designed waveguides can yield very low crosstalk between the two channels both in the OFF and ON states provided that the ratio of the induced phase difference between the two polarizations is an odd integer.[27] In this configuration, the cross talk is

limited only by fabrication imperfections. A minimum length of 1 cm is nevertheless required for such geometry to achieve isolation levels greater than 20 dB.

In the Bragg deflector switch/modulator (planar structures), the OFF state (no applied voltage) emerges with high extinction ratio. Upon the application on an electric field, both polarizations will be deflected if present. If the electro-optic phase shifts of the TE and TM modes differ by nonintegral multiples of $\pi$, one polarization will be deflected more efficiently that the other. For efficient switching, only the wave that is phase matched with the electrode periodicity will be deflected efficiently when the two polarizations are non-degenerate as in the case of $LiNbO_3$. This feature allows for greater difference in deflection efficiencies between the TE and TM modes in $LiNbO_3$. In certain crystal orientations, such as Y-cuts, the electro-optic effect in TM modes is much smaller than that of TE resulting in high crosstalk. Z-cuts and X-cuts, however, can be optimized for very low crosstalk when the length is chosen to be the coupling length for the TM waves and TE waves as well. Near zero crosstalk can be obtained in X-cut crystals optimized for wave propagation at $14^o$ from the optic axis. This happens to be the appropriate orientation for very low crosstalk in the OFF state also.[27]

For the single channel phase modulator, when both polarizations are present, the phase modulation for the TE and TM modes will always be different because of the difference in the electro-optic coefficients for all possible orientations. Phases of the two modes can only be made equal for a singular phase value at a particular length or integer multiples thereof, but it cannot be expected that the voltage modulated phases of the two polarizations to be the same otherwise. Crosstalk in this case will be depended on the ratio of power existing in the waveguides in the two polarizations.

Problems associated with integrated optical device performance limitations due to polarization led to the exploration of device construction which perform independent of polarization. An example of such devices are the Mach-Zender structure with two sets of electrodes, each providing the required phase shift for one of the two polarizations.[28] A polarization

independent optical filter has also been demonstrated by employing wavelength selective mode conversion through a periodic electrode structure.[29] These examples suggest that it is possible to achieve low crosstalk by employing certain pattern circuitry that offers polarization independent device operation.

## REFERENCES


1. R.H. Stolen, V. Ramaswamy, P. Kaisar, and W. Pleibel, "Linear Polarization in Birefringent Single Mode Fibers", Appl. Phys. Lett., 33, 699, 1978.

2. J.D. Love, R.A. Sammut, and A.W. Snyder, Electron. Lett., 15, 615, 1979.

3. V. Ramaswamy and W.S. French, Electron. Lett., 14, 143, 1978.

4. R.A. Sammut, Electron. Lett., 16, 728, 1980.

5. I.P. Kaminow and V. Ramaswamy, "Single Polarization Optical Fibers: Slab Model", Appl. Phys. Lett., 34, 268, 1979.

6. Y. Namihira, M. Kudo, and Y. Mushiano, Trans. Inst. Chem. Eng., 60C, 391, 1977.

7. M. Johnson, "In Line Fiber Optical Polarization Transformer", Appl. Opt., 18, 1288, 1979.

8. R. Ulrich and A. Simon, "Polarization Optics of Twisted Single Mode Fibers", Appl. Opt., 13, 2241, 1979.

9. R. Ulrich, S.C. Rashleigh and W. Eickhoff, "Bending Induced Birefringence in Single Mode Fibers", Opt. Lett., 5, 273, 1980.

10. A. Papp and H. Harms, "Polarization Optics of Liquid Core Optical Fibers", Appl. Opt., 16, 1315, 1977.

11. R. Ulrich, "Representation of Codirectional Coupled Waves", Opt. Lett., 1, 109, 1977.

12. I.P. Kaminow, "Polarization in Optical Fibers", IEEE J. of QE, QE-17, 15, 1981.

13. I.P. Kaminow, "Polarization in Fibers", Laser Focus, pp. 82, June 1980.

14. M. Born and E. Wolf, "Principles of Optics", 3rd Ed. (Pergamon, London, 1964) pp. 31.

15. M. Johnson, "Poincare Sphere Representation of Birefringent Networks", Appl. Opt., 20, 2075, 1981.

16. A. Simon and R. Ulrich, "Evolution of Polarization Along a Single Mode Fiber", Appl. Phys. Lett., 31, 840, 1979.

17. R. Ulrich, "Polarization Stabilization on Single mode Fiber", Appl. Phys. Lett., 35, 840, 1979.

18. S.C. Rashleigh and R. Ulrich, "Magneto-Optic Current Sensing with Birefringent Fibers", Appl. Phys. Lett., 34, 768, 1979.

19. T. Finadkly, "Single Mode Fiber Isolator In Toroidal Configuration", Appl. Opt., 20, 3989, 1981.

20. V. Ramaswamy, W.G. French and R.D. Standley, "Polarization Characteristics of Non-Circular Core Single Mode Fibers", Appl. Opt., 17, 3014, 1978.

21. V. Ramaswamy and W.G. French, Electron, Lett., 14, 143, 1978.

22. E.A.J. Marcatili, "Dielectric Rectangular Waveguide and Directional Coupler for Integrated Optics", BSTS, 48, 2071, 1969.

23. V. Ramaswamy, I.P. Kaminow, and P. Kaiser, "Single Polarization Optical Fiber; Exposed Cladding Technique", Appl. Phys. Lett., 33, 814, 1978.

24. I.P. Kaminow, J.R. Simpson, H.M. Presby, and J.B. MacChensey, "Strain Birefringence in Single Polarization Germano-Silicate Optical Fibers", Electron. Lett., 15, 677, 1979.

25. R.B. Dyott, J.R. Cozens, and D.G. Morris, "Preservation of Polarization in Optical Fiber Waveguides with Elliptical Cores", Electron. Lett., 15, 380, 1979.

26. H. Matsumura, T. Katsuyama and T. Suganuma, "Fundamental Study of Single Polarization Fibers", Presented at the 6th European Conf. Opt. Comm., York, England, Sept. 1980.

27. R.A. Steinberg and T.F. Giallorenzi, "Performance Limitations Imposed on Optical Waveguide Switches and Modulators by Polarization", Appl. Opt., 15, 2440, 1976.

28. W.K. Burns, T. Giallorenzi, R.P. Moeller, and E.J. West, "Interferometric Waveguide Modulator with Polarization Independent Operation", Appl. Phys. Lett., 33, 944, 1978.

29. R.C. Alferness and L.L. Buhl, "Polarization Independent Optical Filter using TE-TM Conversion", Appl. Phys. Lett., 39, 131, 1981.

# 7. LASER AND FIBER COUPLING TO INTEGRATED OPTICS

## 7.1 END-BUTT COUPLING

End-butt coupling is a straightforward, practical technique for couplings between laser diodes, optical fibers and integrated optical chip. In the case of fiber-to-channel waveguide coupling, the large index difference between modes in glass fiber ($n_{eff} \sim 1.50$) and in the channel waveguide ($n_{eff} \sim 2.20$ for $LiNbO_3$) is not a serious problem for an efficient coupling, except the Fresnel reflection loss due to index mismatch at the fiber-waveguide interface. Fresnel reflection at the glass-$LiNbO_3$ waveguide interface is estimated to be less than 4%. Reflection loss can be further reduced by applying a proper index matching liquid or an anti-reflection coating between the fiber and the waveguide. Theoretically, the coupling efficiency can be determined by the overlap integral of the two transverse mode fields at the interface. In this section, we shall investigate the coupling between a circular Gaussian field and an elliptical Gaussian field. These results can be applied to the coupling cases such as laser-to-fiber, fiber-to-channel waveguide and laser-to-channel waveguide.

Power coupling efficiency, $\eta$, between any two transverse optical fields is determined by the normalized overlap integral,

$$\eta = \frac{\left| \int \psi_1 \psi_2^* \, dxdy \right|^2}{\int \psi_1 \psi_1^* \, dxdy \int \psi_2 \psi_2^* \, dxdy} \tag{1}$$

where $\psi_1$ and $\psi_2$ are the transverse optical field distributions of the two modes at the interface. $\psi_1$ and $\psi_2$ are in general complex functions containing both amplitude and phase information. It has been shown that the coupling efficiency between a circular Gaussin beam with beam waist of "a" and an elliptical Gaussian beam with beam waists of $w_x$ and $w_y$ is given by[1]

$$\eta = \frac{4}{\left(\frac{w_x}{a} + \frac{a}{w_x}\right)\left(\frac{w_y}{a} + \frac{a}{w_y}\right)} \tag{2}$$

Equation (2) is derived assuming the longitudinal separation between the beam waists of the Gaussian field is zero. The coupling efficiency will be reduced if the longitudinal separation is not zero, this is due to the mismatch of the curved wavefronts.

By differentiating $\eta$ with respect to the parameter "a," one can easily show that for a given set of elliptical Gaussian field parameters, $w_x$ and $w_y$, the optimum coupling efficiency occurs when

$$a = \sqrt{w_x w_y} \tag{3}$$

Figure 7-1 plots the optimum coupling efficiency versus the ratio of $w_x$ and $w_y$. In order to keep the coupling loss less than 1 dB, i.e. 80% optimum coupling efficiency, the ellipticity of the Gaussin field must satisfy the requirement of $w_x/w_y > 0.4$ or $w_x/w_y > 0.4$. In addition, the condition of Equation (3) should also be satisfied. Equation (2) is a simple equation that calculates the power coupling efficiency based on three Gaussian field parameters.

Equation (2) has been used to estimate the coupling efficiency for laser diode-to-fiber coupling[2] and fiber-to-channel waveguide coupling.[3] In both cases, the transverse field of the single mode fiber, i.e. $HE_{11}$ mode, has been approximately by a circular Gaussian field. An numerical calculation indicates that a 99% power transfer can be achieved between a circular Gaussin beam and the $HE_{11}$ mode of a fiber. In another calculation,[4] the results show the field overlap between, single mode fiber with V = 0.9 to 2.4 and a circular Gaussian field can be better than 0.988. This approximation turns out to be extremely close to the real situation. Gaussian fit to the field distribution in a channel waveguide is a difficult task simply because there exists no close-form equations describing the electrical field inside the waveguide. This situation becomes even worse when the channel waveguide is formed by diffusion such as Ti diffused $LiNbO_3$ waveguides. The general guideline is to fabricate the channel waveguide close to a circular symmetry, as indicated in Figure 7-1. Thus, the discussion here will be limited to the geometric aspect ratio of an isotropically diffused channel waveguides. Readers interested in the Gaussian fit of diffused channel waveguides are referred to Reference 3 and references therein.

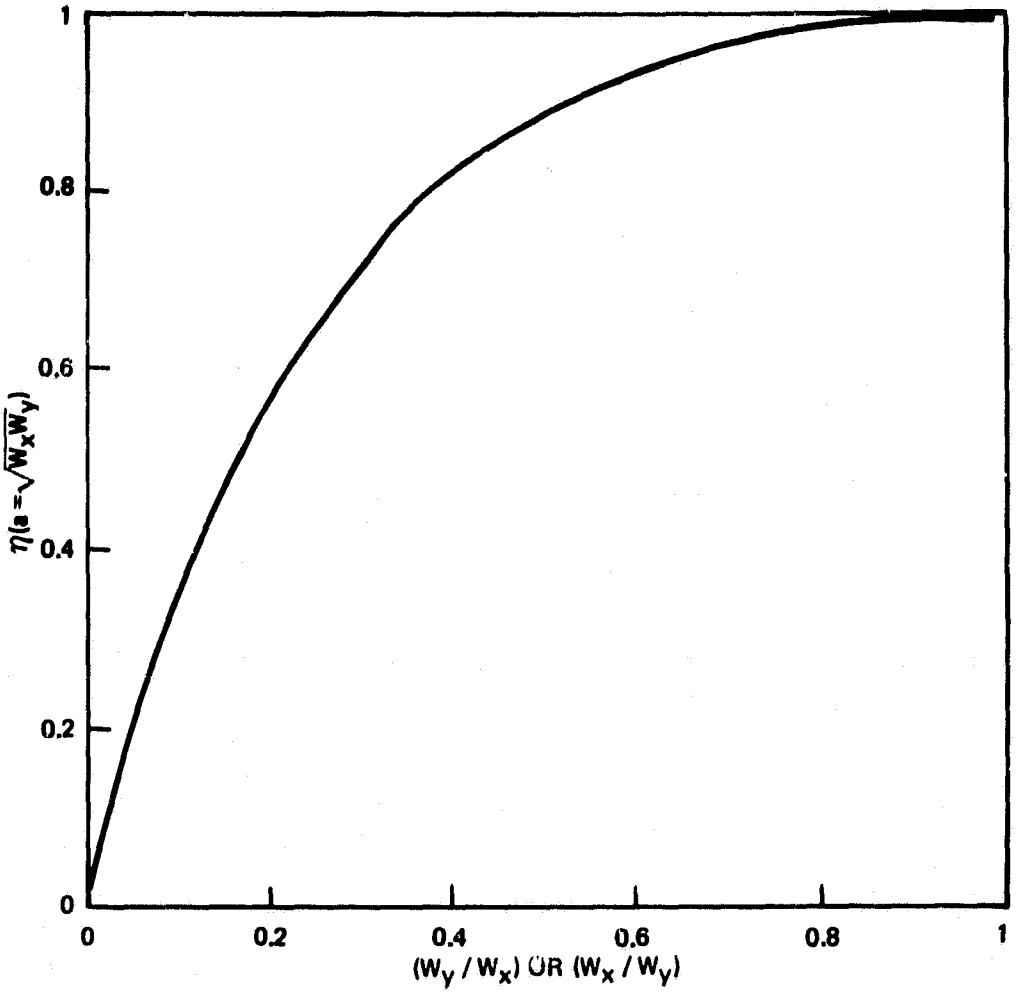


Figure 7-1. Optimum Coupling Efficiency Versus the Ratio of $w_x$ and $w_y$

A 2-D isotropic diffusion model is used to describe the diffused channel waveguides. We assume the diffusion time is long enough to diffuse all the source material from the surface into the bulk substrate and assume the index of refraction profile is linearly proportional to the dopant concentration. The stripe of the diffusion source extends infinitely in the Z-direction and has a width of W along the X-direction. The index profile of the diffused channel waveguide is given by

$$n^2(x,y) = n_o^2 + (n_s^2 - n_o^2)\, f(y/D)\, g(2x/W) \qquad (4)$$

where $n_o$ is the index of refraction of the substrate and $n_s$ is the index of refraction at the surface after diffusion. The diffusion profile along the depth direction is described by a Gaussian function and the profile along the X-direction is described by an error function.

$$f(y/D) = \exp(-y^2/D^2) \tag{5}$$

and

$$g(2x/W) = 1/2 \operatorname{erf}\left[\frac{W}{2D}\left(1 + \frac{2x}{W}\right)\right] + \operatorname{erf}\left[\frac{W}{2D}\left(1 - \frac{2x}{W}\right)\right] \tag{6}$$

where D is the diffusion depth determined by the diffusion coefficient and diffusion time. Because the diffusion process proceeds along with x and y directions, the geometrical aspect ratio of the index profile is different from the ratio of strip width to diffusion length W/D, the equality is true only when W/D >> 1. In y direction, the index change is reduced by a factor 2 at y = 0.83 D. In x direction, the full width at half maximum can be calculated from Equation (6) and is plotted in Figure 7-2. If one multiply $2X_{1/2}/D$ by a factor of 1/0.83, the coordinate of Figure 7-2 becomes the geometrical aspect ratio of the diffused channel waveguide.

Ti:$LiNbO_3$ waveguides are used extensively to fabricate various integrated optical devices such as modulators, switches, and filters. To make those pratically useful for fiber system applications, it requires an efficient coupling to single mode optical fibers. There are several papers reporting the coupling measurement results for different conditions. In Reference 5, He-Ne laser ($\lambda$ = 633 nm) is used as the light source. The channel waveguides are formed by diffusing 3-4 μm wide, 170-220 Å Ti metal into Z-cut, X-propagating $LiNbO_3$ substrates. Single mode fiber has NA ≃ 0.1 and the core diameter is 4.5 μm. When water is used as index matching liquid, the throughput for a fiber-9 mm long channel-fiber configuration are 52% for TE polarization and 51% for TM polarization. Assume the only loss is due to interface coupling, one can translate the results to the fiber-channel waveguide coupling efficiencies of 72% (TE) and 71% (TM). If other losses due to reflection and waveguide attenuation are taken into

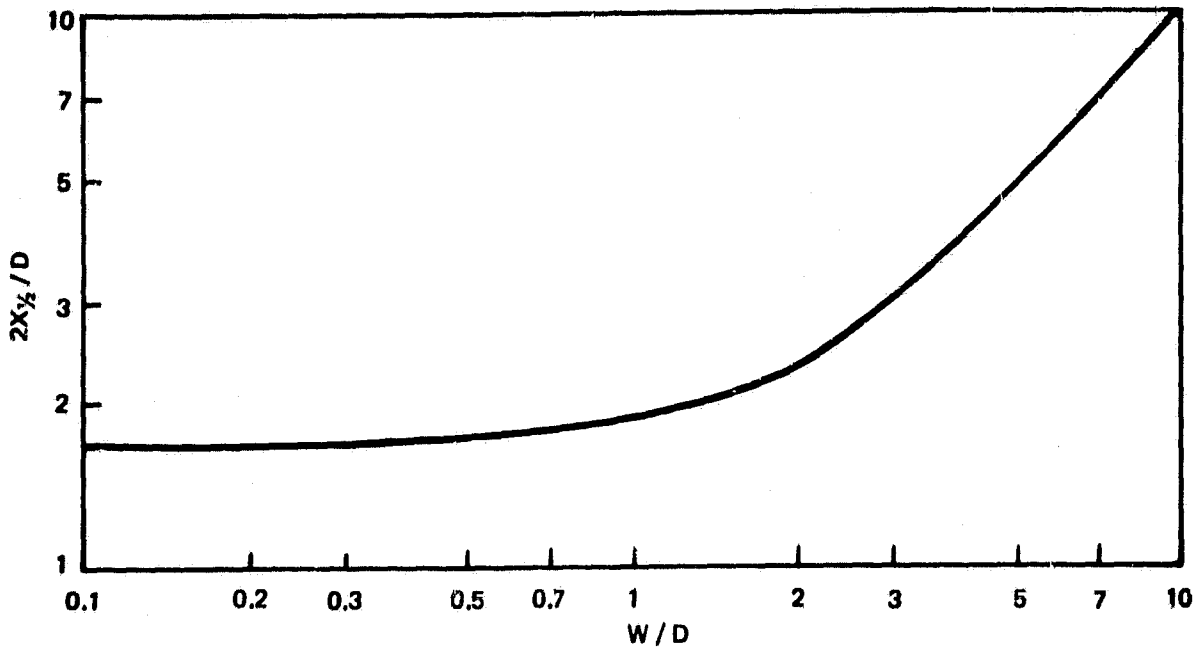


Figure 7-2. Full Width at Half Maximum, $2X_{1/2}$, of index profile versus the ratio of the undiffused channel width W to the diffusion length D.

account, the coupling efficiency as high as 87% has been obtained. Under similar condition, coupling loss of 1 dB has also been measured at 0.83 μm by another reserach group.[6]

In Reference 7, He-Ne laser of $\lambda$ = 1150 nm is used to measure the coupling of fiber to Ti diffused channel waveguides on Y-cut and Z-cut $LiNbO_3$ substrates, 500 Å of Ti metal is diffused at different diffusion temperatures, and the coupling losses and propagation losses are measured. Strip width varies between 6 μm and 10 μm, the fiber mode diameter at half maximum is approximately 5.0 μm. Coupling losses in the Y-cut and Z-cut waveguides are 2.5 dB and 1 dB respectively. Measured coupling losses agree well with the calculations based on the overlap of near field patterns. The higher coupling loss for Y-cut substrates is attributed to the mode mismatch in the lateral direction. This is caused by an unusual large lateral diffusion constant for Y-cut $LiNbO_3$ wafers.

Recently, the coupling loss was further reduced by optimizing the diffusion parameters to reduce the mode mismatch. 720Å thick Ti metal stripes of width ranging from 4 to 10 μm are diffused at 1100°C. Single

mode optical fiber has a mode diameter of 7.8 μm. Measurements of $w_x$ and $w_y$ of the near field mode pattern show that the optimum coupling condition specified by Equation (3) is satisfied for channel width from 7 to 10 μm. Total insertion losses for fiber-waveguide-fiber coupling configuration are approximately 1 dB for TE polarization of a Nd:YAG laser of $\lambda$ = 1302 nm.[8] Coupling loss for TM polarization wave is slightly higher. Index liquid is used to reduce the Fresnel reflection loss.

Another way to improve the coupling efficiency is to modify the fiber mode diameter to satisfy Equation (3). This can be done by forming a conical taper at the end of the fiber. Since the mode diameter of the fiber is a strong function of the core radius, one can easily obtain the optimum fiber mode profile. This technique has been used to demonstrate a coupling efficiency of 95%, an increase of 25% in coupling efficiency.[9] A more elaborate coupling configuration demonstrated involves an optical microlens between the waveguide and optical fiber. The microlens fabricated at the end of the fiber improve the mode mismatch, thus reducing the coupling loss.

## 7.2 COUPLING TOLERANCES

Because of the small dimensions of the waveguides involved, the end-butt coupling between single mode optical waveguides is very critical to the misalignment, both the angular misalignment and lateral misalignment. Coupling, in general, is not sensitive to the longitudinal misalignment. Equation (2) is the maximum coupling efficiency for a given set of parameters of circular and elliptical Gaussian fields. If there is a lateral misalignment, $\delta_x$ and $\delta_y$ along the x and y axes, then the coupling efficiency, normalized to its maximum value $\eta_o$, becomes,

$$\frac{\eta}{\eta_o} = \exp\left\{-\frac{\delta_x^2}{w_x^2 + a^2}\right\} \exp\left\{-\frac{\delta_y^2}{w_y^2 + a^2}\right\} \qquad (7)$$

Coupling efficiency will be reduced by 4.34 dB, i.e. 36.8% its maximum value, when the lateral alignments are more than the characteristic modal radii

$$\delta_x = \sqrt{w_x^2 + a^2} \text{ or } \delta_y = \sqrt{w_y^2 + a^2}.$$

If the Gaussian fields are misaligned angularly by the amounts of $\Theta_x$ and $\Theta_y$, then the coupling efficiency for a perfect positional alignment is given approximately by

$$\frac{n}{n_o} = \exp\left\{-\frac{k^2a^2w_y^2\sin\Theta_x}{2(a^2+w_y^2)}\right\}\exp\left\{-\frac{k^2a^2w_y^2\sin^2\Theta_y}{2(a^2+w_x^2)}\right\} \qquad (8)$$

where $k = 2\pi/\lambda$ is the wavenumber of the optical light. This equation is exact only for small angular misalignments, $\Theta_x$ and $\Theta_y << 1$. From Equation (8), one concludes that for a given modal parameters, coupling efficiency is less sensitive to the angular misalignment for a longer wavelength. In the case of coupling a single mode optical fiber to a Ti:$LiNbO_3$ channel waveguide,[10] the coupling tolerances for a 1 dB degradation of coupling are 2 μm for lateral misalignment, 20 μm for longitudinal misalignment, and $1^o$ for angular misalignment.

In the research laboratory, precise alignment between fiber and channel waveguide can be achieved with the help of differential micrometer or pizoelectrical controlled stages. It is also possible to obtain fairly accurate alignment using the flip-chip approach,[11] as shown in Figure 7-3. Fibers are positioned precisely in preferentially etched V-grooves in Si wafer. Grooves are formed by etching through a $SiO_2$ mask defined by photolithographic technique. On the (100) Si wafer, the etching rate along the depth direction <100> is more than 60 times faster than the etching rate along <111> direction, when etchant solution is used.[11] Thus etching a channel in a <100> silicon surface will result in a V-shaped channel, the side walls of the channel are parallel to the <111> planes. The angle of the V-groove, as determined by crystalline structure, is $54.7^o$. Because of the large difference in etching rates, there is little undercutting beneath the $SiO_2$ mask. Overetching merely results in a deeper, not wider channel until the two <111> planes intersects. This unique feature allows one to fabricate fiber alignment channels with extremely high precision. From a simple trigometric calculation, one can derive the following relationship between the original channel width and fiber diameter for a fiber centered with respect to the wafer surface.

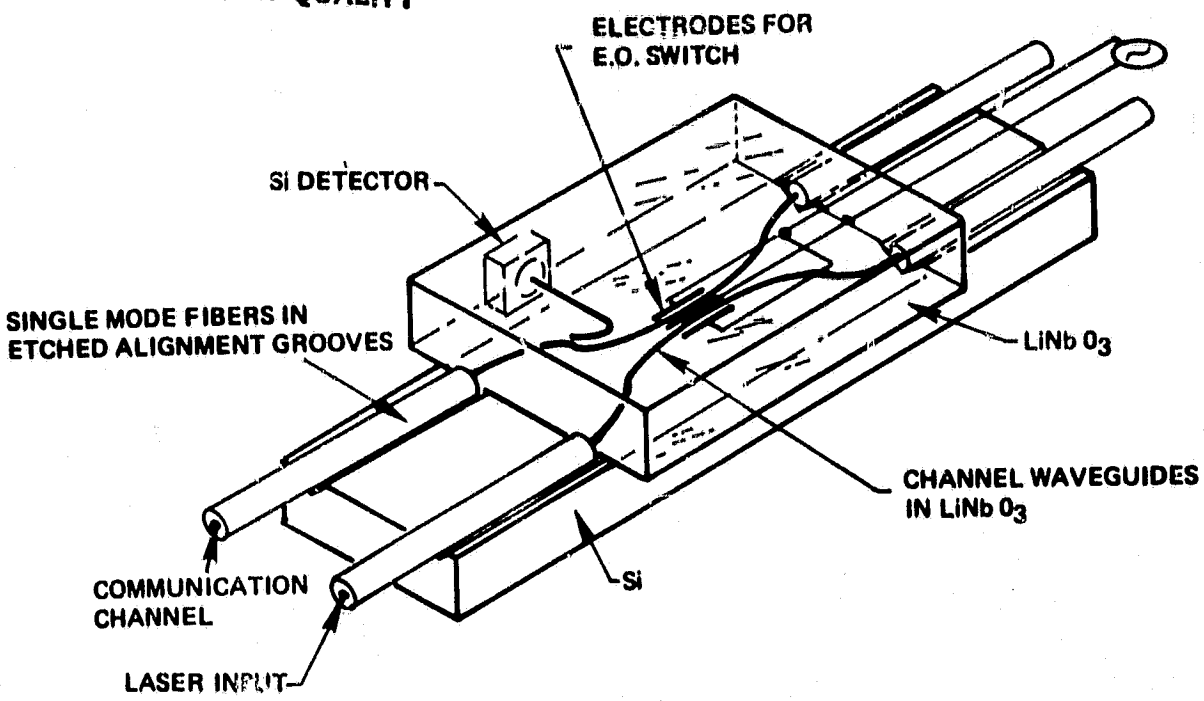


Figure 7-3. Flip-Chip Approach to End-Fire Coupling Between Single Mode Optical Fibers and Channel Waveguides

$$W = D/\sin\theta$$

where W is the width of $SiO_2$ mask and D is the outside diameter (OD) of the fiber, and $\theta$ is the V-groove angle, as shown in Figure 7-4. Experimental results indicate that fiber alignment tolerance of ±1 μm can be achieved by this etching technique. At this time, the biggest difficulties encountered are the fiber dimensional variation and core eccentricity. Commercial single mode fibers are specified with OD variation ±5 μm and core eccentricity of ±1 μm. In order to obtain efficient couplings using prefabricated alignment fixture, there is a lot of improvement to be done in controlling the fiber dimensions.

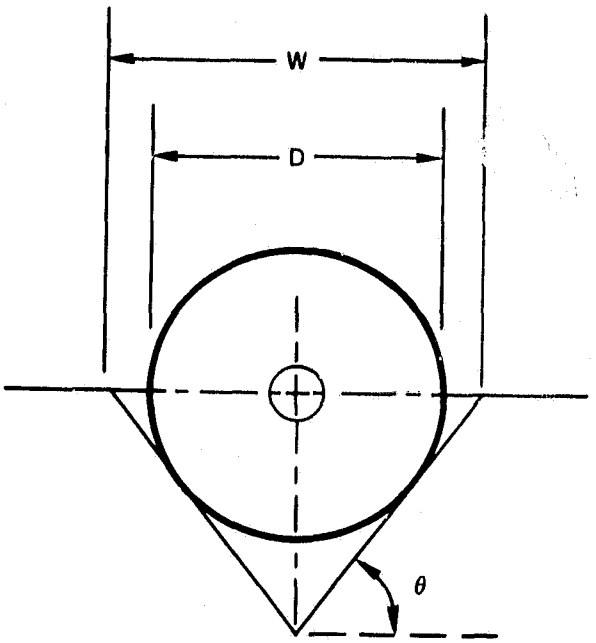


$W = D/\sin\theta$

**Figure 7-4. Relationship Between Etched Si-V Groove and Optical Fiber**

## REFERENCES


1. L.G. Cohen "Power Coupling from GaAs Injection Lasers into Optical Fibers," Bell Syst. Tech. J. 51, 573 (1972).

2. D. Marcuse "Excitation of the Dominant Mode of a Round Fiber by A Gaussian Beam" Bell Syst. Tech. J. 49, 1695 (1970).

3. W.K. Burns and G.B. Hocker, "End Fire Coupling Between Optical Fibers and Diffused Channel Waveguides," Appl. Opt. 16, 2048 (1977).

4. P.J.B. Clarricoats and K.B. Chan, Proc. IEEE 120, 1371 (1973).

5. C.H. Bulmer, S.K. Sheem, R.P. Moeller, and W.K. Burns, "High Efficiency Flip-Chip Coupling Between Single-Mode Fibers and $LiNbO_3$ Channel Waveguides," Appl. Phys. Lett. 37, 351 (1980).

6. O.G. Ramer, "Single-Mode Fiber-to-Channel Waveguide Coupling," J. Opt. Comm. 2, 3 (1981).

7. M. Fukuma and J. Noda, "Optical Properties of Titanium Diffused $LiNbO_3$ Strip Waveguides and Their Coupling-to-a-Fiber Characteristics," Appl. Opt. 15, 591 (1980).

8. R.C. Alferness, V. Ramaswamy, "High Efficiency Single-Mode Fiber to Ti:$LiNbO_3$ Waveguide Coupling at $\lambda = 1.32$ μm," Topical Meeting on Integrated and Guided Wave Optics, Jan. 6-8, 1982, Pacific Grove, CA.

9. M. Papuchon, P. Kayoun, Y. Bourbin, "High Coupling Efficiencies Between Single Mode Optical Fibers and Ti Diffused $LiNbO_3$ Waveguides," Topical Meeting on Integrated and Guided Wave Optics, Jan. 6-8, 1982, Pacific Grove, CA.

10. J. Noda, O. Mikami, M. Minakata, and M. Fukuma, "Single-Mode Optical-Waveguide Fiber Coupler," Appl. Opt. 17, 2092, (1978).

11. H.P. Hsu and A.F. Milton, "Flip-Chip Approach to Endfire Coupling Between Single-Mode Optical Fibers and Channel Waveguides," Elect. Lett., 12, 404 (1976).

# 8. SOURCES FOR OPTICAL COMMUNICATIONS AND FIBER GYRO APPLICATIONS

## 8.1 INTRODUCTION

The main sources for optical communications systems available and in research today can be divided into two main groups according to the wavelength at which they operate. In one group fall the GaAlAs light emitting diodes (LED's) and lasers which operate in the spectral range 800-900 nm, and in the other group fall the InGaAsP quaternary laser diodes which operate in the 1100-1700 nm spectral range.

Mainly for historical reasons the state of development of GaAlAs devices is ahead of that of InGaAsP devices. However, InGaAsP devices are more attractive candidates in the regions of low loss and low signal dispersion of current-technology silica-based optical fibers, namely the 1100-1350 nm and 1500-1700 nm spectral regions.

The main factors to be considered when choosing an optical source for an optical communications system are: device reliability and aging behavior, modulation bandwidth, coupling efficiency to glass fibers, power output, wavelength matching to low loss optical fiber spectral windows, and the potential of devices under research. These factors will be addressed in the following sections.

Another issue of importance when choosing between the GaAlAs and the InGaAsP systems is the question of threshold current temperature stability. Temperature stability is measured approximately by the value of $T_o$ in the relationship

$$J_{th} \sim e^{-T/T_o}$$

where $J_{th}$ is the threshold current density, T the temperature, and $T_o$ a constant material dependent temperature. For GaAs and GaAlAs ternary materials $T_o$ has values between 120-150 °K. For quaternary GaInAsP materials the value of $T_o$ is ≃120°K for T≲ 260°K and it drops to ≃60-80°K for T≳260°K. Thus quaternary materials show higher temperature threshold current sensitivity than GaAlAs material systems and may need temperature stabilization.

## 8.2 LIGHT EMITTING DIODES (LED'S)

### 8.2.1 Light emitting diode geometries

The two main LED geometries developed to date are the surface emitter LED (of the burrus type), shown in Fig. 8.1, and the edge emitter LED, a double heterostructure type diode, shown in Fig. 8.2.

The radiation pattern of surface emitting diodes is of the Lambertian type with a beamwidth of 120°. Light is coupled out of the diode into a fiber by imbedding it into a well etched into the GaAs substrate. The matching of diode to fiber is aided by the use of an index matching epoxy that also provides structural strength.

In the case of edge emitters, the radiation is guided by the waveguide produced by the AlGaAs heterolayers. Radiation is thus confined to narrower beamwidths [1]. For example, for active layers of the order of 500Å the beamwidth in the plane perpendicular to the heterolayers is about 30° [2], and the width of the emitting region in the junction plane is typically 50-80 μm, depending on the fiber into which the light is to be coupled.

### 8.2.2 LED characteristics

Two major areas of concern when using LED's in optical communication systems are their modulation characteristics (modulation bandwidth and distortion properties) and their coupling to optical fibers.

Due to their relatively large emission spectra (one or two orders of magnitude larger than that of laser diodes) and their poorer coupling efficiencies to low NA fibers, LED's are second to laser diodes in high-data-rate applications (~50 Mbit/sec). However, in many low data rate applications LED's are preferable to laser diodes due to their better linearity, smaller temperature dependance of emitted power, and slower degradation than laser diodes.

Both surface-emitters and edge emitters provide several milliwatts [3] of power output into air in the 800-900 nm (GaAlAs) spectral range at drive currents of 100-200 mA.

A comparison[3] of surface-emitting and edge-emitting LED's has shown that for fibers with numerical apertures NA≤0.3 edge emitters are coupled more efficiently into fibers than surface emitters, whereas for NA ≥0.3 the opposite is true. Coupling can be aided by the use of coupling

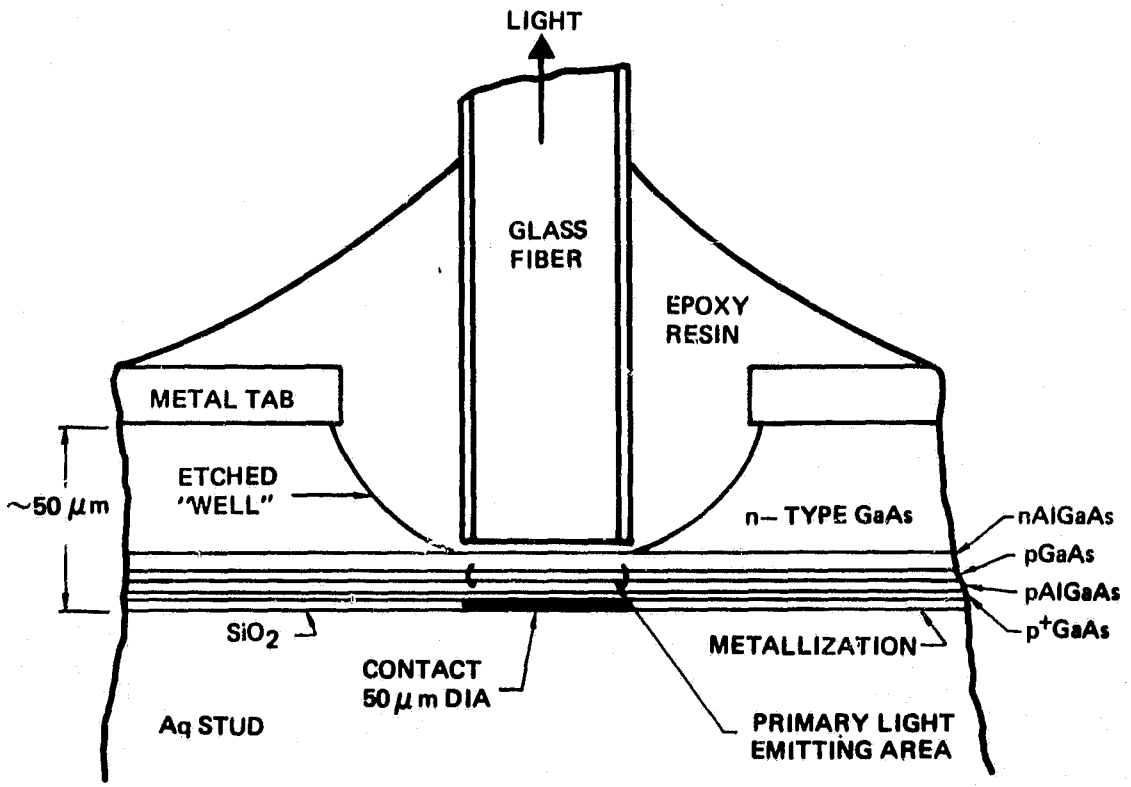


Figure 8.1 Surface-mitting (Burrus) diode

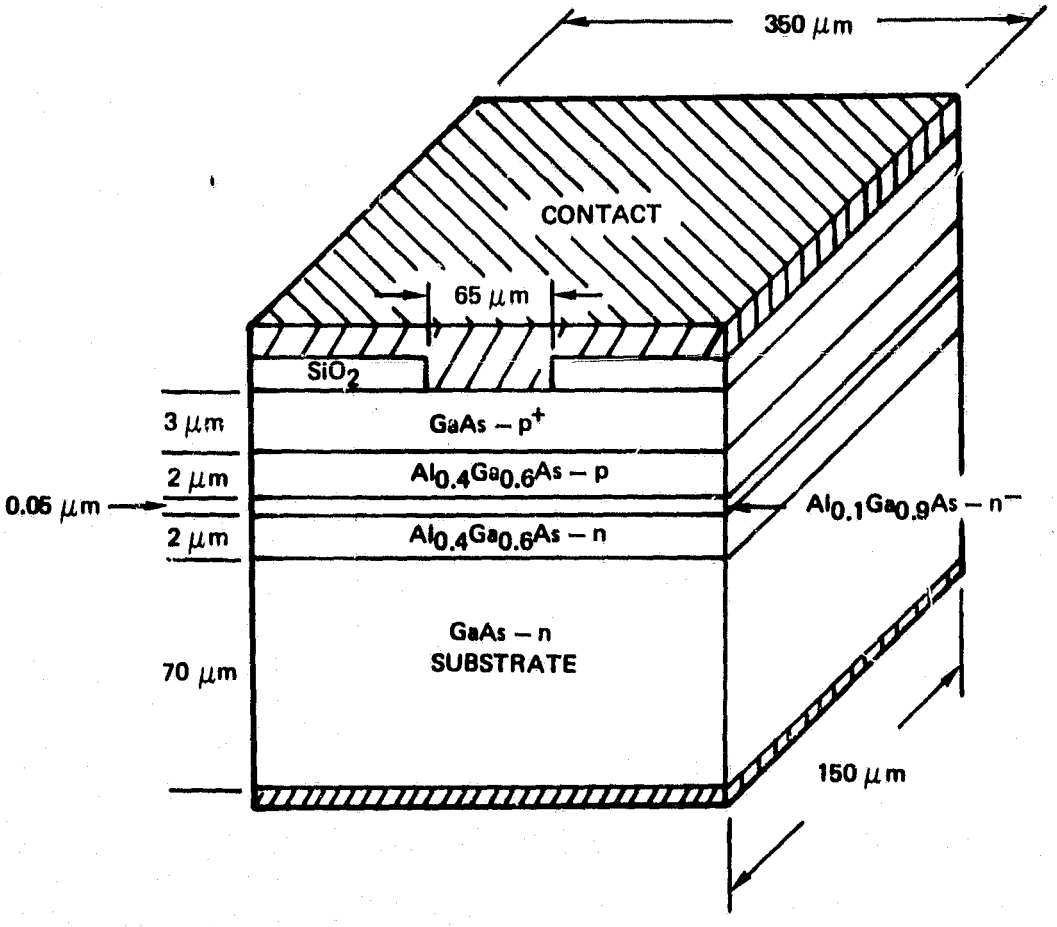


Figure 8.2. High-radiance edge-emitting diode

lenses and matching fluids. For example, the coupling efficiency of a 35-μm-dot contact diameter surface emitting LED to a 0.14 NA 85-μm core diameter step-index fiber was increased from 2.3 to 10 percent by forming a sphere on the fiber end.[4] And by using self-aligned spherical lenses, a monolithic array of surface LED's has been used to couple 600 μW into a 0.39 NA ten-core flat fiber cable at a drive current level of 100 mA[7].

Non-linear distortion has been reduced to very low levels (-60 to -80 dB) by using compensation techniques[5] such as complementary distortion, feedback and feedforward.

In the longer wavelength range (1100-1700 nm) of lower fiber loss InGaAsP LED's have been shown to exhibit characteristics similar or better to those of GaAlAs LED's.

A main drawback of InGaAsP LED's is their relatively high spectral bandwidth ($\Delta\lambda \simeq$ 90 nm) with respect to that of GaAlAs LED's ($\Delta\lambda \simeq$ 30 nm). In spite of this fact transmission bandwiths of up to 1 Gbit km/s could be achieved by using α-optimized[6] graded-index fibers in the minimum dispersion region 1300 nm $< \lambda <$ 1350 nm.

## 8.3 LASER DIODES

### 8.3.1 Laser diode geometries and properties

Laser diodes offer definite advantages over LED's[3,8]. Their spectral bandwidth is of the order of 2 nm, one order of magnitude narrower than that of GaAlAs LED's ($\simeq$30 nm) and two orders of magnitude narrower than that of InGaAsP LED's ($\simeq$90 nm). They can be modulated at rates of several GHz (several hundred MHZ for LED's), and offer larger coupling efficiencies to low NA optical fibers ($\simeq$50 vs. 2-10 percent for LED's). One of the main concerns in the development of laser diodes for high-data-rate long-haul optical communications systems is the stabilization of their transverse and longitudinal mode patterns to a single mode. Fig. 8.3 shows several geometries used to achieve single mode transverse operation. All these geometries accomplish transverse mode stability by confining the optical radiation to a narrow region within a gain or refractive-index defined waveguide. It has been found that in many cases, for yet unknown reasons, stabilization of the transverse mode pattern leads to simultaneous stabilization of the longitudinal mode pattern to a single mode.

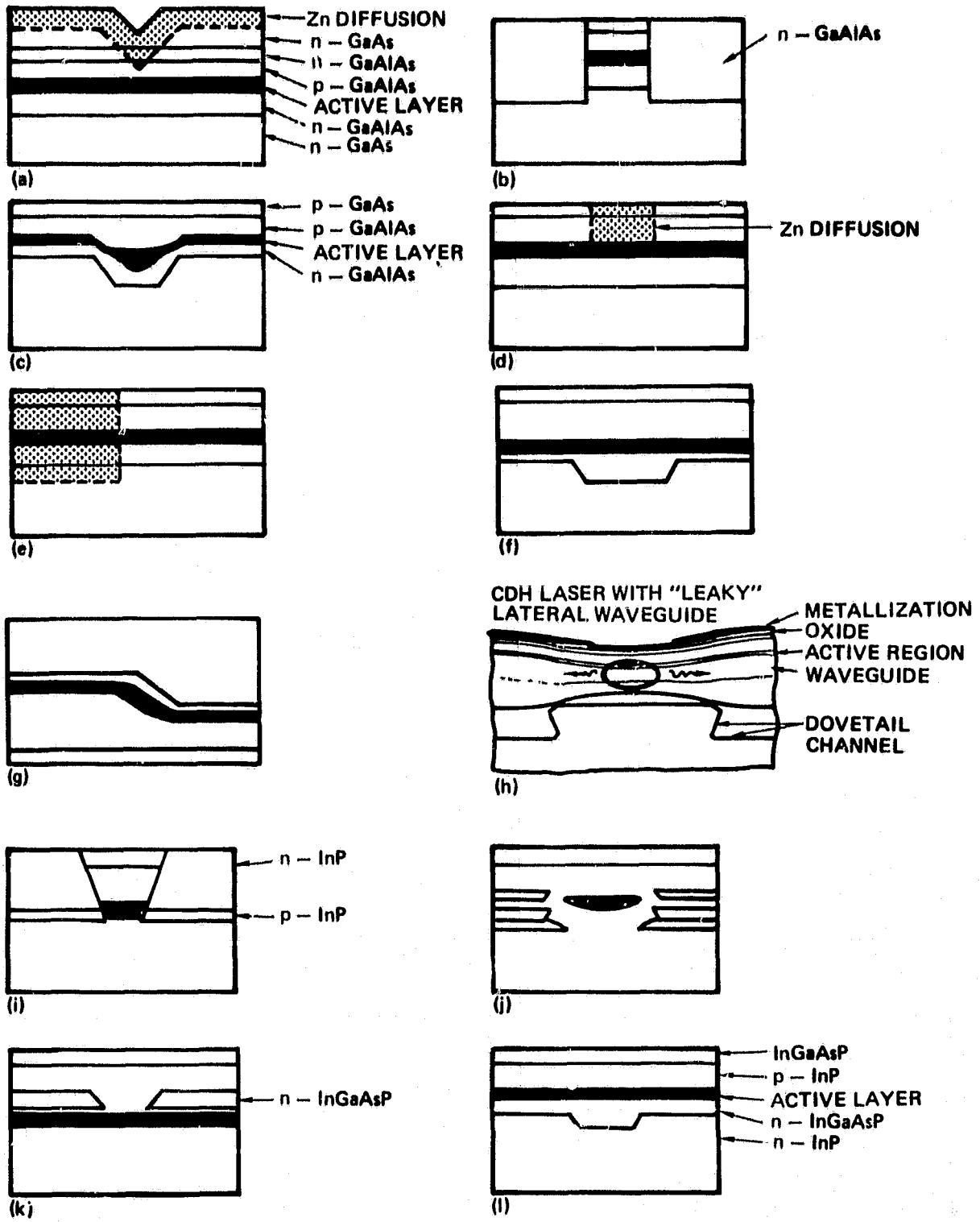


Figure 8.3. Schematic structures of GaAlAs/GaAs(a) V groove lasers; (b) BH; (c) embedded structure; (d) deep-difusion stripe; (e) TJS; (f) channeled-substrate planar; (g) terraced substrate; (h) CDH-LOC. Schematic structures of InGaAsP/InP index guide lasers; (i) BH; (j) buried crescent; (k) self-aligned structure and (l) plano-convex waveguide.

Index-guided lasers have smaller emitting areas (1-3 μm as opposed to 3-8 μm) than gain-guided devices. For this reason they operate at lower threshold currents and have better single-transverse-mode stability. Both index-guided and gain-guided lasers can be modulated at rates in excess of a few GHz.

The main properties of each of the main laser geometries are presented in the Tables 8.1 and 8.2. Table 8.1 shows data for GaAlAs and Table 8.2 shows data for InGaAsP lasers. Commercially available laser diodes and their properties are shown in Table 8.3.

Longitudinal mode control in laser diodes can be achieved also intentionally[9-11] by means of distributed-feedback (DFB) and distributed-Bragg-Reflection (DBR). In these geometries the laser cavity itself or the end mirrors are formed by periodic waveguides which show high wavelength selectivity and improve temperature stability of the lasing wavelength. The temperature sensitivity of the lasing wavelength is reduced from ≃4Å/°C to ≃1Å/°c by this means. DFB and DBR lasers also have the added advantage of easy integrability with other devices onto a single chip.

## 8.4 DEVICE RELIABILITY

Extensive efforts have been made towards identifying and understanding the causes of device degradation both in AlGaAs [12-16] and in InGaAsP [17-20]. Many of these causes have been eliminated but some failure mechanisms still have not been fully understood.

The main known failure mechanisms fall within one of the following categories:

1. Facet Damage
   (a) catastrophic
   (b) slow erosion
2. Dark Line Defect
3. Thermal Resistance and Ohmic Contact
4. Self Pulsation
5. Optical Nonlinearity

Table 8.1 AlGaAs Lasers Reported in Research Literature and Their Characteristics

| Geometry | Fig. no. | Threshold Current (mA) | Power Output (mW) | Single Trans. Single Long. Mode | References | Comments |
|---|---|---|---|---|---|---|
| V-grooved | 8.3a | 50 | 3 | No | (26,27,63) | Gain guided 1Gbit mode rates demonstrated |
| BH-LOC | 8.3b | 20-30 | 10 | Yes | (28,29,41,64) | High diff. quantum eff: 80% |
| Embedded | 8.3c | 30 | 5 | Yes | (25,30,31) | |
| Deep Diffused Stripe | 8.3d | 20-30 | 20 | Yes | (32) | Linear output |
| TJS | 8.3e | 20-30 | 20 | Yes | (33) | |
| CSP | 8.3f | 70 | 15 | Yes | (25,34) | |
| CDH-LOC | 8.3h | 75 | 40 | Yes | (35,38) | Free of kinks up to 100mW |
| TS | 8 g | 95-110 | 150 | Yes | (36) | Linear up to $10xI_{th}$ Pulsed operation |
| PCW | | N/A | 36 | Yes | (37) | |

Table 8.2 InGaAsP Quaternary Lasers Reported in Research Literature and Their Characteristics

| Geometry | Fig. no. | $I_{th}$ Threshold Current/mA | Power Output (mW) | Single Transverse Single Longitudinal | References | Comments |
|---|---|---|---|---|---|---|
| Gain guided stripe | — | 150 | 1 | No | (39) | No satisfactory laser demonstrated at acceptable low $I_{th}$ |
| (BH) Buried Heterostructure | 8i | 20-30 | 40 | Yes | (40,41,43) | No kink up to I=230 mA |
| (BC) Buried Crescent | 8j | 28 | 6 | Yes | (42) | Stable single mode up to $2xI_{th}$ |
| (SAS) Self Aligned Struct. | 8k | 70 | — | Yes | (44) | |
| (PCW) Plano-Convex Waveguide | 8ℓ | 100 | 10 | Yes | (25,42) | |
| (TS) Terraced Substrate | — | — | — | — | (45) | |

Table 8.3 Commercial Laser Diodes

| Manufacturer/ Model no. | Power (mW)/ Drive Current (mW) | Threshold Current (mA) | Max Mod. Bandwidth (MHz) | Beam Divergence (m rad) | Single Mode Wavelength | Comments |
|---|---|---|---|---|---|---|
| Hitachi HL8301 | 3@75 | 60 | 1000 | 12°x27° | 0.8-0.85 | |
| Mitsubishi ML-4001 | 3@60 | 50 | 2000 | - | .78 | |
| General Optronics GOLS-SLM | 7@110 | 91 | 1250 | 780 | .78-.85 | |
| Laser Diode Lab. SCW-20,21 | 7@70 | 35 | 2000 | 610x175 | .8 -.88 | 10,000hr warr. |
| Laser Diode Lab. SCW-30,31 | 5@70 | 35 | 2000 | | .8 -.88 | very low beam divergence, integrated lens |
| Mitsubishi ML-3001 | 3@60 | 50 | 2000 | | .83 | |
| Lasertron QL51300 | 7@150 | 100 | | 10°x40° | 1.3 | |
| Lasertron QL51500 | 5@150 | 100 | | 10°x40° | 1.5 | |
| General Optronics GO-DIG, GO-ANA | 5@130 | 120mA | 1000 | | 1.3 | with fiber pigtail |

Reliability and aging tests are reproduced on large numbers of devices at elevated temperatures and the results are extrapolated to room temperature by assuming an Arrhenius statistical relationship of the form

$$\tau\ (T) \propto \exp\ (E_a/kT)$$

between lifetime $\tau$ (time for a specific degree of degradation over a specified temperature range) and absolute temperature T. k is Boltzman's constant and $E_a$ is an "activation energy" characteristic of each degradation mechanism. The criteria for failure are not yet standardized. The most commonly used are:

1. 50% increase in threshold current
2. 50% decrease in output power
3. Power drop below 1 μW
4. No lasing at elevated temperature
5. No lasing at room temperature
6. Total collapse
7. Appearance of kinks in the PI characteristics
8. Inability to withstand large currents (∿20x threshold) for several minutes

In this way expected room-temperature lifetimes in excess of $10^6$ hours have been obtained by several authors for GaAlAs laser diodes.[21-24] Real-time room temperature continuous laser operation of over two years has also been reported.[24]

InGaAsP devices are somewhat sturdier than their GaAlAs counterparts and their facet degradation due to facet oxidation is slower. Facet degradation has been barely observable in tests of up to $10^4$ hours without facet coatings.

LED's have been found to degrade slower than laser diodes and extrapolated room-temperature lifetimes of $\simeq 4x10^7$ hours for AlGaAs LED's and $\simeq 5x10^9$ hours for [17]. InGaAsP LED's have been reported.

## 8.5 CONCLUSION

At the present time GaAlAs laser diodes and LED's offer the best solution for short range optical data links ( intraurban or shorter). This choice is aided by the commercial availability of low cost photodetectors for the 800-900 nm spectral region.

For high-data-rate long-haul applications, however, InGaAsP laser diodes, with their excellent match to the low-loss low-dispersion spectral region of fibers (1100-1700nm), seem to offer the best alternative. They also appear to be less susceptible to degradation than GaAlAs diodes.

For optical gyroscope applications, where a short coherence length is required for freedom of interference of the optical beams with themselves due to backward Rayleigh scattering, a super-radiant laser diode offers the best match. Super-radiant diodes can be obtained from most of the laser diodes by anti-reflection coating the mirror facets appropriately and by starting with a not too narrow stripe laser geometry capable of multimode oscillation.

It appears that the main efforts in research should be concentrated in the areas of improving the mode stability of single-transverse and single-longitudinal mode laser diodes. This is of particular importance when lasers are modualted at several GHz frequencies. Other issues to be addressed include higher output power and improved performance at higher currents and higher temperatures.

## References


1. J.P. Witke, "Spontageous-Emission-Rate Alteration by Dielectric and other Waveguiding Structures", RCA Rev., Vol. 36, pp. 655-656, Dec. 1973.

2. M. Ettenberg, H. Uressel, and J.P. Witke, "Very High Radiance Edge-Emitting LED's", IEEE J. Quantum Electron., vol. QE-12, pp. 360-364, June, 1976.

3. D. Botez and U. Ettenberg, "Comparison of Surface-An Edge-Emitting LED's for Use in Fiber-Optical Communications", IEEE Trans. Electron Devices, vol. ED-26, pp. 1230-1238, Aug. 1979.

4. M. Abe, I. Umebu, O. Hasenawa, S. Yamaroshi, T. Yamaoka, T. Rotani, H. Okada, and H. Takanashi, "High Efficiency Long-Lived GaAlAs LED's for Fiber Optical Communications", IEEE Trans. Electron Devices, vol. ED-24, pp. 990-994, July, 1977.

5. J. Straus and O.I. Szentesi, "Linearized Transmitter for Optical Communications", Proc. IEEE Int. Symp. Circuits and Systems", Phoenix, AZ, pp. 288-292, April, 1977.

6. M. J. Adams, D. N. Payne, F. M. E. Sladen, and A. H. Hartog, "Optimum Operating Wavelength for Chromatic Equalisation in Multimode Optical Fibers", Electron. Lett., vol. 14, no. 3, pp. 64-66, Feb. 2, 1978.

7. S. Horiuchi, T. Tanaka, K. Ikeda, and W. Susaki, "A Monolithic Linear Array of High-Radiance AlGaAs Double Heterostructure LEDs with Self-Aligned Spherical Lenses", Proc. IEEE, vol. 66, pp. 42-43, Feb. 1978.

8a. H. Kressel and J. K. Butler, Semiconductors Lasers and Heterojunctions LEDs. New York: Academic Press, 1977.

8b. T. P. Lee and A. G. Dentai, "Power and Modulation Bandwidth of GaAs-AlGaAs High Radiance LEDs for Optical Communication Systems", IEEE J. Quantum Electron., vol. QE-14, pp. 150-159, Mar. 1978.

9. M. Nakamura, K. Aiki, J. Umeda, and A. Yariv, "CW Operation of Distributed Feedback GaAs-GaAlAs Diode Lasers at Temperatures up to 300°K", Appl. Phys. Lett., vol. 27, pp. 403-405, Sept. 1975.

10. A. Doi, T. Fukuzawa, M. Nakamura, R. Ito, and K. Aiki, "InGaAs/InP Distributed Feedback Injection Lasers Fabricated by One-Step Liquid Phase Epitaxy", Appl. Phys. Lett., vol., 35, pp. 441-443, Sept. 1979.

11. K. Utaka, K. Kobayashi, K. Uishino, and Y. Suematsu, "1.5-1.6 μm GaInAsP/InP Integrated Twin-Guide Lasers with First-Order Distributed Bragg Reflectors", Electron. Lett., vol. 16, pp. 455-456, June, 1980.

12. A. R. Goodwin, P. A. Kirkby, I. G. A. Davies, and R. S. Baulcomb, "The Effects of Processing Stresses on Residual Degradation in Long-Lived $Ga_{1-x}Al_xAs$ Lasers", Appl. Phys. Lett., vol. 34, no. 10, pp. 647-649, May 15, 1979.

13. M. Ettenberg, "A Statistical Study of the Reliability of Oxide-Defined Stripe CW Lasers of (AlGa)As," J. Appl. Phys. vol. 50, pp. 1195-1203, Mar. 1979.

14. H. Imai, M. Morimoto, K. Hori, and M. Takusagawa, "Long-Lived High Power GaAlAs DH Laser Diodes at 70°C", in Tech. Dig. Topical Meeting on Optical Fiber Communication (Washington DC) Paper ThB1, pp. 90-91, Mar. 1979.

15. I. Ladany, T. R. Furman, and D.P. Marinelli, "Internal Stress and Degradation in Short-Wavelength AlGaAs double-Heterojunction Devices", Electron. Lett., vol. 15, no. 12, pp. 342-343, June 7, 1979.

16. S. Yamakoshi, T. Sugahara, O. Hasegawa, Y. Toyama, and H. Takanashi, "Growth Mechanism of (100) Dark Line Defects in High Radiance GaAlAs LEDs," in Proc. IEDM Conf. (Washington DC), pp. 642-645, Dec. 1978.

17. S. Yamakoshi, M. Abe, S. Komiya, and Y. Toyama, "Degradation of High Radiance InGaAsP/InP LED's at 1.2-1.3 μm Wavelength", in Tech. Dig. Int. Electron Device Meet., Paper 5.6, pp. 122-126, Dec. 1979.

18. G. N. Olsen, M. Ettenberg, and C. J. Nuese, "Reliability of Vapor-Grown(In, Ga)/As and (In, Ga)(As, P) Heterojunction Laser Structures", IEEE J. Quantum Electron., vol. QE-15, pp. 688-694, Aug. 1979.

19. T. Yamamoto, K. Sakai, and S. Akiba, "10000-h Continuous CW Operation of $In_{1-x}Ga_xAs_yP_{1-y}$/InP DH Lasers at Room Temperature", IEEE J. Quantum Electron., vol. QE-15, pp. 684-688, Aug. 1979.

20. R. Yeats, Y. G. Chai, T. D. Gibbs, and G. A. Antypas, "Perpornance Characteristics and Extended Lifetime Data for InGaAsP/InP LED's, IEEE Electron Device Lett., vol. EDL-2, no. 9, Sept. 1981.

21. H. Kressel, M. Ettenberg, and I. Ladany, "Accelerated Step-Temperature Aging of $Al_xGa_{1-x}As$ Heterojunction Laser Diodes", Appl. Phys. Lett., vol. 32, no. 5, pp. 305-308, Mar. 1978.

22. T. Kajimura, K. Saito, N. Shige, and R. Ito, "Stable Operation of Buried-Heterostructure $Ga_{1-x}Al_xAs$ Lasers during Accelerated Aging", Appl. Phys. Lett., vol. 33, no . 7, pp. 626-628, Oct. 1978.

23. S. Nita, H. Namizaki, S. Takamiya, and W. Susaki, "Single-Mode Junction-up TJS Lasers with Estimated Lifetime of $10^6$ Hours", IEEE J. Quantum Electron., vol. QE-15, no. 11, pp. 1208-1210, Nov. 1979.

24. R. L. Hartman, N. E. Schumaker, and R. W. Dixon, "Continuously Operated (Al,Ga)As Double-Heterstructure Lasers with 70°C Lifetimes as long as Two Years", Appl. Phys. Lett., vol. 31, no. 11, pp. 756-758, Dec. 1977.

25. M. Nakamura and S. Tsuji, "Single-Mode Semiconductor Injection Lasers for Optical Fiber Communications", IEEE, J. Quantum Electro., vol. QE-17, no. 6, June, 1981.

26. T. Kobayashi, H. Kawaguchi and Y. Furukawa, "Lasing Characteristics of Very Narrow Planar Stripe Lasers", Japan. J. Appl. Phys., vol. 16, pp. 601-607, April 1977.

27. P. Marschall, E. Schlosser, and C. Wolk, "A New Type of Diffused Stripe Geometry Injection Laser", in Proc. 4th European Conf. Opt. Commun. pp. 94-97, Sept. 1978.

28. T. Tsukada, "GaAs-$Ga_{1-x}Al_xAs$ Buried-Heterostructure Injection Lasers," J. Appl. Phys., vol. 45, pp. 4899-4909, Nov. 1974.

29. K. Saito and R. Ito, "Buried-Heterostructure AlGaAs Lasers," IEEE J. Quantum Electron., vol. QE-16, pp. 205-215, Feb. 1980.

30. P.A. Kirkby and G.H.B. Thompson, "Channeled Substrate Buried Heterstructure GaAs-(GaAl)As Injection Lasers", J. Appl. Phys., vol. 47, pp. 4578-4589, Oct. 1976.

31. R. D. Burnham and D. R. Scifres, "Etched Buried Heterostructure GaAs/GaAlAs Injection Lasers", Appl. Phys. Lett., vol. 27, pp. 510-511, Nov. 1975.

32. H. Yonezu et al., "New Stripe Geometry Laser with High Quality Lasing Characteristics of Horizontal Transverse Mode Stabilization", Japan, J. Appl. Phys., vol. 16, pp. 209-210, Jan. 1977.

33. H. Namizaki,"Transverse-Junction-Stripe Lasers with a GaAs p-n Junction", IEEE J. Quantum Electron., vol QE-11, pp. 427-431, July, 1975.

34. K. Aiki, M. Nakamura, T. Kuroda, and J. Umeda, "Channeled-Substrate-Planar Structure (AlGa)As Diode Lasers", Appl. Phys. Lett., vol. 48, pp. 649-651, June 1977.

35. D. Botez and P. Zory, "Constricted Double-Heterostructure (AlGa)As Diode Lasers", Appl. Phys. Lett., vol. 32, pp. 261-263, Feb. 1978.

36. T. Sugi, M. Wada, H. Shimizu, K. Ito, and I. Teramoto, "Terraces-Substrate GaAs-(GaAl)As Injection Lasers." Appl. Phys. Lett., vol. 34, pp. 270-272, Feb. 1979.

37. Y. Ide, T. Furuse, I. Sakuma, and K. Nishida, "Transverse MOde Stabilized AlGaAs/GaAs plano-convex waveguide Laser Made by a Single-Step Liquid Phase Epitaxy", Appl. Phys. Lett., vol 36, pp. 121-123, Jan. 1980.

38. D. Botez,"CW High-Power Single-Mode Operation of Cousticted Double-Heterojunction AlGaAs Lasers with Large Optical Cavity" Appl. Phys. Lett., 36, 190 (1980).

39. R. E. Nahory, M. A. Pollack, and J. C. DeWinter,"Temperature Dependence of InGaAsP Double Heterostructure Laser Characteristics", Electron. Lett., vol. 15, pp. 695-696, Oct. 1979.

40. H. Kano and K. Suglyama, "Operation Characteristics of Buried-Stripe GaInAsP/InP DH Lasers Made by Melt-Back Method", J. Appl. Phys. vol. 50, pp. 7934-7938, Dec. 1979.

41. H. Nagai, Y. Noguchi, K. Takahei, Y. Toyoshima, and G. Iwane, "InP/GaInAsP Buried Heterostructure Lasers of 1.5 μm Region", Japan, J. Appl. Phys. vol. 19, pp. L218-L220, Apr. 1980.

42. T. Murotani, E. Oomura, H. Higuchi, H. Namizaki, and W.Susaki, "InGaAsP/InP Buried Crescent Laser with very Low Threshold Current ($\lambda$=1.3 $\mu$m)," Electron. Lett., vol. 16, pp. 566-568, July 1980.

43. K. Kishino, Y. Suematsu, and Y. Itaya, "Mesa-Substrate Buried Heterostructure GaInAsP/InP Injection Lasers", Electron. Lett., vol. 15, pp. 134-135, Feb. 1980.

44. M. Yano, H. Nishi, and M. Takusagawa, "Oscillation Characteristics in InGaAsP/InP DH Lasers with Self-Aligned Structure", IEEE J. Quantum Electron., vol. QE-15, pp. 1388-1394, Dec. 1979.

45. K. Moriki, K. Wakao, M. Kitamura, K. Iga, and Y. Suematsu, "Single Transverse Mode Operation of Terraced Substrate GaInAsP/InP Lasers at 1.3 $\mu$m Wavelength," Japan, J. Appl. Phys., vol 19, pp. 2191-2196, Nov. 1980.

# 9. DETECTORS

## 9.1 INTRODUCTION

Detectors for optical communications should have high sensitivity and fast response to allow long-haul high-data-rate information transmission.

In the 800-900 nm spectral region of GaAlAs laser diodes and LED's, both PIN (without internal gain) and avalanche photodiodes (APD's, with internal gain) have sufficiently high speed of response to allow detection of Gbit/sec signals[1]. Si APD's and PIN diodes with rise-times below 80ps and 35 ps, respectively, are now commercially available. Quantum efficiencies of commercially available Si PIN diodes are around 85%. In this spectral region and at modulation rates up to 1 Gbit/sec, dark currents are sufficiently low to introduce negligible system noise, and the receiver sensitivity is primarily limited by the amplifier noise.

The basic geometries for PIN and APD's are shown in Fig. 9.1. Various Si APD structures are commercially available. APD's increase receiver sensitivity by internal avalanche multiplication of the signal photocurrent. In the 800-900nm spectral region the best detectors have been considered to be the Si APD's. However, new developments in the GaAlAs/GaAs alloy system make that choice less clear in the near future. The GaAlAs/GaAs alloy system provides excellent lattice matching and is thus very useful in heterostructure devices. Double heterostructure photodetectors in this material system have demonstrated high quantum efficiencies.[2,3] Others [4] have reported on GaAlAs/GaAs APD's of high quantum efficiency: 65 percent without anti-reflection coating and 95 percent with anti-reflection coating; very short rise times: 35 ps or less; avalanche gains of ~100, and dark current densities of about $3.4 \times 10^{-8}$ A/cm$^2$ at one-half breakdown voltage. The GaAlAs/GaAs material system is therefore superior to the Si system in both speed and quantum efficiency, but it is inferior to it in noise properties. The larger noise is believed to be due to direct bandgap tunneling as evidenced by the somewhat larger dark currents. As of yet, no diodes in this material system are commercially available in this spectral range.

In the 1100-1700 nm range, however, the choices are broader. Possible candidates are Ge, InGaAs, GaAlSb, InGaAsP and GaAlAsSb devices.

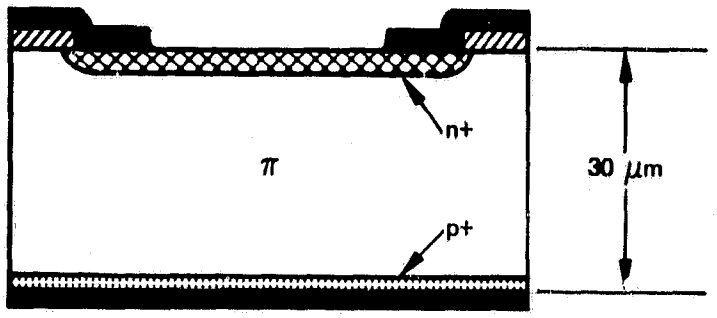


(A) PIN PHOTODIODE

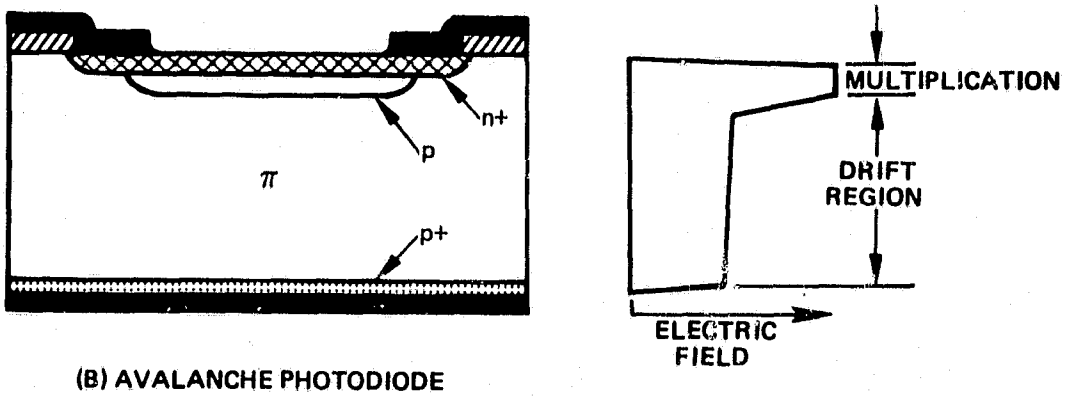


(B) AVALANCHE PHOTODIODE

Figure 9-1. Silicon p-i-n and avalanche photodiode structures.

Ge is sensitive to wavelengths below 1800nm and its broadband quantum efficiency is about 40 percent. It suffers, however, from an inherently high noise level. The dark current level at gain of 1 is about 0.1 μA.

The III-V alloy direct-bandgap materials mainly, mainly under research, can be tailored to the wavelength by proper choice of the alloy mixture. This results in lowered dark currents by eliminating thermal noise below the bandgap energy. Another added advantage of this alloys is that they can be fabricated in heterojunction geometries,improving the detector speed.

The ternary alloys (InGaAs, GaAlSb on GaSb) have been investigated as photodiode materials for the 1000-1400 nm range. Their main drawback is the appearance of lattice mismatch defects during crystal growth, which are believed to cause increased dark current and microplasma sites. The existence of microplasma sites limits avalanche performance.[6] In addition, lattice mismatch is generally associated with shorter life-times. Thus lattice-matched quaternary alloys appear to offer a better chance for obtaining high performance avalanche photodiodes. GaAlAsSb/GaSb heterojunction APD's show very fast rise-times [4,7]. The response time [8] of InP based devices has also been drastically improved by geometries that locate the heterojunction close to the p-n junction. Rise-times for these systems are now in the <100 ps range.

A GaAlAsSb APD has been integrated [7] with an FET for improved performance by reducing the capacitance between components. The integrated receiver had a sensitivity 10-20 times higher than that of a Ge APD with the same preamplifier over a bandwidth of 100 MHz.

However, unlike silicon,III-V alloy material systems all suffer from a common fundamental problem: the ionization coefficients for electron and holes are similar, thus both carriers are multiplied in the avalanche and excess noise is generated (in silicon the ionization coefficient for electrons can be 10 to 100 times larger than that of holes so only one carrier type is multiplied significantly). Therefore low noise PIN detector/amplifier combinations have been proposed as the choice for long wavelength receivers, rather than avalanche photodiodes. APD's

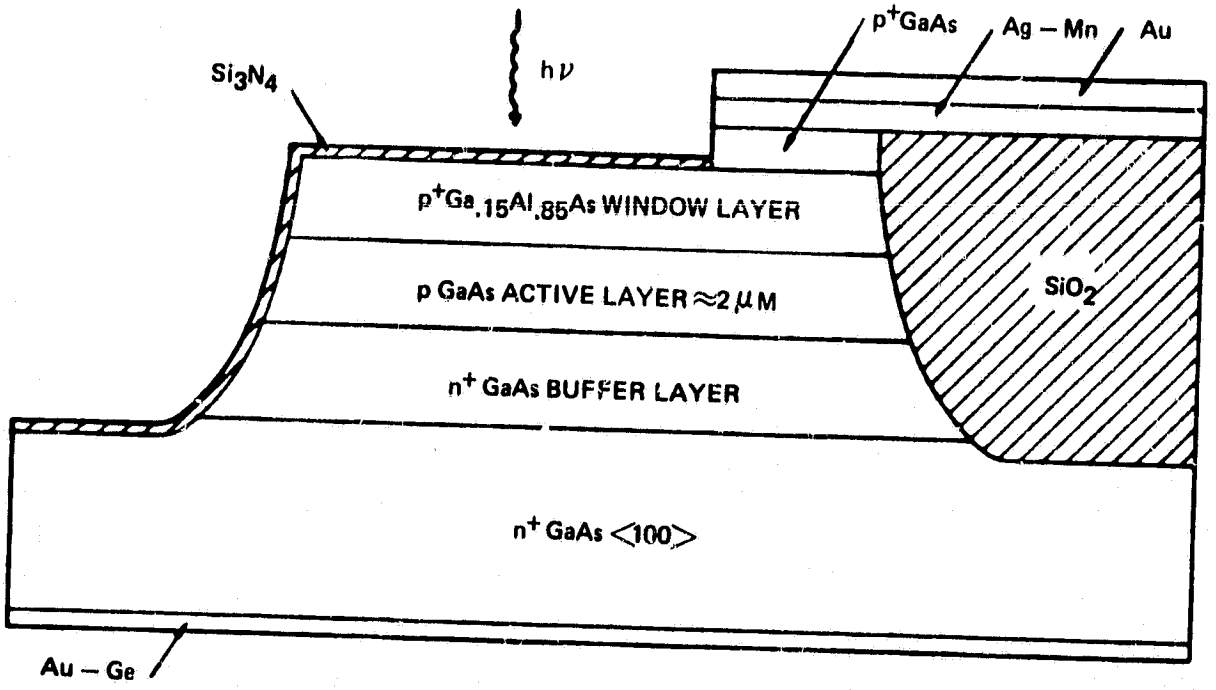


Figure 9-2. Structure of GaAlAs/GaAs diode.

offer a few dB better sensitivity than PIN diode/preamplifier combinations and require high operation voltages and complicated control circuitry.

Another choice in this spectral range is the InGaAsP/InP alloy system.[4] APD's in this material system have been found to offer lower dark current, faster response time, and higher operating temperatures than Ge devices.[19]

## 9.2 DETECTOR GEOMETRIES

### 9.2.1 PIN detectors geometries

The typical PIN detector geometry is shown in Fig 9-1a. It consists of an $n^+$ (or $p^+$) thin layer separated by a thick $\pi$(or $\nu$) region from a $p^+$(or $n^+$) region. Contacts are attached to the $n^+(p^+)$ and $p^+(n^+)$ regions. Due to the almost intrinsic characteristics of the $\pi(\nu)$ region, the depletion region reaches from the $\pi(\nu)$ side of the $n^+(p^+)$ region clear across the $\pi(\nu)$ region, into the $p^+(n^+)$ region, increasing the collection efficiency of the photons.

This device can be operated in two modes: without a bias voltage (the photovoltaic mode) or with a bias voltage (the photoamperic mode). The frequency response of this device is limited by the transient time across the $\pi(\nu)$ region and the capacitance between $p^+(n^+)$ and $n^+(p^+)$ regions.

Since the gain of this structures is usually low, PIN diodes have been integrated with GaAs FET's in order to improve their gain. In integrated configuration they have been operated [8] successfully at 274 Mbits/sec with sensitivities comparable or better than those of Ge APD at 1.3 μm.

### 9.2.2 APD geometries

The typical geometry of an avalanche photodiode is shown in Fig. 9-1b. In this geometry a thin p(n) layer is added between the $n^+(p^+)$ and the $\pi(\nu)$ regions. The APD is operated at an reverse bias thus the p(n) region is a region of very high electric field in which the current is multiplied by avalanche processes providing for internal gain before it goes to the next amplifier.

A slightly modified geometry is shown in Fig. 9-2. This structure has been used in the realization of GaAlAs/GaAs APD's. It consists of an $n^+$ GaAs substrate onto which several layers are grown in succession:

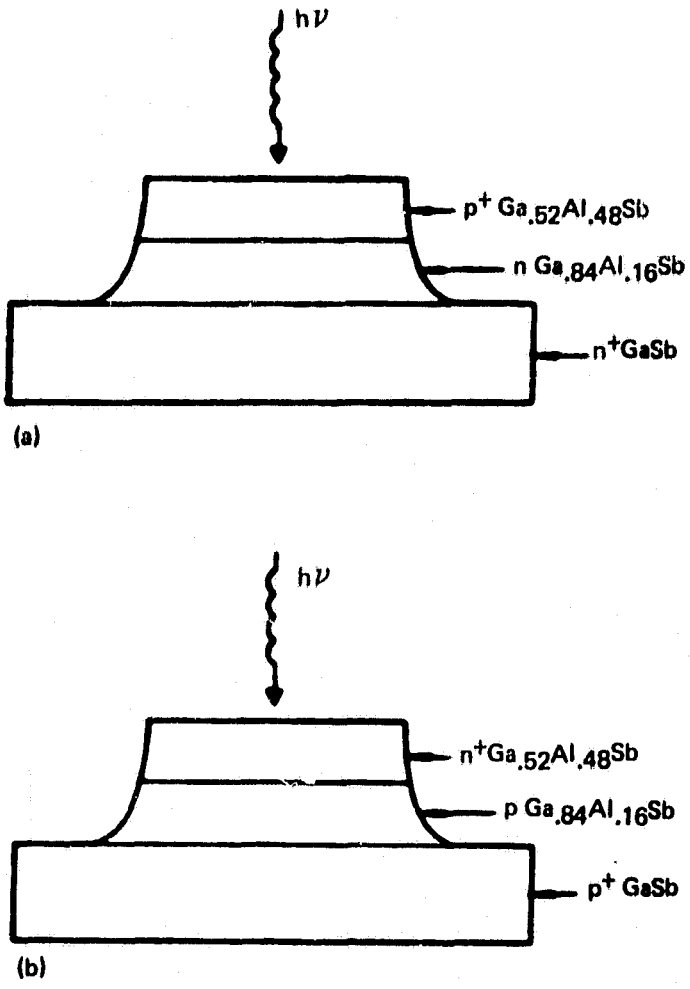


Figure 9-3. (a) Structure of the GaAlSb diode for electron injection; (b) structure of the GaAlSb diode for hole injection.

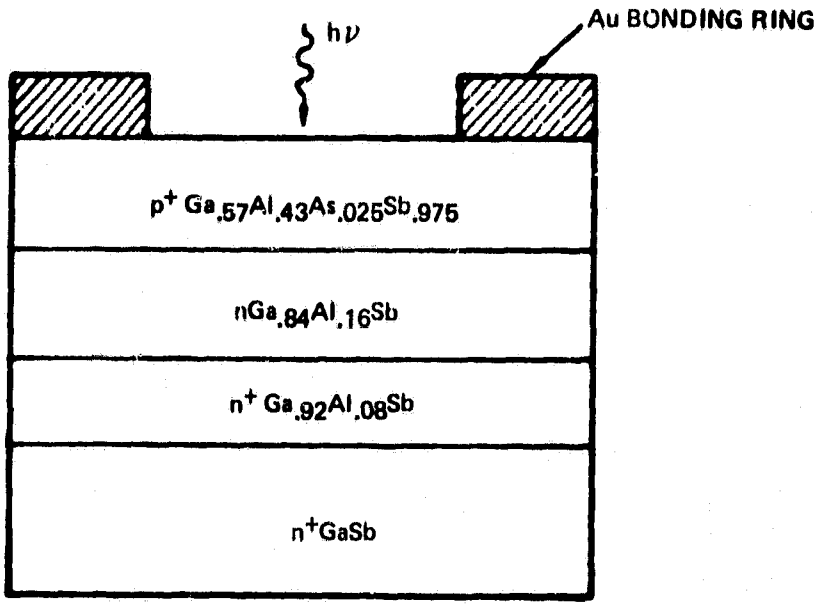


Figure 9-4. Structure of GaAlAsSb diodes for electron injection.

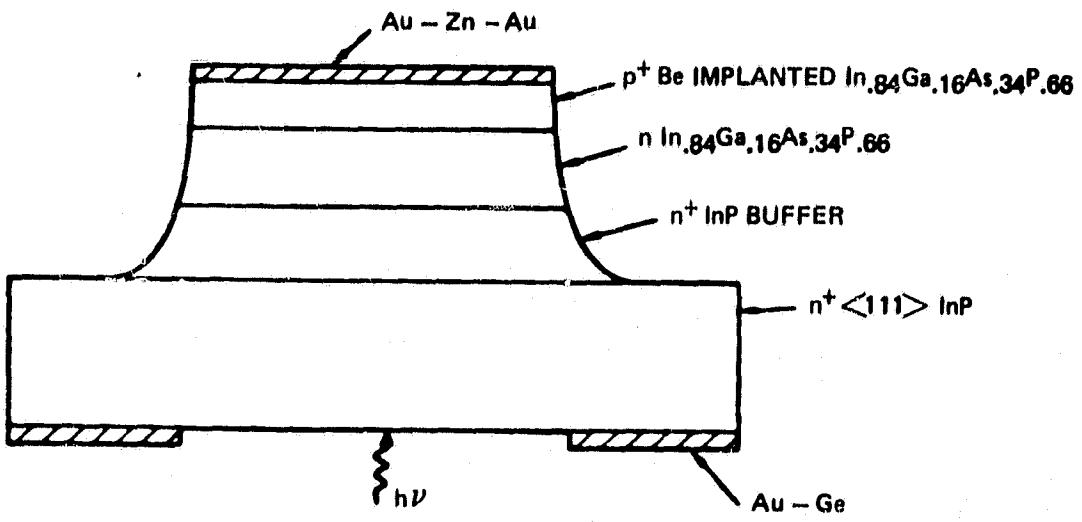


Figure 9-5. Structure of Be implanted InGaAsP diodes.

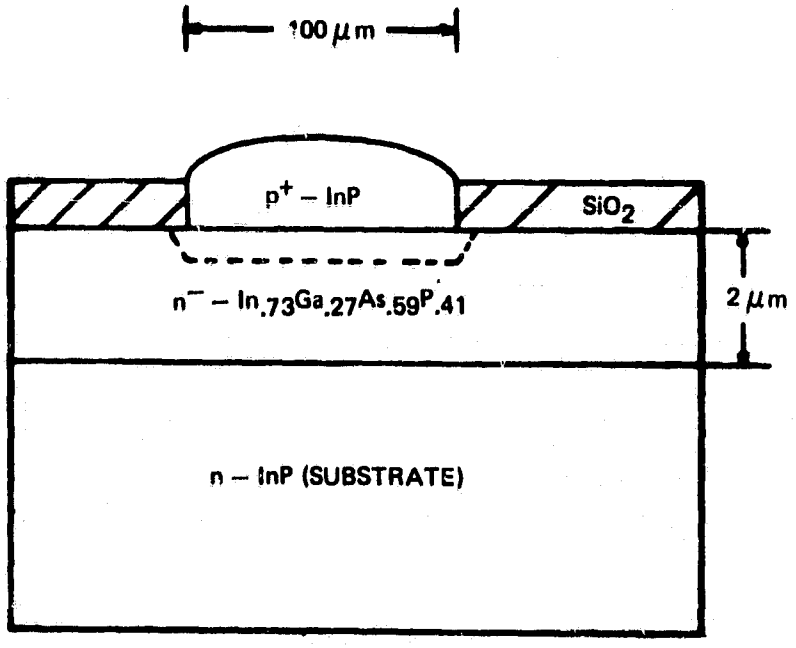


Figure 9-6. "Buried" planar avalanche photodetector grown by oxide defined vapor-phase epitaxy.

C-2

An $n^+$ Te doped GaAs buffer layer, a 2 μm Ge doped p GaAs active layer, a Ge doped GaAlAs p window layer, and a very thin(≈.2 μm) Ge doped $p^+$ GaAs contact layer. The external quantum efficiency of this device is 95 percent at λ=530 nm when antireflection coatings are used. Response times of less than 35 ps were observed with this device.

Another detector structure[4] used with the GaAlSb alloy system is shown shown in Fig. 9-3. With this structures internal quantum efficiencies of 60 percent at 1060 nm dropping to 45 percent at 1270 nm have been obtained without antireflexion coating.

The geometry shown on Fig. 9-4 has been used with the GaAlAsSb material system. This system offers the advantages of better surface morphology and lower dark current densities (up to three times lower). The main limitation on this system appears to be surface breakdown at the interface between the p $Ga_{.84}Al_{.16}Sb$ and the $n^+$ $Ga_{.57}Al_{.43}As_{.025}Sb_{.975}$ layers caused by the incorporation of Sb. The solution of this problem is undoubtedly possible and will make this system a much better candidate at longer wavelengths.

Another structure of interest is the Be implanted InGaAsP of Fig. 9-5. Be implantation is used to form the $p^+$ layer instead of Zn, avoiding the problems generated by the high and concentration dependent diffusion coefficient of the latter, which makes control of the position of the p-n junction difficult. With this structure dark currents as low as $4x10^{-6}$ A/cm$^2$ at 10V and $1.9x10^{-5}$ A/cm$^2$ at 10V reverse bias have been achieved. These devices also show very fast rise times of approximately 60 ps and FWTM times of approxiamtely 180 ps.

Another novel geometry in InGaAsP/InP recently reported[9] is the "buried" avalanche detector shown in Fig. 9-6. The structure is grown in a two-step vapor phase epitaxy process whereby an undoped InGaAsP layer is first covered with $SiO_2$. 100 μm holes are then etched into the $SiO_2$ prior to vapor deposition of a Zn-doped p-type InP layer. Zinc diffuses from the InP into the InGaAsP layer and encloses the p-n InGaAsP homojunction. Avalanche gains as high as 20 were reported.

Another type of detector recently reported [10] and which might provide an interface between digital logic circuits and input/output optical fibers in the 1300 nm spectral range is the p-n-p-n optical switch shown

in Fig. 9-7. This device exhibits a nonlinear (negative-resistance) I-V characteristic which can be useful in switching from low to high current, triggered by small currents in the μA range. The signal current is provided by light injected via a step-index multimode fiber. Switching was reported with powers as low as 3 μW of light at 1060 nm. This device has potential use as a light-signal repeater.

The device of Fig. 9-8 is a novel structure recently reported in the literature[11]. This is a device compatible with planar technology and lends itself to integration with MESFETS and other microwave integrated circuits. It has response times between 50 and 60 ps and operating voltages below 25V at $\lambda$=830 nm.

Photoconductive devices made either of high-sensitivity semiconductors[1] or of conductive materials, have received attention recently[12]. The first rely on the recombination of photogenerated carrier for their speed and the second achieve fast sweep out of carriers by the application of a d.c. bias. Response times below 100 ps have been reported with a 48x48 μm large device (fi (Fig. 9-9) fabricated on an InP substrate.

## 9.3 CONCLUSION

In the 800-900 nm spectral range Si PIN and APD devices seem to offer the best match, followed closely by the high quantum efficiency, fast, lattice-matched GaAlAs/GaAs alloy devices, which have been improved greatly in the last year and should mature more in the next few years of research.

In the 1100-1700 nm spectral range the detector choices are less clear and several systems should play a role in the years to come. The contenders are Ge-PIN detectors with integrated preamplifiers and noise improved Ge-APD's; and the III-V Ternary and quaternary systems, whose response times and dark current levels have been improved significantly over the past years and will probably undergo further development in the future.

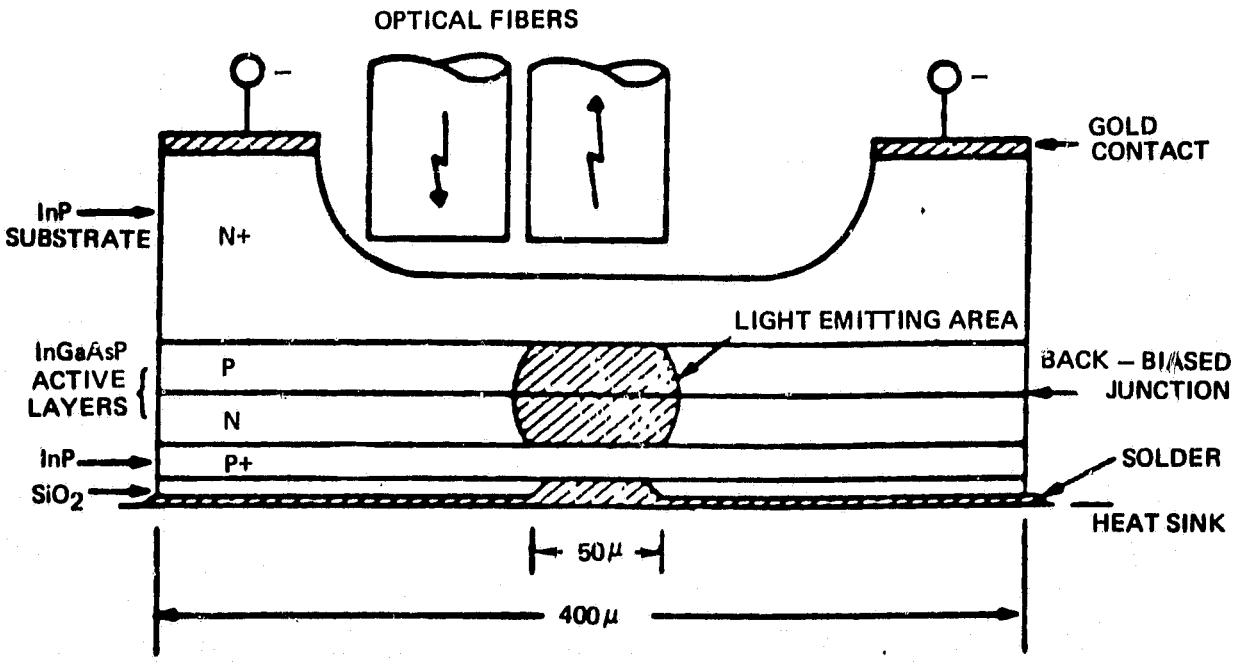


Figure 9-7. p-n-p-n- detector and LED structure.

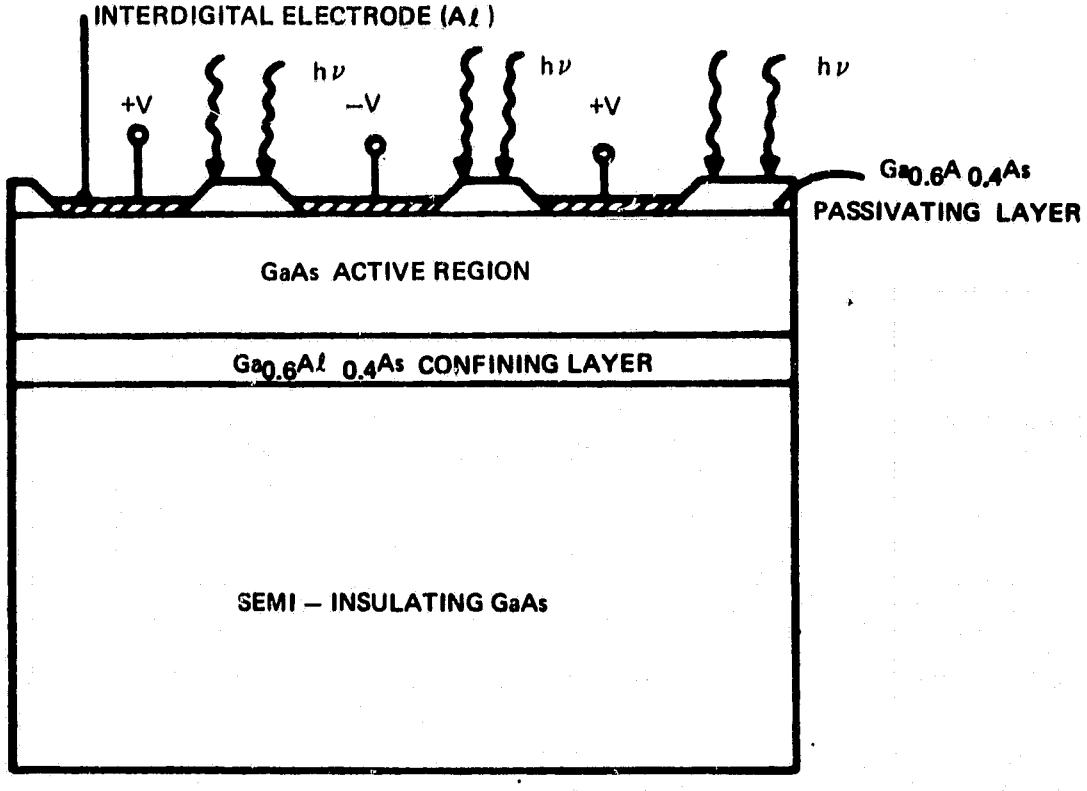


Figure 9-8. Schematic cross section of the HIP detector.

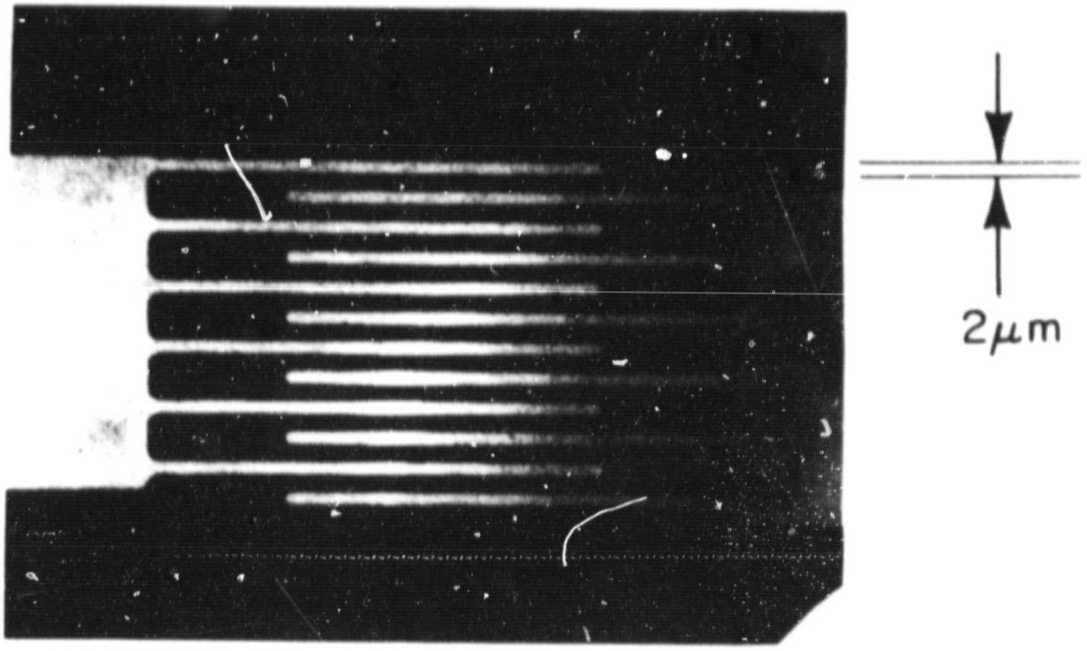


Figure 9-9. Photograph of the InP optoelectronic switch.

## References


1. H. Melchior, "Detectors for lightwave communication", Physics Today, vol. 30, pp. 32-39, Nov. 1977.

2. J. L. Merz, R. A. Logan, P. L. McBride, and A. M. Sergent, "GaAs double heterostructure photodetectors," J. Appl. Phys., vol. 48, pp. 3580-3587, Aug. 1977.

3. E. Eickhoff, P. Marshall, and E. Schlosser, "Transparent, highly sensitive GaAs/(GaAl)As photodiodes," Electron Lett., vol. 13, pp. 493-494, Aug. 1977.

4. H. David Law, K. Nakano, and L. R. Tomasetta, "III-V alloy heterostructure high speed avalanche photodiodes", IEEE J. Quantum Elect. vol. QE-15, no. 7, July 1979.

5. H. Ando, H. Kanbe, T. Kimura, T. Yamaosa, and T. Kaneda, "Characteristics of germanium avalanche photodiodes in the wavelength region of 1-1.6 μm," IEEE J. Quantum Electron., vol. QE-14, pp. 804-809, Nov. 1978.

6. T. P. Lee, C. A. Burrus, Jr., and A. G. Dental, "InGaAsP/InP photodiodes: Microplasma-limited avalanche multiplication at 1-1.3 μm wavelength," IEEE J. Quantum Electron., vol. QE-15, pp. 30-35, Jan. 1979.

7. L. R. Tomasetta, D. Low, R. C. Eden, I. Dehimy, and K. Nakano, "High sensitivity optical receivers for 1.0-1.4 μm fiber-optic systems," IEEE J-QE, pp. 800-804, Nov. 1978.

8. T. P. Lee, C. A. Burrus, and A. G. Pentai ,"InGaAs/InP pin photodiodes for lightwave communications at the .95-1.65 μm wavelength", IEEE, JQE, vol. QE-17, no. 2, pp. 232-238, Feb. 1981.

9. G. H. Olsen and H. Kressel, "Vapor-grown 1.3 m InGaAsP/InP avalanche detectors," Electron Lett., Mar-Apr. 1979.

10. K. Ogawa, "Optical repeater gain achievable with light-activated p-n--p-n LEDs," in Tech. Dig. Topical Meet. Optical Fiber Communication (Washington, DC), Paper ThB5, pp. 94-95, Mar. 1979.

11. L. Figueroa and C. W. Slayman, "A novel heterostructure interdigital photodetector (HIP) with picosecond optical response", IEEE Electron. Lett., vol. EDL-2, no. 8, August 1981.

12. A. G. Foyt, F. J. Leonberger, and R. C. Williamson, "Picosecond InP optoelectronic switches", Appl. Phys. Lett. 40, 447 (1982)